UNIVERSITÀ
DEGLI STUDI
FIRENZE

DOTTORATO DI RICERCA IN
SCIENZE CHIMICHE

CICLO XXVI

COORDINATORE Prof. Andrea Goti

NANOSTRUCTURED AFFINITY BIOSENSORS FOR CANCER BIOMARKERS DETECTION

Settore Scientifico Disciplinare CHIM/01

Dottorando
Dott. Ravalli Andrea

_____

Tutore
Prof. Marrazza Giovanna

_____

Coordinatore
Prof. Goti Andrea

_____

Anni 2011/2013

Abstract

Detecting cancer at early stage is one of the most important factors associated with successful treatment outcome.

Cancer biomarkers are able to detect a specific disease early and help to provide treatments before it becomes incurable in later stages. Biomarkers are also extremely important to determinate the recurrence of the disease and to evaluate the follow-up of the patients after a chemio- or radio- therapic and surgery treatments.

The classical methods (such as ELISA immunoassays) for detection of cancer biomarkers may take several hours, or even days from when tests are ordered to when results are received. These methods can be tedious, time consuming and often require extra care and expensive instruments making early diagnosis of cancer more difficult especially for the cancer patients who are admitted to an emergency department. In addition, if we consider that qualified personnel are needed for clinical analysis, the natural necessity for alternative analytical technologies is presented.

For this purpose, electrochemical biosensors can act as an option for solving problems mentioned before, or become a helpful tool at least.

The advance in nanotechnology have led to the discovery and the employment of a great number of new materials in nanoscale dimensions (comprise between 1 and 100 nm, even for biological application dimensions can raise up to 500 nm and rarely up to 700 nm). Because the common biological systems (such as protein, viruses, membrane etc.) are nanostructured and their interaction take place at nanometric scale, nanomaterials becomes an ideally candidates for the development of advanced biosensing devices. Nanostructures present several advantages in analytical applications and can be mainly used as transducers (due to their unique optical, chemical, electrical, and catalytic properties) or as a component of the recognition element of a biosensing device (due to increase of the area/volume relationship that increases the number of attached bioreceptors in the sensing surface).

In this thesis different strategies for the development of electrochemical nanostructured biosensors for the determination of a pattern of cancer biomarkers (in particular CA125, HER2, VEGF, MUC1) related to the early detection of ovarian and breast cancers were presented.

In particular this dissertation is subdivided in seven chapters.

In Chapter 1 the definitions of electrochemical biosensor and biomarker were introduced. Moreover, the use of antibodies, aptamers and Affibodies® as bioreceptors in electrochemical biosensors for clinical applications were discussed. Finally, recent applications of nanostructured biosensors for detection of cancer biomarkers were reviewed.

In Chapter 2 the electrochemical techniques (cyclic voltammetry, differential pulse voltammetry and electrochemical impedance spectroscopy) used in this work were introduced.

From Chapter 3 to Chapter 7 the development of nanostructured electrochemical biosensors for the determination of CA125, VEGF, HER2 and MUC1 cancer biomarkers were presented.

Chapter 3: a label-free impedimetric immunosensor for the detection of tumour marker CA125 based on gold nanoparticles-modified graphite screen-printed electrodes was reported. Experimental conditions of each step for the developed immunosensor were studied and optimised. The electrochemical immunosensor allowed unambiguous identification of CA125, while no significant non-specific signal was detected in the case of all negative controls. The analytical usefulness of the impedimetric immunosensor was finally demonstrated analysing human serum samples.

Chapter 4: two simple and sensitive approaches for CA125 detection were presented by using antibody immobilized on poly-anthranilic acid-modified graphite screen printed electrodes. The first proposed approach was a label free impedimetric immunosensor. The immunoassay was based on poly-anthranilic acid (PAA) modified graphite screen-printed electrodes with subsequent covalently monoclonal antibody anti-CA125 immobilization. The modified screen-printed electrodes were used to capture the protein from the sample solutions. The second approach was based on a sandwich format. The monoclonal anti-CA125 antibodies immobilized on poly anthranilic acid-modified graphite screen-printed electrodes were used to capture the protein from the sample solution. The sandwich assay

was then performed by adding secondary anti-CA125 antibodies labelled with gold nanoparticles (AuNPs). The antibody-AuNPs captured onto immunosensor surface induced the silver deposition from a silver enhancer solution. The deposited AgNPs were measured by anodic stripping voltammetry (ASV) in acid solution. The performance of both immunosensors in terms of sensitivity, reproducibility and selectivity were studied.

Chapter 5: an aptamers sandwich biosensor based on gold nanostructured (AuNPs) graphite screen-printed electrodes for the determination of VEGF cancer biomarker was proposed. First, thiolated anti-VEGF aptamer was covalently immobilized on the surface of gold nanoparticles-modified graphite screen printed electrodes (AuNPs-GSPEs) followed by the formation of a mixed self-assembly monolayer SAM. VEGF antigen was then incubated with the sensors and subsequently the sandwich was completed by interaction with secondary biotinylated anti-VEGF aptamer. Streptavidin-alkaline phosphatase was finally incubated with the sensors and the electrochemical behaviour of alpha-naphthol was analysed by differential pulse voltammetry (DPV) in order to construct the calibration curve. Each phases involved in the assembly of the aptasensors were evaluated by electrochemical impedance spectroscopy (EIS) technique. The performance of the immunoassay in terms of sensitivity, reproducibility and selectivity has been also studied.

Chapter 6: the development of a label-free gold nanostructured biosensor using anti-HER2 Affibody® as bioreceptor for the detection of HER2 breast cancer biomarker was reported. The biosensor was based on the immobilization of the terminal cysteine-modified Affibody® on the surface of AuNPs-modified GSPEs *via* Au-SH bond. After the formation of self-assembly monolayer, bioreceptor-antigen affinity reaction was evaluated by means of electrochemical impedance spectroscopy (EIS) technique. Preliminary experiments in commercial serum samples spiked with HER2 protein were also conducted. Each phases of the construction of the assay were characterized and evaluated by means of EIS measurements. Finally, the reproducibility and selectivity were determined.

Chapter 7: different electrochemical bioassays for Mucin1 (MUC1) tumor marker using magnetic beads coupling screen-printed arrays were developed and used for analysis in

biological samples. The bioassays were based on a sandwich format in which aptamers or antibodies were coupled respectively to Streptavidin or Protein G-modified magnetic beads. The modified beads were then used to capture the protein from the sample solution and the sandwich assay is performed by adding a secondary aptamer or antibody. The enzyme alkaline phosphatase (AP) and its substrate (1-naphthyl phosphate) were then used for the electrochemical detection by differential pulse voltammetry (DPV). All parameters involved in each step of the affinity sensors were optimized. The analytical performance of the designed assays was compared in terms of sensitivity, selectivity and reproducibility. The results showed that although a comparable sensitivity was obtained for all tested assays, however, the aptamer-based approaches exhibit higher selectivity for MUC1, allowing also the detection of the protein in complex matrices. The developed aptasensor for multiplex detection was applied on serum samples obtained from cancer patients, providing promising perspectives for future clinical applications.

Curriculum Vitae

Nato a Prato il 02/05/1982.

Diploma di Perito Chimico Tintore, conseguito presso l' I.T.I.S. T. Buzzi (Prato) nell'anno 2001, con votazione 80/100.

Attestato di Tecnico per la Sicurezza sul Lavoro, rilasciato dalla Regione Toscana (2004)

Laurea triennale in Chimica Applicata, conseguita presso l'Università di Firenze il 22/04/2005 con votazione 106/110.

Laurea specialistica in Chimica dell'Ambiente e dei Beni Culturali (Classe S/62), conseguita presso l'Università di Firenze il 20/07/2009 con votazione 109/110.

Giugno – Settembre 2010: Contratto a progetto presso il gruppo Sensori e Biosensori (Dipartimento di Chimica – Università di Firenze): "*Valutazione di una strumentazione analitica integrata per analisi rapide e decentrate di patogeni alimentari"*.

Settembre – Novembre 2010: Contratto a progetto con Ecobioservices & Researches s.r.l (attività svolta presso il Dipartimento di Chimica – Università di Firenze, gruppi Sensori e Biosensori): "*Biosensori per la determinazione rapida (POCT) della celiachia e delle allergie"*.

Dicembre 2010 –Novembre 2012: Borsa di studio per attività di ricerca presso il gruppo Sensori e Biosensori (Dipartimento di Chimica – Università di Firenze): *"Realizzazione di sensori elettrochimici"*.

Gennaio 2011: iscritto al I anno del corso di Dottorato di ricerca in Scienze Chimiche XVVI ciclo (tutor scientifico: prof. Giovanna Marrazza).

Novembre – Dicembre 2011: Stage della durata di 1 mese nell'ambito del programma di azioni integrate Italia-Spagna 2010-2012 "Nanobiosensori per la valutazione di marcatori

tumorali", presso ICN-CIN2 (Istituto Catalano di Nanotecnologia – Centro di Investigazione in Nanoscienza e Nanotecnologia), Bellaterra (Barcellona, Spagna); tutori scientifici: Prof. Giovanna Marrazza, Prof. Arben Merkoci.

Gennaio 2012: iscritto al II anno del corso di Dottorato di ricerca in Scienze Chimiche XVVI ciclo (tutor scientifico: prof. Giovanna Marrazza).

Aprile 2012: 1 settimana trascorsa come Vsiting Student presso l' Università di Cranfield (UK), supervisore: prof. Sergey Piletsky.

Dicembre 2012: abilitazione all'esercizio della professione di Chimico.

Gennaio 2013: iscritto al III anno del corso di Dottorato di ricerca in Scienze Chimiche XVVI ciclo (tutor scientifico: prof. Giovanna Marrazza).

Giugno 2013: partecipazione alla "Summer School on Electrochemistry for Environmental and Biomedical Applications" (Cluj-Napoca (Romania), 17 – 21 Giugno 2013).

Settembre 2013: vincitore di una borsa di studio (esame titoli) per la partecipazione al XXIV Congresso Nazionale di Chimica Analitica (Sestri Levante, 15 – 19 Settembre 2013).

Publications

Ravalli A., Rivas L., De la Escosura-Muñiz A., Pons J., Merkoçi A., Marrazza G., Sandwich aptamers assay based on gold nanostructured graphite screen-printed electrodes for VEGF cancer biomarker detection, *Submitted to Journal of Nanoscience and Nanotechnology*, 2013.

Ravalli A., Da Rocha C. G., Yamanaka H., Marrazza G., Affibody®-based label-free gold nanostructured biosensor for HER2 breast cancer biomarker detection, *Submitted to Talanta*, 2013.

Florea A., Ravalli A., Cristea C., Sandulescu R., Marrazza G., Electrochemical Aptasensor for multiplex detection of MUC1 tumor marker addressable to hospital patients for cancer screening, *Submitted to Clinica Chimica Acta*, 2013.

Ravalli A., Rivas L., De la Escosura-Muñiz A., Merkoçi A., Marrazza G., Electrochemical antibody – aptamer assay for VEGF cancer biomarker detection, *Sensors and Microsystems AISEM proceeding*, 2013.

Ravalli A., Florea A., Cristea C., Sandulescu R., Marrazza G., Electrochemical immunoassay for Mucin 1 detection as diagnostic tool in ovarian cancer, *Sensors and Microsystems AISEM* proceedings, 2013.

Ravalli A., Pilon dos Santos G., Ferroni M., Faglia G., Yamanaka H., Marrazza G., New label free CA125 detection based on gold nanostructured screen-printed electrode, *Sensors and Actuators B: Chemical*, 2013, 179, 194-200.

Taleat Z., Ravalli A., Mazloum-Ardakani M., Marrazza G., CA 125 Immunosensor Based on Poly-Anthranilic Acid Modified Screen-Printed Electrodes, *Electroanalysis* 2013, 25, 269-277.

Congress participations

1. GS2013 e SIOF (Sestri Levante,19 – 20 Settembre 2013):
   Poster: "Polymer-modified thin-film interdigitated array for (bio)sensing applications", Autori: Andrea Ravalli, Giovanna Marrazza.

2. XXIV Congresso della divisione di Chimica Analitica della SCI (Sestri Levante, 15 – 19 Settembre 2013)
   Orale: "New aptasensors for early diagnosis of breast cancer". Autori: Andrea Ravalli, Giovanna Marrazza.

3. COST thematic workshop "Bioinspired Nanotechnology for Biosensing" (Stiges, 16 Maggio 2013)
   a. Poster: "Polymer-modified thin-film interdigitated array for (bio)sensing applications".
      Autori: Autori: Bianca Ciui, Andrea Ravalli, Cecilia Cristea, Robert Sandulescu, Giovanna Marrazza.

   b. Poster: "Electrochemical apatsensor for multiplex detection of MUC1 addressable in hospital patients for cancer screening".
      Autori: Anca Florea, Andrea Ravalli, Cecilia Cristea, Robert Sandulescu, Giovanna Marrazza.

4. XVII Congresso AISEM 2013 (Brescia, 5 – 7 Febbraio 2013)
   a. Orale: "Electrochemical immunoassay for MUC1 detection as diagnostic tools in ovarian cancer". Autori: Anca Florea, Andrea Ravalli, Cecilia Cristea, Robert Sandulescu, Giovanna Marrazza.

   b. Poster: "New Aptasensor for VEGF biomarker detection". Autori: Andrea Ravalli, Lourdes Rivas, Alfredo de la Escosura-Muñiz, Josefina Pons, Arben Merkoçi, Giovanna Marrazza.

c. Poster: “Electrochemical immunoassay for CA125 detection based on silver-enhanced gold nanoparticle label”. Autori: Andrea Ravalli, Zahra Taleat, Giovanna Marrazza.

5. XXIII Congresso della divisione di Chimica Analitica della SCI (Isola d’Elba, 16 – 20 Settembre 2012)
   a. Orale: “Electrochemical immunoassay for CA125 detection based on silver-enhanced gold nanoparticle label”. Autori: Andrea Ravalli, Zahra Taleat, Giovanna Marrazza.

   b. Poster: “New Aptasensor for VEGF biomarker detection”. Autori: Andrea Ravalli, Lourdes Rivas, Alfredo de la Escosura-Muñiz, Josefina Pons, Arben Merkoçi, Giovanna Marrazza.

   c. Poster: “Electrochemical immunoassay for MUC1 detection as diagnostic tools in ovarian cancer”. Autori: Anca Florea, Andrea Ravalli, Cecilia Cristea, Robert Sandulescu, Giovanna Marrazza.

6. 63rd Annual Meeting of the International Society of Electrochemistry (Praga, 19 – 24 Agosto 2012):

   Orale: “Gold nanostructures for affinity biosensing applications”. Autori: Andrea Ravalli, Giovanna Marrazza.

7. 14th International Conference on Electroanalysis (ESEAC) (Portorož, Slovenia, 3 – 7 Giugno 2012):

   Poster: “Gold nanostructures for affinity biosensing applications”. Autori: Andrea Ravalli, Glauco Pilon dos Santos, Hideko Yamanaka, Giovanna Marrazza.

8. Convegno Nazionale Sensori (Roma, 15 – 17 Febbraio 2012):

   Orale: “Colorimetric dot assay for cancer biomarkers using gold nanorods”. Autori: Sonia Centi, Fulvio Ratto, Andrea Ravalli, Francesca Tatini, Zahra Taleat, Franco Fusi, Giovanna Marrazza, Roberto Pini.

9. XXIV Congresso Nazionale SCI (Lecce, 11-16 Settembre 2011):

   Orale: “Gold nanostructures for affinity biosensing applications”. Autori: Andrea Ravalli, Glauco Pilon dos Santos, Hideko Yamanaka, Giovanna Marrazza.

10. GS2010 III Workshop (Università degli Studi di Firenze 26 - 28 Ottobre 2010):

    Poster: “Realization and characterization of gold nanostructures for affinity biosensor development”. Autori Francesca Berti, Andrea Ravalli, Monica Revenga Parra, María Encarnación Lorenzo Abad, Marco Mascini, Giovanna Marrazza.

Table of contents

List of figures and tables

Figure 2.4. Nyquist plots and equivalent circuits for: A) Faradic EIS experiments, B) Non-Faradic EIS experiment. Legend: R_s: solution resistance, R_{ct}: charge transfer resistance, C_{dl}: double layer capacitance, W: Warbug impedance.

Figure 3.1. Randles equivalent circuit used to fit EIS spectra (R_s: electrolyte resistance, C_{dl}: double layer capacitance, R_{ct}: charge transfer resistance, W: Warburg impedance).

Figure 3.2. Scheme of AuNPs-based label-free immunosensor for CA125 detection: A) electrodeposition of AuNPs on GSPEs, B) Functionalization of gold nanoparticles with MUDA, C) Mixed SAM formation with MCH, D) activation of –COOH groups with EDAC/NHS and mAb-CA125 immobilisation, E) blocking step with rIgG, F) Ab-Ag affinity reaction.

Figure 3.3. A) R_{ct} as function of number of cycles (1, 10, 20, 50) using different concentrations of $HAuCl_4$: (■) 0.0002, (●) 0.0006 and (▲) 0.001 M; scan Rate: 0.1 V s^{-1}. B) R_{ct} as function of scan rate (0.025, 0.05, 0.1, 0.2 V s^{-1}) using 0.0006 M and 25 cycles. EIS measurements were performed in 0.01 M $[Fe(CN)_6]^{3-/4-}$ equimolecular mixture in 0.1 M KCl; each point was repeated at least 3 times using different gold nanostructured graphite screen-printed electrodes (AuNPs/GSPEs).

Figure 3.4. Nyquist plot of 0.01 M $[Fe(CN)_6]^{3-/4-}$ equimolecular mixture in 0.1 M KCl solution for the bare (■, curve a) and AuNPs modified GSPEs (●, curve b) obtained using 0.0006 M $HAuCl_4$, 25 cycles and scan rate 0.1 V s^{-1}. Inset: average and standard deviation respect to the R_{ct} for bare graphite screen-printed electrodes (Bare GSPEs) and for gold nanostructured graphite screen-printed electrodes (AuNPs/GSPEs). The measurements were repeated at least 3 times using different GSPEs.

Figure 3.5. A) Cyclic voltammograms obtained in 0.5 M H_2SO_4 solution for the bare GSPEs (- -) and AuNPs/GSPEs (—). B) Cyclic voltammograms obtained in 0.01 M $[Fe(CN)_6]^{3-/4-}$ 0.1 M KCl solution for the bare GSPEs (- -) and GSPEs modified with AuNPs (—).

Figure 3.6. SEM image of AuNPs electrodeposed onto graphite screen-printed electrodes prepared in optimised experimental conditions (0.0006 M $HAuCl_4$, 25 cycles 0.1 V s^{-1}), using different detectors: A) In-Lens and B) EsB detector.

Figure 3.7. Nyquist plot of AuNPs-modified GSPEs (●, curve a) and after the MUDA chemisorption (■, curve b) obtained in 0.01 M $[Fe(CN)_6]^{3-/4-}$ equimolecular mixture in 0.1 M KCl. Inset: average and standard deviation respect to the R_{ct} for gold nanostructured graphite screen-printed electrodes (AuNPs/GSPEs) and after the MUDA chemisorption (MUDA/AuNPs/GSPEs). The measurements were repeated at least 3 times using different GSPEs.

Table 3.1. Sensor surface characterisation of the single steps of the immunoassay performed in 0.01 M $[Fe(CN)_6]^{3-/4-}$ equimolecular mixture solution in KCl 0.1 M, PBS 0.1 pH 7.4. Each measurement was repeated at least 3 times using different screen-printed electrodes. Legend: A) AuNPs electrodeposed on GSPEs, B) Functionalization of gold nanostructured graphite screen-printed electrodes with MUDA, C) mixed SAM formation with MCH; D) immobilisation of mAb-CA125, E) blocking step with rIgG, F) affinity reaction with 30 U mL^{-1} CA125 solution.

Figure 3.8. A) Calibration curve for CA125 antigen. Inset: aspecific calibration curve with PSA (0, 50, 100 mg L^{-1}). B) Nyquist plot of mAb-CA125-CA125 interaction. EIS measurements were obtained using 0.01 M $[Fe(CN)_6]^{3-/4-}$ equimolecular mixture prepared in 0.1 M PBS pH 7.4. Each concentration was repeated at least 3 times using different gold nanostructured screen-printed electrodes.

Figure 3.9. A) Average and standard deviation respect to the R_{ct} for the immunosensor response in buffer, serum and serum samples spiked with CA125 (20 and 30 U mL^{-1}) and PSA (aspecific control, 100 mg L^{-1}) obtained in 0.01 M $[Fe(CN)_6]^{3-/4-}$. B) Nyquist plot of the immunosensor response in buffer, serum and serum samples spiked with CA125 (20 and 30 U mL^{-1}) and PSA (aspecific control, 100 mg L^{-1}) obtained in 0.01 M $[Fe(CN)_6]^{3-/4-}$ equimolecular mixture in 0.1 M PBS pH 7.4. The measurements were repeated at least 3 times using different GSPEs.

Figure 4.1. UV-Vis spectra of AuNPs colloidal solution obtained by citrate reduction method. Inset: bright red colour of AuNPs (16 nm) colloidal solution synthesized by citrate reduction method.

Figure 4.2. Scheme of the immunosensors: electropolymerization of anthranilic acid (AA) (a), activation of polymer (b), mAb-CA125 immobilization on the modified GSPEs surface (c), COOH-free sites blocking with ethanolamine (d), incubation with CA125 protein (e). Route A): EIS measurements for label-free CA125 detection.
Route B): reaction with AuNPs/pAb-CA125 conjugate (f), silver enhancement (g) dissolution of silver nanoparticles in HNO_3 1M (h) ASV for silver detection (i).

Figure 4.3. Cyclic voltammograms of anthranilic acid electropolimerization. A) Cyclic voltammograms: bare graphite screen-printed electrode (GSPE, curve a); 15^{th} cycle of poly-anthranilic acid modified graphite screen-printed electrode (curve b, PAA/GSPE) in 1 M H_2SO_4, 0.1 M KCl solution. The scan rate was 0.05 mV s^{-1}. B) Magnification of 1, 5, 10, 15 cycles obtained using 0.05 M anthranilic acid (AA) in 1 M H_2SO_4, 0.1 M KCl solution, and with a scan rate of 0.05 mV s^{-1}.

Figure 4.4. R_{ct} responses of bare graphite screen-printed electrodes (GSPEs) and poly-anthranilic acid modified graphite screen-printed electrodes (PAA/GSPEs) using 0.01 M $[Fe(CN)_6]^{3-/4-}$ redox probe prepared in different buffered solutions. Each point was repeated at least 3 times using different graphite screen-printed electrodes. The polymerization was carried out using 50 mM AA by cyclic voltammetry.

Figure 4.5. Optimization of acid anthranilic acid (AA) concentration for electropolymerization. A) Rct measurements of PAA/GSPEs prepared starting from different monomer concentrations (0.01, 0.05, 0.08 mM), using 15 cycles and a scan rate of 0.05 V s^{-1}. B) Nyquist plot of bare GSPE (■) and of PAA-modified GSPEs using different AA concentrations: 0.01 M (●), 0.05 M (▲), 0.08 M (◆). Electrochemical impedance spectra were performed in 0.01 M $[Fe(CN)_6]^{3-/4-}$ in 0.01 M TRIS (pH 7.4). Each point was repeated at least 3 times using different screen-printed graphite electrodes.

Figure 4.6. Optimization of electropolymerization cycles. A) R_{ct} measurements of poly-anthranilic acid modified graphite screen-printed electrodes (PAA/GSPEs) prepared starting from AA 50 mM, with a scan rate of 50 mV s^{-1}, using different cycles (1, 5, 10, 15). B) Nyquist plot of bare GSPE (■) and of poly-anthranilic acid modified graphite screen-printed electrodes (PAA/GSPEs) using different polymerization cycles: 1 (●), 5 (▲), 10 (◆) and 15 (✳). Electrochemical impedance spectra were performed in 0.01 M $[Fe(CN)_6]^{3-/4-}$ prepared in 0.01 M TRIS (pH 7.4). Each point was repeated at least 3 times using different screen-printed graphite electrodes.

Figure 4.7. Optimization of primary antibody anti-CA125 (mAb-CA125) concentration: 20 mg L^{-1} (■), 30 mg L^{-1} (●), 40 mg L^{-1} (▲) on the EIS response for CA125 using 0.01 M $[Fe(CN)_6]^{3-/4-}$ prepared in TRIS 0.01 M pH 7.4. The values reported in the graphics represent the mean value of 3 different measurements.

Figure 4.8. Calibration curve for label-free CA125 detection by EIS measurements performed in 0.01 M $[Fe(CN)_6]^{3-/4-}$ prepared in TRIS 0.01 M pH 7.4. Inset: aspecific test with PSA (0, 50, 100 mg L^{-1}). Each point was repeated at least 3 times using different modified graphite screen-printed electrodes.

Figure 4.9. A) Calibration plots for CA125 detection through sandwich assay using pAb-CA125 antibody labelled-gold nanoparticles and silver enhancement. Inset: aspecific signal obtained with PSA (50, 100 mg L^{-1}). B) Voltammograms by differential pulse anodic stripping voltammetry of silver using different CA125 concentrations, from down to top: 0, 5, 10, 25 U mL^{-1}, respectively. Each point was repeated at least 3 times using different modified screen-printed graphite electrodes.

Table 5.1. List of the aptamers sequences (form 5' to 3') used in this work. 15 thymine nucleobases – T(15) – were used as spacer.

Figure 5.1. Schematic representation of the steps involved in the development of aptamers sandwich assay for VEGF detection: a) electrodeposition of gold nanoparticles AuNPs on graphite screen-printed electrodes (GSPEs); b) incubation with thiolated primary anti-VEGF aptamer (Apt1-VEGF); c) incubation with MCH protein; d) affinity

reaction with VEGF; e) addition of biotinylated secondary anti-VEGF aptamer (Apt2-VEGF); f) incubation with streptavidin-alkaline phosphatase (streptavidin-AP); g) addition of the substrate (alpha-naphthyl phosphate) h) DPV measurements as described in materials and methods section.

Figure 5.2. A) Nyquist plot of bare graphite screen-printed electrode (GSPE, ●) and of gold nanoparticles-modified graphite screen-printed electrode (AuNPs/GSPE, ■). Inset: magnification of AuNPs/GSPEs EIS spectrum. B) Average and standard deviation respect to the R_{ct} for bare GSPEs and for (AuNPs/GSPEs). EIS measurements were performed as reported in materials and methods section using 3 different electrodes.

Figure 5.3. A) Nyquist plot of gold nanoparticles-modified graphite screen-printed electrode (AuNPs/GSPEs, ■) and after the functionalization with thiolated primary anti-VEGF aptamer (Apt1-VEGF/AuNPs/GSPEs, ●) and after formation of mixed SAM monolayer with 6-mercapto-1-hexanol (MCH/Apt1-VEGF/AuNPs/GSPEs, ▲). B) Average and standard deviation respect to the R_{ct} for bare AuNPs/GSPEs, Apt1-VEGF/AuNPs/GSPEs and MCH/Apt1-VEGF/AuNPs/GSPEs. EIS measurements were performed as reported in materials and methods section using 3 different electrodes.

Figure 5.4. A) Calibration plots for VEGF detection through aptamers sandwich assay obtained by DPV measurements. Inset: aspecific signal obtained with HER2 protein (50, 100 μg L^{-1}). B) DPV voltammograms obtained through aptamers sandwich assay for VEGF concentration: 0, 50, 100, 200, 250 nM. Each point was repeated at least 3 times using different modified screen-printed graphite electrodes.

Figure 6.1. Schematic representation of Affibody®-based label-free gold nanostructured biosensor for HER2 breast cancer biomarker detection. a) electrodeposition of gold nanoparticles (AuNPs) on graphite screen-printed electrodes (GSPEs) b) functionalization with anti-HER2 Affibody® molecules); c) Incubation with MCH; d) affinity reaction with HER2 protein; e) label-free HER2 determination by electrochemical impedance spectroscopy (EIS) measurements.

Figure 6.2. A) Nyquist plot of gold nanoparticles-modified graphite screen-printed electrodes (AuNPs/GSPEs, ■), after the functionalization with anti-HER2 Affibody® (anti-HER2 Af/AuNPs/GSPEs, ●) and with 6-mercapto-1-hexanol (MCH/anti-HER2 Af/AuNPs/GSPEs, ▲) obtained in 0.01 M $[Fe(CN)_6]^{3-/4-}$ equimolecular mixture in 0.1 M PBS, pH 7.4. B) Average and standard deviation respect to the R_{ct} for AuNPs/GSPEs, anti-HER2 Af/AuNPs/GSPEs, MCH/anti-HER2 Af/AuNPs/GSPEs. The measurements were repeated at least 3 times using different GSPEs.

Figure 6.3. A) Calibration curve for HER2 cancer biomarker and aspecific test with 40 μg L^{-1} VEGF (●). B) Nyquist plot of Affibody®-HER2 affinity reaction obtained in 0.01 M $[Fe(CN)_6]^{3-/4-}$ equimolecular mixture in 0.1 M PBS, pH 7.4. The measurements were repeated at least 3 times using different GSPEs.

Figure 6.4. Nyquist plot of the biosensors response in serum samples spiked with HER2 (10, 20, 30 μg L^{-1}) obtained in 0.01 M $[Fe(CN)_6]^{3-/4-}$ equimolecular mixture in 0.1 M PBS pH 7.4. The measurements were repeated at least 3 times using different GSPEs.

Figure 7.1. A) Schematic representation of the steps involved in the development of different MUC1 assays: a. Antibody – Antibody assay (Ab – Ab): 1) incubation of protein G-modified magnetic beads with primary anti-MUC1 antibody (mAb-MUC1); 2) blocking step with milk powder 5% prepared in 0.1 M PBS buffer pH 7.4; 3) affinity reaction with MUC1 protein; 4) incubation with secondary anti-MUC1 antibody (pAb-MUC1); 5) incubation with alkaline phosphatase (AP)-labelled anti-rabbit IgG tertiary antibody (Ab-AP). b. Aptamer – Antibody assay (Apt – Ab): 1) incubation of streptavidin-modified magnetic beads with biotinylated primary anti-MUC1 aptamer (Apt1-MUC1); 2) blocking step with biotin; 3) incubation with MUC1 protein; 4) incubation with secondary anti-MUC1 antibody (pAb-MUC1); 5) incubation with alkaline-phosphatase (AP) labelled anti-rabbit IgG tertiary antibody (Ab-AP). c. Aptamer – Aptamer assay (Apt – Apt): 1) incubation of streptavidin-modified magnetic beads with biotinylated primary anti-MUC1 aptamer (Apt1-MUC1); 2) blocking step with biotin; 3) incubation with MUC1 protein; 4) incubation with secondary biotinylated anti-MUC1 aptamer (Apt2-MUC1); 5) incubation with streptavidin-alkaline phosphatase.

B) Electrochemical measurements: screen-printed array were placed on a magnetic support and modified-magnetic beads were deposited on the surface of each working electrode of the array.

Table 7.1. Experimental parameters optimization for antibody – antibody sandwich assay. $I_{MUC}1/I_{blank}$ represent the ration between the current obtained using respectively 5 ng mL^{-1} and 0 ng mL^{-1} MUC1 buffered solution. Letters and numbers present in Assay step column are referred in accordance of Figure 7.1 A.

Figure 7.2. Selectivity of the different developed assays performed in MUC1 (5 ng mL^{-1}), MUC4 (5 ng mL^{-1}) and MUC16 (35 U mL^{-1}) buffered solution (a. Ab – Ab assay; b. Apt – Ab assay; c. Apt – Apt assay). Blank signal was substracted from each measurements.

Table 7.3. Experimental parameters optimization for aptamer – aptamer sandwich assay. $I_{MUC}1/I_{blank}$ represent the ratio between the current obtained using respectively 5 ng mL^{-1} and 0 ng mL^{-1} MUC1 buffered solution. Letters and numbers present in Assay step column are referred in accordance of Figure 7.1 A.

Table 7.4. Analytical performances of antibody – antibody (Ab – Ab), aptamer – antibody (Apt – Ab), aptamer – aptamer (Apt – Apt) assays performed in MUC1 buffered solutions. Letters a, b., c. are referred in accordance of Figure 7.1 A.

Figure 7.2. Selectivity of the different developed assays performed in MUC1 (5 ng mL^{-1}), MUC4 (5 ng mL^{-1}) and MUC16 (35 U mL^{-1}) buffered solution (Ab – Ab assay: white histograms; Apt – Ab assay: dark grey histograms; Apt – Apt assay light grey histograms). Blank signal was subtracted from each measurement.

Figure 7.3. Experiments with commercial serum sample 1:200 diluted spiked with MUC1 at different concentrations using aptamer assay.

Table 7.5.MUC1 determination in 1:200 diluted serum sample form cancer patients performed with aptamers sandwich assay using standard addition method.

List of abbreviations and symbols

AA	Anthranilic Acid
Ab	Antibody
AC	Alternate Current
AgNPs	Silver nanoparticles
Ag	Antigen
AP	Alkaline Phosphatase
Apt	Aptamer
ASV	Anodic Stripping Voltammetry
AuNPs	Gold nanoparticles
BSA	Bovine Serum Albumin
CA125, MUC16	Carbohydrate Antigen CA125
CA15-3, MUC1	Carbohydrate Antigen 15-3
CEA	Carcinoembryonic Antigen
CNTs	Carbon nanotubes
CV	Cyclic Voltammetry
DC	Direct Current
DEA	Diethanolamine
DNA	Deoxyribonucleic acid
DPV	Differential Pulse Voltammetry
EA	Ethanolamine
EDAC	1-Ethyl-3-(3’-dimethylaminopropyl) carbodiimide
EGFR	Epidermal Growth Factor Receptor
EIS	Electrochemical Impedance Spectroscopy
ELISA	Enzyme-Linked Immunosorbent Assay
Fab	Fragment-antigen binding domain
Fc	Fragment crystallisable domain
GOx	Glucose Oxidase
GSPEs	Graphite Screen-Printed Electrodes
HER2,	Human Epidermal Growth Factor Receptor 2
HRP	Horseradish Peroxidase

IgG	Immunoglobulin G
LSPR	Localized Surface Plasmon Resonance
MAb	Monoclonal antibody
MCH	6-mercapto-1-hexanol
MES	2-(N-morpholino) ethanesulfonic acid
MNPs	Magnetic nanoparticles
MUDA	11-Mercaptoundecanoic acid
MWCNTs	Multi-Walled Carbon Nanotubes
NHS	N-hydroxysuccinimide
PAA	Polyanthranilic acid
PAb	Polyclonal antibody
PANI	Polyaniline
PBS	Phosphate Buffer Saline
PCR	Polymerase Chain Reaction
PLGF	Placenta Growth Factor
PSA	Prostate Specific Antigen
RIAs	Radiation Immunological Assays
RNA	Ribonucleic acid
SAM	Self-assembly monolayer
SELEX	Systematic Evolution of Ligands by Exponential Enrichment
SEM	Scanning Electron Microscope
TRIS	Tris(hydroxymethyl) aminomethane hydrochloride
VEGF	Vascular Endothelial Growth Factor

CHAPTER 1

1. Biosensors: introduction

1.1. Definitions

As define by International Union of Pure and Applied Chemistry (IUPAC), a chemical sensor is a small and compact device composed by a chemical (molecular) recognition system (receptor) in spatial connection with a physic–chemical transducer that transforms chemical information, related to the sample or total concentration of a specific component, into an analytically useful signal.

Biosensors are chemical sensors in which the recognition system utilizes a biochemical mechanism.

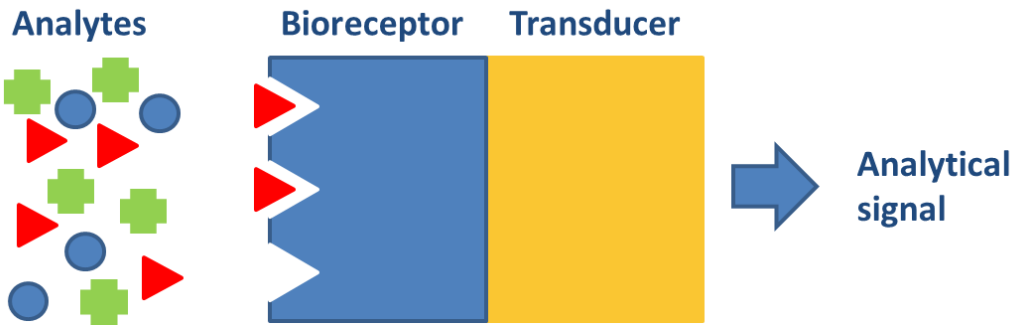

Figure 1.1. Schematic representation of biosensor.

According to the nature of the biorecognition process, biosensors can be classified in two main categories: catalytic (in which the bioreceptor is constituted by mono- or multi-enzymes, whole cells, i.e. bacteria, fungi or eukaryotic cells, or by animal or plant tissue slice) and affinity biosensors (in which the bioreceptor is capable to bind selectively and reversibly a specific ligand in order to obtain a useful analytical signal) [1].

Biosensors can be also classified in relation of the transduction methods in: electrochemical (based on the determination of electroactive species that can be bound, produced or consumed on the surface of the electrochemical cell [2]), optical (which exploits the change in the optical property of biomolecule as a results of its interaction with the target analyte, or the use of different kinds of labels and probes [3]), piezoelectric (in which the analytical signal is produced by the application of a mechanical stress on the surface of a piezoelectric crystal related to the interaction

between the bioreceptor and the analyte [4]), thermometric (based on the measurement of the heat absorbed or evolved during a biochemical reaction [5]) and magnetic (which reveals the variation of the magnetic properties of the system for the detection of the analyte [6]).

Among this, electrochemical biosensors have found a broad range of application due to their low cost, speed of detection, high sensitivity, portability and high compatibility with miniaturization techniques.

Electrochemical detection techniques are normally divided into six main categories: amperometric, voltammetric, impedimetric, conductimetric, potentiometric and field-effect.

Amperometric and voltammetric biosensors are based on the application of a potential to a working electrode (respect to a reference electrode) and on the measurement of the current resulting from the electrochemical reduction or oxidation of an electroactive substance.

In particular, in amperometry technique, the changes in the current generated by the electrochemical reaction are evaluated continuously respect to the application of a constant DC (or stepped DC, for chronoamperometry) potential, while for voltammetric measurements (including cyclic voltammetry, linear sweep voltammetry, differential pulse voltammetry, stripping voltammetry etc.), the potential is scanned over a selected potential range.

In both cases the measured current is proportional to the concentration of the electroactive specie [7].

In contrast, in the impedimetric measurements the impedance of an interface in AC (alternate current) steady state with constant DC bias condition was measured.

With this approach the change in the impedance values at the electrode-solution surface is related to the analyte-probe biorecognition [8].

In conductimetric, potentiometric and field-effect techniques the evaluation of the biological reaction were performed recognizing the charge or ion concentration changes.

Conductometric system measure the capability of an analyte to conduct an electrical current between electrodes, while in potentiometry the accumulation of a charge potential at the working electrode (compared to the reference electrode) when no or square-wave current (for chronopotentiometry) flows into the system, was measured. At last, in field-effect transistor an electrical field was used to control the conductivity of a channel (a

zone depleted of charge carrier) between two electrodes (defined as source and drain) in a semiconducting material (gate). Briefly, the biocatalytical reaction changes the presence of accumulated charge carrier producing thus an electrical signal (drain current) proportional to the analyte concentration

1.2. Electrochemical biosensors for clinical applications

Today's situation in clinical diagnostics and monitoring requires rapid and accurate analyses. Very important factors complicating these procedures are mainly related to the prices of analytical devices and expenses for whole measurements. In addition, if we consider that qualified personnel are needed for clinical analyses, the natural necessity for alternative analytical technologies is presented.

For this purpose, biosensors can act as an option for solving problems mentioned before, or become a helpful tool at least.

Electrochemical devices are extensively applied in the field of detection of cancer biomarkers, which are tumour associated antigens and mutations.

While cancer-related assays are more complex than home self-testing of glucose, modern electrochemical bioaffinity sensors, such as DNA- or immunosensors, have recently demonstrated great potential for monitoring cancer-related protein markers and DNA mutations.

The classical methods (such as ELISA immunoassays) for diagnosis of cancer may take several hours, or even days from when tests are ordered to when results are received. These methods can be tedious, time consuming and often require extra care and expensive instruments making early diagnosis of cancer more difficult especially for the cancer patients who are admitted to an emergency department. Therefore, measurement of carcinomatous markers is critical in assisting the diagnosis of cancer and electrochemical biosensors can satisfy the rapid diagnosis requirements in cancer marker detection during early stages of the disease [9-12].

2. Biomarkers

2.1. Definitions

According to the US National Institutes of Health's (NIH) and Biomarkers Consortium, a biomarker is a "characteristic that is objectively measured as an indicator of normal

biological processes, pathogenic processes, or a pharmacological response to a therapeutic intervention" (www.biomarkersconsortium.org).

Moreover, the NIH's National Cancer Institute (NCI), describes biomarkers in its dictionary of cancer terms as "a biological molecule found in blood, other body fluids, or tissues that is a sign of a normal or abnormal process, or of a condition or disease. A biomarker may be used to see how well the body responds to a treatment for a disease or condition. Also called molecular marker and signature molecule" (http://www.cancer.gov).

Finally, the United Nations' World Health Organization (WHO) defines a biomarker as "indicator of changes or events in biological systems. Biological markers of exposure refer to cellular, biochemical, analytical, or molecular measures that are obtained from biological media such as tissues, cells, or fluids and are indicative of exposure to an agent" (WHO, IPCS Risk Assessment Terminology).

2.2. Cancer biomarkers

It is now well established that early detection of cancer represents the best opportunity to cure. The diagnosis of cancer when a tumor is still small to be completely removed surgically, drastically increases the survival rate of patients. Unfortunately, most cancers dot not produce symptoms until the tumors are either too large to be removed or until metastatic processes are presents [13].

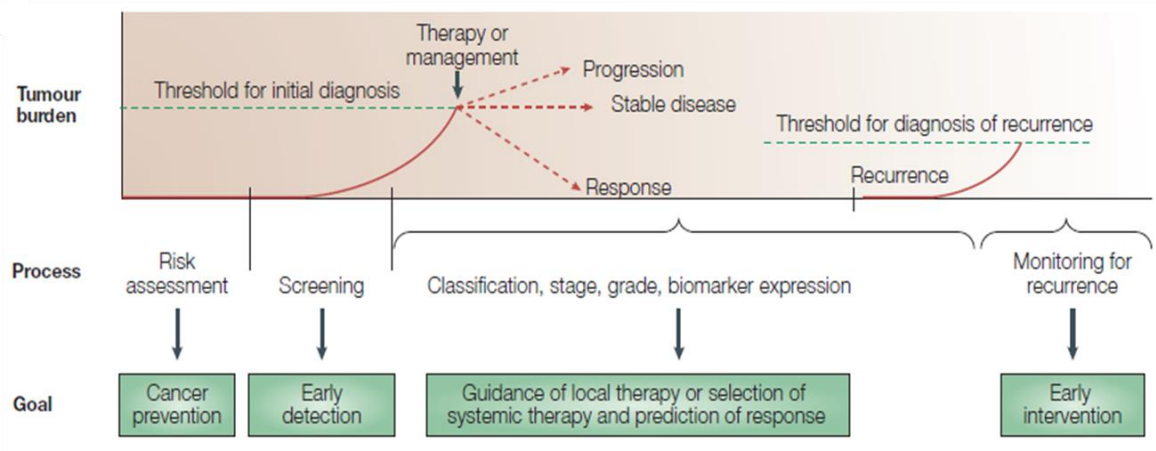

Figure 1.2. Schematic representation of the uses of cancer biomarkers in the different phases of evolution of cancer [14].

It is also known that in every disease, there is a latency period and that, if it is possible to detect the disease in this stage, treatments can be performed before it become lethal.
Cancer biomarkers are able to detect a specific disease early and help to provide treatments before it becomes incurable in later stages. Biomarkers are also extremely important to determinate the recurrence of the disease and to evaluate the follow-up of the patients after a chemio- or radio- therapic and surgery treatments [14].

Ideally cancer biomarker should possess common characteristics [15]:

1. High sensitivity and specificity with low false negatives and low false positives results.
2. High differentiation rate between healthy and tumor patients.
3. High prediction of early recurrence and prognostic properties.
4. Easily assayable and able to identify changes in cancer patients receiving treatments.

Nevertheless, in reality, an ideal tumor marker does not exist.
In fact if we consider the prostate specific antigen (PSA), the most common used cancer biomarker, it suffers from several major limitations: for instance, PSA concentration could increase in individuals with benign conditions (prostate enlargement, inflammation or infection) and its level do not correlate well with tumor aggressiveness [16].
Similar behaviour can be found considering CA125 (carbohydrate antigen 125), a biomarker related to the ovarian cancer.
CA125 is used for early detection of ovarian cancer (since increased levels of CA125 may precede clinical detection by more than a year) and can be also useful to evaluate chemotherapy responses, to distinguish malignant pelvic masses from benign masses, to detect the recurrence of the cancer, and to improve clinical trial design.
However, its level in serum can be found high in patient with other not tumoral diseases (such as peritoneal irritation, endometriosis, and pelvic inflammation) or pregnancy status [17].
To solve this problem, during the last decades the evolution of -omics sciences (i.e., genomics, transcriptomics, proteomics, peptidomics, and metabolomics) led to the study and the discovery of a large number of new molecules eligible to become a new cancer biomarkers. Despite this, the number of biomarkers receiving US Food and Drug

Administration (FDA) clearance has declined substantially over the last 10 years to less than one protein biomarker per year.

For this reasons, in the future, cancer screening tests will probably combine the results of multiple diagnostic tests or biomarker assays with prior testing histories and patient specific risk factors. Recent advances in quantitative methods use all of this information to identify individuals with positive test results who are most in need of surgical intervention.

The ability to optimally combine information on multiple markers is important because single markers typically lack the sensitivity and specificity that is necessary for useful mass screening [18].

2.2.1. Classification of cancer biomarkers

Different strategies have been suggested to define and classify cancer biomarkers, but general consensus has yet to be established.

Theoretically, any biologically derived entity or processes which lead to the cancer detection, at the stage of diagnosis (and allow to determinate the prognosis) or post diagnosis (in therapy and treatment modules) are potential candidates to become cancer biomarkers [19].

Mainly it can be classified, referred to the disease state, in: prognostic (based on the recognizing features between benign and malignant tumors and on the differentiation status of tumors which can influence clinical treatments), predictive (utilized to assess the effect of administer drug and to select the best chemotherapeutic agent for a patient), pharmacodynamics (utilized to select the doses of chemotherapeutic agents for a specific set of tumor-patient conditions) and diagnostic (that can help to determinate the stage and the recurrence of a tumor or the clinical follow-up of patients).

Biomarker can also divide respect to the nature of biomolecules in: DNA, RNA (and micro-RNA) and protein biomarkers.

Circulating DNA was probably the first evaluated markers to detect the cancer staging. DNA serum levels can be also related to the presence of metastatic cancer. Moreover, single nucleotide polymorphism in many genes was used as cancer biomarker. For instance, mutations in XRCC1 (X-ray Repair Cross-Complementing protein 1), ATM

(Ataxia Telangiectasia Mutated) or cellular tumor antigen p53 genes were extensively studied to detect the presence of lung, head and neck cancers.

Analysis of epigenetic regulation of transcription and translation and of the associated protein (histones and non-histones) is also important to define carcinogenesis process. For instance, gene silencing by CpG (regions of DNA where a cytosine nucleotide occurs next to a guanine nucleotide in the linear sequence of bases along its length) methylation is one of the best studied epigenetic modification and the degree of methylation in prostate cancer tissue or serum are strictly related to the severity of the lesions [20].

While most DNA markers were evaluated singularly, most RNA-based biomarkers consist in the analysis of multi-gene molecular patterns or "fingerprints". This kind of procedures are more accurate than a single-molecule marker, but new development in biostatistics and bioinformatics is needed to select which gene includes in the evaluated patterns [20].

Moreover, expression of specific populations of micro-RNA (miRNA, small and non-coding RNAs) in a tissue and in time-dependent way, is associated with clinical behaviour of several cancer types (such as leukaemia, prostate, colorectal, lung and pancreatic) and can be used to classify, to determinate the diagnosis and the prognosis as well as the stage, the risk and drug-response of human tumors.

Protein-based cancer biomarkers are the most studied and the most used biomarkers. Because proteins influence the molecular pathways in normal and malignant cells, they are strictly related to disease state, initiation and progression.

In fact, the only FDA (US Food and Drug Administration)-approved cancer biomarkers available for clinical use are protein markers [21].

Cancer-specific alterations in proteins may occur at the level of protein abundance or post-translational protein modification (such as glycosylation or phosphorylation). If the protein biomarker is present in a body fluid, bioreceptors to these specific changes represent a formidable instrument for the development of cancer biomarkers detection assays.

Many cancer biomarkers proteins were discovered first immunizing animals with extracts from tumors or cancer cell lines and after selecting the monoclonal antibodies that recognize "cancer-associated" antigens [22]. Recently, the complete discovery of human genomic coupled with the advance in proteomic and nano-proteomic (which aims to

characterize the entire protein complement expressed by the genome) technologies led to an exponential increase on the discovery and the study of new and low abundant protein cancer biomarkers.

Up to date, tumour-associated protein are studied by the use of classical two-dimensional (2-D) fluorescence difference gel electrophoresis (DIGE); polycarylamide gel electrophoresis (PAGE); and high throughput platforms, such as Mass Spectroscopy (MS), Matrix Associated Laser Absorption Desorption Ionization Time of Flight (MALDI-TOF), Surface Enhanced Laser Absorption Desorption Ionization Time of Flight (SELDI-TOF), and reverse phase microarray [23-28].

In this thesis, different strategies were investigated for the development of nanostructured biosensors for the detection of several cancer biomarkers associated with the diagnosis and the prognosis of ovarian and breast cancers.

In particular, in the next paragraph, the properties of CA125, MUC1, HER2 and VEGF cancer biomarkers will be detailed described from biological and clinical point of view.

2.2.2. Mucins

Mucins are large, abundant, filamentous glycoproteins that are present at the interface between epithelia and their extracellular environments. This interface is often the lumen of a hollow organ within the body such as the gastrointestinal tract, lungs and urogenital tract. Several of these mucins are known to form mucus layers, whereas others form the glycocalyx on the intestinal enterocytes.

Physiologically, these bulky and abundant glycoproteins are strategically positioned to mediate the interactions between epithelial cells and their milieu. They act both keeping unwanted substances and organisms at an arm's length either serving as an outside-to-inside signal that alters the proliferation, differentiation or cell adhesion status of the epithelial cells.

The mucins family includes proteins that contain tandem repeat structures with a high proportion of prolines, threonines and serines (known as PTS domain). Mucins are further defined by extensive glycosylation of the PTS domain through N-acetylgalactosamine linked with *O*-linkages at the threonine and serine residues. Mucins are classified into two main classes: membrane-bound mucins (MUC1, MUC3A, MUC3B, MUC4, MUC12,

MUC13, MUC15, MUC16, MUC17, and MUC20) and secreted or gel-forming mucins (MUC2, MUC5AC, MUC5B, MUC6, MUC7, MUC8 and MUC19) in which the numbers represent the protein-coding gene.

Cancer cells express aberrant forms and larger amounts of mucins (compared with normal cells). These forms arise as a consequence of the deregulation of expression of mucin core proteins and the enzymes that modify them during the transformation of tumour cells. The expression of distinct oligosaccharide structures, together with differential glycosylation of mucin core proteins, confers on tumour cells an enormous range of potential ligands for interaction with other receptors at the cell surface. These facts suggest that the aberrant expression of mucins may be implicated in the development and progression of different kind of cancers diseases [29-31].

MUC16 (also known as carbohydrate antigen 125, CA125) was discovery by Bast *et al.* in 1981 using monoclonal antibody OC125 [32].

CA125 is an *O*-linked glycoprotein of high molecular mass ranging in normal conditions, from 2.5 to 5 MDa. The core domain retains the capacity to bind both OC125 and M11 class monoclonal antibodies.

As with other mucins belong to this class, MUC16 has a large ectodomain (estimated to extend up to 500 nm from the cell surface into the glycocalyx), a single pass membrane-spanning domain, and a small cytoplasmic tail.

The ectodomain is composed of a heavily *O*-glycosylated N-terminus area (composed by tandem repeat region with over 60 tandem repeats of 156 amino acids each), and a region with several SEA domains near the membrane-spanning sequence.

The cytoplasmic tail is not well characterized, but it contains several potential tyrosine phosphorylation sites [33, 34].

Measurement of serum CA125 concentration plays a central part in the clinical management for EOC (Epithelial Ovarian Cancer) patients. Elevated presence of CA125 in serum (> 35 U/mL) is common in patients with advanced disease (~ 90%). Moreover, the rise and the fall of CA125 concentration in serum are correlated with progression and regression of the disease.

However, up to 20% of patients with advanced EOC have normal serum level of CA125 and, furthermore, CA125 levels can be elevated in various benign diseases including menstruation, first trimester pregnancy, endometriosis, adenomyosis, salpingitis, uterine

fibroids, chronic renal failure or in inflammation of the pleura, peritoneum or pericardium [35, 36].

MUC1 (also known as carbohydrate antigen 15-3, CA15-3) is a type I transmembrane glycoprotein, that is mainly overexpressed in breast and ovarian carcinomas.

CA15-3 possesses a molecular mass ranging from 300 to 600 kDa, which is apically expressed in the majority of glandular and ductal epithelia of various organs.

It consists of two subunits, which are proteolytically derived from a common precursor peptide, and form a stable heterodimeric complex.

The smaller subunit contains a C-terminal cytoplasmic domain of 72 amino acids, followed by the hydrophobic membrane-spanning domain (or transmembrane domain) of 31 amino acids, and a short extracellular sequence which is non-covalently linked to the larger extracellular subunits.

The extracellular subunits contain the VNTR (variable number tandem repeat) domain varying from 20 to 125 repeats, which exhibits high contents of proline, serine and threonine (PTS region).

The expression of the MUC1 protein is greatly upregulated on tumors, where it undergoes changes in glycosylation and distribution, resulting in the exposure of the core protein of the tandem repeat regions. The overexpression of mucin and distribution on cell surface are assumed to influence the biological behaviour of the tumor cells during malignant transformation and tumor progression, suggesting that the protein may be important for the maintenance or generation of the tumor[37, 38].

The disease status in breast and recently in ovarian cancer patients is routinely assessed by monitoring the serum levels of circulating CA15-3 protein.

Elevated levels of CA15-3 (> 20 U/mL) in the serum are always associated with poor survival. Moreover, the determination of CA15-3 protein has been exploited as a measure of tumor burden and used to monitor the response on of the patients to clinical treatments [39-41].

2.2.3. Human Epidermal Growth Factor Receptor 2 (HER2)

Human Epidermal Growth Factor Receptor 2 (HER2), also known as ErbB2, c-erbB2 or HER2/neu, is a 185 kDa protein with an intracellular tyrosine kinase domain and an extracellular ligand binding domain. In humans, HER family includes four structurally

related members, HER1 (ErbB1, also known as EGFR), HER2 (ErbB2), HER3 (ErbB3) and HER4 (ErbB4).

In particular, HER2 is a type 1 transmembrane glycoprotein composed of three distinct regions: an N-terminal extracellular domain (ECD), a single α-helix transmembrane domain (TM), and an intracellular tyrosine kinase domain. As the largest part of HER2, the N-terminal ECD contains approximately 600 residues (90–110 kDa) which could be divided into four subdomains (I–IV). Subdomains I and III can form a binding site for the receptor's potential ligands, while the subdomains II and IV are involved in the homodimerization and heterodimerization processes.

It has been demonstrated that HER heterodimers are more potent in signal transduction than homodimers and HER2 represent the preferred dimerization partner of all other HER receptors. In normal cells, HER2 is mainly involved in the enhancement of signaling pathways which activate biological responses such as cell proliferation, apoptosis inhibition, angiogenesis, migration and invasion.

HER2 is frequently overexpressed in breast cancer, gastric cancer, ovarian cancer and prostate cancer.[42-44]

Overexpression of HER2 usually results in malignant transformation of cells accounts for ~25% of all breast cancer cases (clinical cut off: 15 ng/mL) and it is always associated with more aggressive tumor phenotypes. The overall survival rate and relapse time for HER2 positive breast cancer patients are significantly shorter than patients without HER2 overexpression [45, 46]. The role of HER2 in ovarian cancer is not clear as in breast cancer. However, it was suggested that the HER2 overexpression is more frequent in advanced stage of ovarian tumor [47, 48].

2.2.4. Vascular Endothelial Growth Factor (VEGF)

Vascular Endothelial Growth Factor is referred to a family of dimeric glycoprotein including five members (VEGF-A, VEGF-B, VEGF-C, VEGF-D, placenta growth factor, PGF) and their associated receptors (VEGFR-1, VEGFR-2, VEGFR-3). Homologs of VEGF protein are also discovered in the genome of some viruses (VEGF-E) [49] or in the venom of some snakes (VEGF-F) [50, 51]. Because VEGF-A was the first and the most studied protein (in particular related to oncology and cancer biology), often in literature (and in this text) the term VEGF strictly indicate the VEGF-A member.

VEGF is a dimeric glycoprotein which is covalently linked by 2 disulfide bridges, encoded by the gene located at chromosome 6p213 constituted by 8 exons separated by 7 introns. Related to alternative exon splicing of exons 6 and 7, it can be distinguished in many different isoform of which VEGF121, VEGF165 and VEGF189 (constituted respectively by 121, 165 and 189 amino acids) were the most well-studied [52].

Crystallographic research conducted by Muller *et al.* [53] reveal that VEGF is formed by an antiparallel homodimer covalently linked by two disulfide bridges, in similar way of platelet-derived growth factor (PDGF). Respect to VEGF121 and VEGF189, VEGF165 shown intermediate properties because is both secreted (as diffusible protein or as bioactive fragments) and partially bound to the cell surface and to the extracellular matrix (ECM) [54].

From biological point of view, VEGF and its receptors play a main role in the formation of cardiovascular system.

Briefly, the first of this process, consist in the differentiation of the angioblasts into the hemangioblast, followed by the reorganization of the endothelial cells (angiogenesis process) which start the production of VEGF that lead to the formation of new blood vessels [55].

VEGF importance in angiogenesis were furthermore demonstrated in several studies in which the targeted disruption of VEGF and its receptor during embryogenesis, led to early embryonic mortality due to severe defects in vascular system [56, 57].

VEGF play also a critical role in carcinogenesis and in tumor metastasis: in fact, recent studies revealed the ability of the tumoral cells to create new vasculatures (increasing the production of VEGF proteins) in order to receive a large number of nutrient and oxygen necessary for their growth.

Moreover, because new tumoral vasculatures are functionally abnormal (highly disorganized, tortuous, dilated) and consequently blood tumor flow is chaotic and variable, hypoxic and acidic zones surrounding the tumor are formed. Thus, tumoral cells increase in the production VEGF to form new vessels and VEGF concentration in blood raise up [58, 59].

VEGF concentration in blood and serum (which values is much higher than 100 pM in pathological condition) can be thus used as biomarker associated with diagnosis and prognosis of different type of cancer diseases with particular reference to the presence of metastasis processes [60, 61].

3. Bioreceptors

In order to develop an optimal device for the determination of cancer biomarkers useful for clinical diagnosis, the selection and the immobilization of the biorecognition element play a critical step.

The most widely used bioreceptor is represented by the antibody molecules, because provides the specificity and sensitivity required for low levels of molecular detection. However, recently, synthetic molecular recognition elements have been fabricated as affinity receptors and used for analyte detection and analysis with the aim to overcome the limitation related to the own nature of the antibodies.

In the next paragraphs the characteristic and the structure of antibodies, aptamer and new engineered scaffold protein molecules will be discussed.

Subsequently, the use of these bioreceptors for the detection of cancer biomarkers coupled with nanomaterials will be reviewed.

3.1. Antibodies

Antibodies (Abs), also called immunoglobulin (Ig), are proteins found in the plasma and in the extracellular fluids that are produce by the specialized lymphocyte B cells of the host, in order to neutralize and/or eliminate the presence of a foreign molecules or organisms (also called antigens, Ags).

Thus, antibodies represent the first response and comprise one of the principal instruments of the adaptive immune system.

Structurally, antibodies are large Y-shaped glycoprotein (of molecular weight about 150 kDa) composed by two identical copies of both heavy (H, ~ 50 kDa) and light (L, ~ 25 kDa) chains bind together by disulphide and non-covalent bonds.

These chains include variable regions (V), which constitute the Fab (fragment-antigen binding) domain, and constant regions (C), which constitute the Fc (fragment crystallisable) domain.

In particular, Fab domain is composed both by heavy and light variable regions (respectively V_H and V_L) bind together to form the Ab-Ag binding domains (called complementary-determining regions, CDRs).

This region is also called paratope and recognizes a complementary site on two antigens (generically identical) called epitope. Fc domain is instead composed by two heavy

chains that include two or three constant domain (C_H), depending on the class of the antibodies. This region modulate immune cell activity and, because can bind to various cell receptors, it mediates different physiological effects.

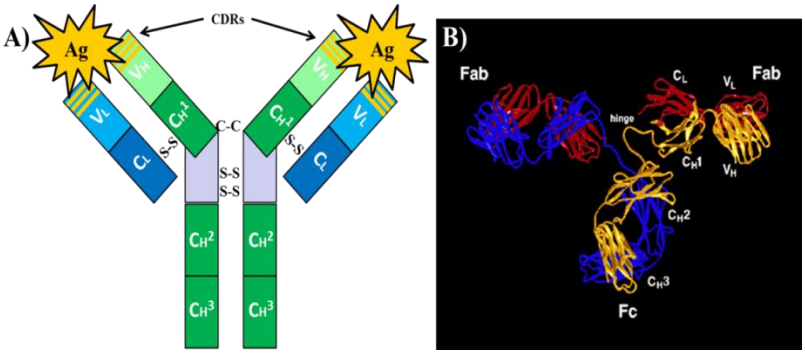

Figure 1.3. A) Schematic representation of Y-shaped Ab structure: C_H 1-3, constant region of heavy chain; C_L, constant region of light chain; V_H, variable region of heavy chain; V_L, variable region of light chain; CDRs complementary-determining regions, Ag, antigen (adapted from ref. [2]).B) Ribbon structure of the first Ab (IgG2A) every crystallized [62].

Based on the sequence of their heavy chain constant region, mammals Abs can be divided in five classes (IgM, IgD, IgG, IgE and IgA). IgG represents about 75% of serum immunoglobulin in human and was the most used Abs in bioaffinity devices and for cancer immunotherapy [63, 64].

3.1.1. Polyclonal and monoclonal antibodies

A high number of antigens possess a very complex structure with numerous epitopes that can be recognized. If each lymphocyte is activated to proliferate and differentiate into plasma cells, the resulting antibodies response is polyclonal (PAbs). In contrast, monoclonal antibodies (MAbs) are produced by a single B lymphocyte clone.

Both polyclonal and monoclonal antibodies are produced in animal that receive injection of antigen or antigen/adjuvant mixture for the induction of complete antibody responses (in the case of PAbs) or to induce specific B cells obtained from the spleen of lymph node to establish hybridomas (in the case of MAbs).

The principal advantages of MAbs are their specificity (coupled to their homogeneity) and consistency that make them useful to evaluating changes in molecular conformation, protein-protein interactions (reducing the probability of cross reaction), or to be used in targeted therapy (in particular in cancer disease). However this high monospecificity may

also limit their usefulness: in fact, small changes in the structure of an epitope present on an antigen can markedly affect the recognizing properties of the specific MAb.
In contrast PAbs are heterogeneous and recognize different antigen epitopes; furthermore, the effect of change on a single or small number of epitopes is less likely to be significant. PAbs stability is also less influenced by variations of pH and salt concentrations.
Finally, PAbs could be useful when the nature of the antigen in unknown and can be also obtained within a short time (4-8 weeks) in comparison of MAbs (3-6 months) with a significant reduction of the production costs [65, 66].

3.2. Aptamers

Despite the wide use of Abs for biosensing applications, some limitations still remain presents. In particular, antibodies (both monoclonal either polyclonal) are selected and produced using animals. Consequently, antibodies generation, as well as presenting ethical issues, becomes difficult with molecules which are toxic or not well tolerated by the host.
Furthermore, antibodies are sensitive to temperature variations and the performance of the same antibody tends to vary using different batches.
In order overcome these limitations, recent progresses and advances in biotechnology and chemical synthesis have led to the discovery and the introduction of a new class of bioreceptor that offers a promising alternative to antibodies.
Aptamers (from the Latin “aptus” – fit and Greek “meros” – part) are oligonucleotide sequences (DNA or RNA) or peptide molecules capable to bind a target molecule with high affinity and specificity. Aptamers offer unique properties compared to other targeting agents such as chemical synthesis (without the use of animals and with reduced cost of production), high degree of purity (which reduce batch to batch variations), high temperature stability, the possibility of reversible denaturation and the inclusion in the molecule of several functional groups [67].
Aptamers (introduced by Ellington and Szoztak [68], and by Tuerk and Gold [69] in 1990) are isolated from combinatorial libraries by a process of in vivo evolution called SELEX (Systematic Evolution of Ligands by Exponential enrichment).
In this process a random sequence of oligonucleotide library (composed approximately by 10^{15} – 10^{16} individual molecules), flanked by constant 5’ and 3’ ends (primer) sequences,

is incubated with a target of interest in a proper buffer at selected temperature. During this step, only a small fraction of the starting sequences is capable to bind the target (generally immobilized on a solid support) and the unbound sequences are further separated from the rest of the library by a simple washing step.

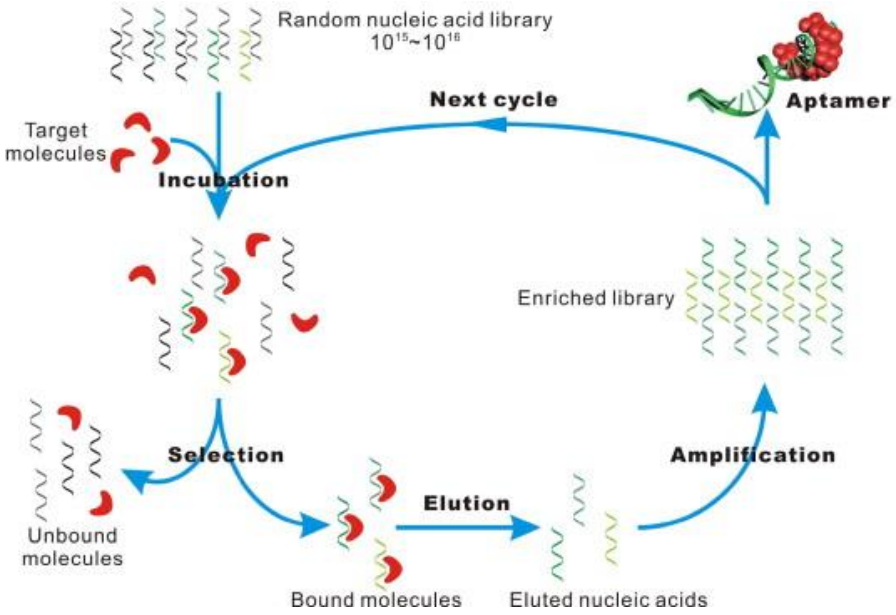

Figure 1.4. Representation of SELEX process. First, random nucleic acid library is incubated with a target molecule. Then, unbound molecules are separated from bound molecules by washing step. Bound nucleic acids are finally eluted, amplified by PCR and used as an enriched library for the next cycle [70].

Next, the bound sequences are eluted, amplified by PCR (Polymerase Chain Reaction) and prepared for the next cycle of selection.

Once affinity saturation is achieved after several rounds (generally 8-15 cycles) of selection/amplification, the enriched library is cloned and sequenced to obtain the sequence information of each member. Selected sequences are then truncated (in order to remove the primer sequences that are not important for the aptamer/target interaction) and finally characterized on the basis of their affinity to the target of interest.

3.3. Engineered protein scaffolds molecules (Affibody®)

Parallel to aptamers, in order to overcome immunoglobulin limitation, another field of investigation is represented by the development of alternative binding proteins (based either on scaffold with the immunoglobulin fold or on completely different protein topologies), called collectively engineered protein scaffolds.

Usually, this scaffold is derived from a robust and small soluble monomeric protein (such as the Kunitz inhibitors or the lipocalins) or from a stably folded extramembrane domain of a cell surface receptor (e.g. protein A, fibronectin or the ankyrin repeat). Compared with antibodies or their recombinant fragments, these protein scaffolds often provide practical advantages including elevated stability, high production yield in *in vitro* systems and possibility to modulate desired properties (such as solubility, thermal stability, protease resistance etc.) [71-73].

Among this classes of engineered protein Affibody® received particular attentions and found application in several studies especially for *in vivo* diagnostic imaging [74, 75] and targeted therapy [76, 77] applications.

Affibody molecules are being developed by a Swedish biotechnology company (*Affibody AB,* www.affibody.com) and are an engineered version (Z domain) of one of the five stable three-a-helix bundle domains from the immunoglobulin Fc-binding region of staphylococcal protein A. Affibody® molecules are constituted by only 58 amino acids without disulphide bonds and can therefore be produced in simpler organism such as prokaryote, rather than the animal system required in antibody synthesis [78].

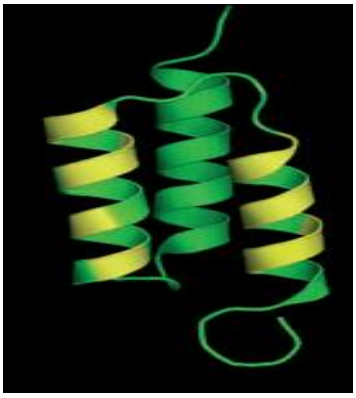

Figure 1.5. Schematic representation of the three-helix bundle Affibody® protein Z scaffold (green) with the 13 position randomized during affibody protein library development [78].

Moreover, due to their small size they can also be chemically synthesised using solid phase peptide synthesis (SPPS), which eliminates the need for biological systems for production, but also means that specific site modification can be performed.

Affibodies can include specific labels, such as fluorophores, radioactive labels and other moieties, such as biotin, which can be used to couple the affibody to surfaces or other molecules, including enzymes [79].

4. Nanostructured affinity biosensors for cancer biomarker detection

The advance in nanotechnology have led to the discovery and the employment of a great number of new materials in nanoscale dimensions (comprise between 1 and 100 nm, even for biological application dimensions can raise up to 500 nm and rarely up to 700 nm).
Because the common biological systems (such as protein, viruses, membrane etc.) are nanostructured and their interaction take place at nanometric scale, nanomaterials becomes an ideally candidates for the development of advanced biosensing devices.

Nanostructures present several advantages in analytical applications and can be mainly used as transducers (due to their unique optical, chemical, electrical, and catalytic properties) or as a component of the recognition element of a biosensing device (due to increase of the area/volume relationship that increases the number of attached bioreceptors in the sensing surface).

Because the high number of nanomaterials utilized in biosensor technologies, the next paragraph is dedicated to the recent works present in literature (from 2009 up to now) regarding the employment of gold and magnetic nanoparticles for cancer biomarkers detection.

4.1. Gold nanoparticles (AuNPs)-based biosensors for cancer biomarkers detection

Among metal nanomaterials, gold plays a special role. A literature research conducted on SciFinder Scholar using "gold nanoparticles" as key word, returned more than 3000 entries (including journal articles and review in English) only in the current year. If the research was expanded from 2010 up to now the results obtained were about 13700. Thus, gold nanoparticles (AuNPs) are one the most (if not the most) studied and applied nanomaterial.
In particular due to their properties (common with other nanomaterials) coupled to their easy synthesis, high compatibility with biological system and enhanced scattering an adsorption, particular attention has been focused on the use of AuNPs for biosensors and for *in vivo* applications (such as cancer cell imaging, cancer therapy and drug delivery) [80-84]. Gold nanoparticles are a colloidal suspension of nanometric-dimension particles of gold.

Even AuNPs first application can be dated to Roman age (utilized to colour glasses, as for instance the famous Lycurgus cup) [85], the modern evaluation of colloidal gold began with the study of Faraday (in 1850s) [86] which revealed that colloidal gold solution shows different properties respect to bulk gold.

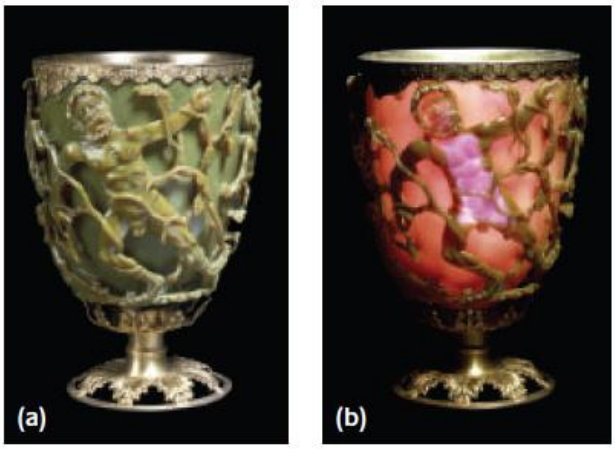

Figure 1.6. Lycurgus cup in reflected (a) and transmitted (b) light [87].

In fact, AuNPs colloidal solutions possess an intense colour, varying from red to purple (respectively for small and larger particles) in contrast with bright yellow colour of massive gold materials.

This phenomenon is due to their unique interaction with light called localized surface plasmon resonance (LSPR). When the oscillating electric field of the incidence light interact with AuNPs, the free electrons of metal nanoparticles undergo an oscillation respect to the metal lattice. At a particular frequency this process is resonant and allow the adsorption of a specific photon (with energy comprise in the visible range of the spectrum) that confer the characteristic intense colour of AuNPs dispersions (i.e. spherical AuNPs of about 10 nm size shows a LSPR at 520 nm resulting in a brilliant red colour of their colloidal solutions) [88].

Numerous studies demonstrated also that LSPR a phenomenon is strictly dependent by the shape, size, and dielectric constants of both the metal and the surrounding material. For instance gold nanorods (AuNRs) solution exhibit a broad range of colour (respect to spherical AuNPs) due to the presence of two LSPR band along the short and the long axis, mainly related to their aspect ratio (represent by the ratio between length and width). Because the longitudinal LSPR of AuNRs can be tuned up to NIR region (~1000 nm) in

which biological tissue are transparent to the incident light, these nanomaterials (with proper functionalization) have found an interesting applications for cancer cells imaging and cancer thermal therapy [89, 90].

Synthesis of spherical AuNPs is classically achieved by citrate-mediated reduction of hydrogen tetrachloroaurate (III) ($HAuCl_4$) in aqueous solution. This procedure pioneered by Turkevich in 1951 [91] and subsequently modified by Frens in 1973 [92] provided the formation of AuNPs in a range between 15 and 150 nm (depending on the citrate concentration). However, particles larger than 20 nm present a high polydispersity and a low concentration.

This problem was then solved by Brown and Natan using a seeding procedure, based on the catalytic reduction of Au^{3+} by hydroxylamine, mediated by AuNPs surface [93].

Via seed procedures are also extensively used to produce AuNPs with different shapes and sizes (rod, triangular, polygonal rods, star etc.); these methods begin with the production of small size (1 – 3 nm) gold nanoparticles (called seed) through the reduction of hydrogen tetrachloroaurate with a strong reducing agent (generally sodium borohydride) followed by the addition of a growth gold solution including weak reducing agent (i.e. ascorbic acid), $HAuCl_4$, silver and surfactant (i.e. cetyltrimethylammonium bromide; CTAB). Controlling the amount and the nature of reducing agent and the condition of the growth, synthesis of AuNPs with different shapes and dimension has been achieved [94-97].

Other synthetic strategies include physical, photochemical, biological techniques and the realization of bimetallic or silica-core based nanoparticles. These procedures have been well-reviewed in ref. [98].

Exploiting the high affinity between gold and thiol groups, AuNPs has been successfully coupled with different biorecognition elements (such as aptamers/DNA probe, antibodies etc.) and has been extensively used in broad range of sensing/signal amplification approaches both in sandwich or label-free assays.

In this work, two different application procedures, mainly related to the capability of AuNPs to immobilize a higher number of biorecognition elements (capture and detection probe) respect to bulk material-based support, of AuNPs in biosensors development were considered:

- in the first one AuNPs were directly deposed onto a solid support (i.e. the working electrode of electrochemical cell) in order to be functionalized with more capture probe allowing the recognition of an higher number of target of interest (i.e. label-free biosensors).

- in the second one, after the immobilization of the capture probe on the solid support, AuNPs-modified detection probe were introduce in the system to form a sandwich assay. The amplification were achieved both by the using an enzyme-labelled detection probe either exploiting catalytic properties of AuNPs surface (i.e. sandwich assay-based biosensors).

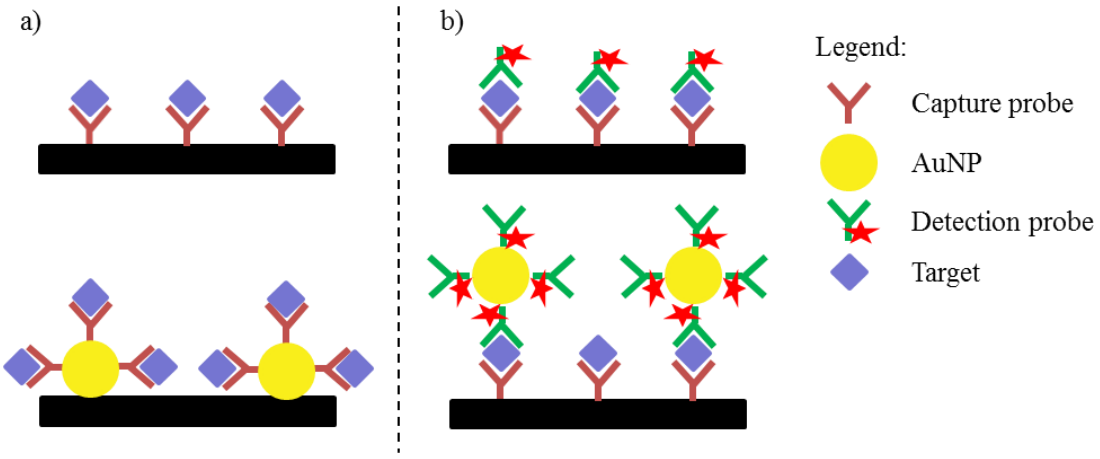

Figure 1.7. Different approaches utilized for AuNPs-signal amplification: a) Capture probe-modified AuNPs can be immobilized on a solid support increasing the number of target that can be recognized by the bioreceptor. b) Amplification of analytical signal by AuNPs modified with enzyme-labelled detection probes.

Electrode surface can be easily modified by AuNPs. A simple method consists into the directly electrodeposition of AuNPs. Several strategies were reposted by different groups. Electrodeposition of AuNPs was generally performed starting from an aqueous solution of $HAuCl_4$ prepared in acidic medium and containing different types of electrolytes. Subsequently, Au(III) was reduced to form AuNPs (in a form of cluster aggregates) by the application of a constant negative potential (or step potential) for a fixed time or varying the potentials for a different number of cycles at an optimal scan rate [99-103].
For instance, Rathod *et al.* [101] reported the electrodepostion of AuNPs on the surface of an working electrode (composed by carbon cloth microfibers) staring from a 0.6 mM

$HAuCl_4$ solution prepared in sulphuric acid 0.5 M and cycling the potential from -0.2 to 1.6 V at 0.1 V s^{-1} *vs.* Ag/AgCl reference electrode for 25 cycles.

Electrodeposition of AuNPs was also performed on polycrystalline Au electrodes using a 6 mM $HAuCl_4$ solution prepared in 0.1 M KNO_3 and scanning the potential from -0.2 to -1.2 V *vs.* Ag/AgCl for 20 cycles [100]. Moreover, Dai *et al.* [104] reported the formation of AuNPs on ITO electrode by the application of a step potential from 1.055 V to -0.0045 V for a fixed time.

Other groups report also the inclusion of pre-formed AuNPs in a monomer solution (generally pyrrole, aniline and chitosan) followed by the synthesis of the polymer or the growth of AuNPs on a pre-formed polymer [105-111].

For instance, glucose biosensors based on chitosan–glucose oxidase (GOx)–AuNPs biocomposite was prepared by one-step electrodeposition staring from a solution including chitosan monomer, pre-formed AuNPs and GOx. Chitosan hydrogel formed during the electrodeposition incorporated AuNPs that enhance the stability of the enzyme and facilitate the oxidation of hydrogen peroxide at the electrode [107].

Saberi *et al.* [109] reported the development of DNA biosensor based on the formation of polyaniline (PANI) film on the surface of graphite screen-printed cells, followed by electrochemical deposition of AuNPs obtained from a $HAuCl_4$ acid solution. This study revealed the enhancement of the AuNPs-modified PANI-based DNA biosensor due both to the intrinsic increase of the performance of AuNPs-modified PANI sensors at neutral pH, either to the correct alignment of DNA capture probe that allowed an improvement of hybridization reaction.

Finally, AuNPs can also immobilized on the electrode surface by layer-by-layer deposition exploiting the high affinity of Au with several functional group (such as -SH, -NH_2, -CN) or in addition with other nanostructured materials, such as multi-walled carbon nanotubes, MWCNTs.

An interest study was reported by Xiao *et al.* [112] in which COOH-modified AuNPs was immobilized to the surface of Au electrode by means of a dithiol linker. Then, amino ethyl-FAD cofactor was covalently linked to COOH-AuNPs and apo-GOx was finally reconstituted. Results showed that AuNPs act as nanoelectrode able to transport the electrons from the FAD centre to the electrode surface activating the bioelectrocatalytic function of the enzyme.

With this approach, the turnover rate of electrons from the enzyme redox site to the electrode was estimated to be eight time higher than the rate of electron transfer from the cofactor site to the native acceptor of the enzyme.

Colloidal AuNPs can be also easily functionalized with different types of signalling bioreceptors (such as antibody, DNA, aptamer etc.) by means of covalent or electrostatic interactions and used in an ELISA-modified assay. In particular capture probe was first immobilized on a solid support, followed by the sandwich formation between antigen and AuNPs-functionalized detection probe.
For instance, Cui *et al.* [113] described the detection of human-IgG using gold nanoparticles AuNPs/CNT modified electrode (to increase the amount and the stability of the immobilized capture Ab) coupled with horseradish peroxidase (HRP)-functionalized AuNPs label, that allowed an enhancement of analytical signal due to the higher number of HRP molecules loaded on the surface of AuNPs.
Similar assays were also studied for the development of immunochromatographic test strips (widely used for pregnancy test) in which AuNPs act as colorimetric label [114, 115] and also used for the amplification of the detection of DNA hybridization reaction [116].

Another amplification techniques exploit the intrinsic catalytically properties of AuNPs to reduce metal (generally silver) allowing the use of the sensible electrochemical stripping metal analysis. Wang described this application for the determination of DNA segments related to the BRCA1 breast cancer gene. In particular detection DNA probe was immobilized on the surface on magnetic beads followed by hybridization with AuNPs-modified complementary target and finally, functionalized beads was placed in a silver-enactment solution. AuNPs catalyse the reduction from Ag(I) to Ag(0) with the formation a metallic silver nanoparticles tags. Ag(0) was then dissolved in acid medium to form Ag(I) ions that are subsequently accumulated at a disposable thick-film carbon electrode by the application of a negative potential (-0.8V) and detected using a potentiometric stripping protocol [117].
AuNPs is also capable to catalyse the reduction of Au(III) to Au(0): in this case an increasing of AuNPs dimension was observed and its application in colorimetric assay has been reported [118-120].

Finally the chronoamperometric detection of the hydrogen produced from acid medium (catalysed by AuNPs) was also studied [121].

AuNPs-modified electrode and AuNPs-coated detection probe strategies were successfully applied for the determination of cancer biomarkers.

AuNPs were extensively used to improve the sensibility both for classic ELISA tests either for immunosensor devices.

Ambrosi *et al.* [122] reported the development of AuNPs-modified ELISA immunoassay for the determination of MUC1 (CA15-3) antigen. In particular, primary anti-CA15-3 antibody was immobilized in a classical 96 well microtiter plate followed by the interaction with CA15-3 antigen and the addition of AuNPs-modified anti-CA15-3-HRP secondary antibody. In comparison with classical assay (Ab-Ag-Ab HRP) the possibility to immobilize a higher amount of signalling antibody on AuNPs surface provided both an increase of sensibility either a reduction of time required for the completion of the assay.

In a different approach, AuNPs were used to modified (via chemical plating) the surface of ELISA microtiter plate followed by the immobilization with the antigen and by the incubation labelled-antibody.

In this case, the fabrication of AuNPs layer results in a higher efficiencies on the protein binding maintaining also unchanged the protein activity. This AuNPs-modified assay was successfully applied for the determination of CEA cancer biomarker (utilized for the diagnosis and the monitoring of colorectal carcinoma) and anti-thrombin model protein in buffered solutions [123]. The same authors also reported the application of this approach for the detection of CEA antigen in human plasma [124].

AuNPs-based electrochemical immunosensor for cancer biomarkers detection were also developed. Elshafer and co-worker reported the development of label-free impedimetric immunosensor based on AuNPs-modified Au electrode for the detection of epidermal growth factor receptor (EGFR) [100], a cancer biomarker associated with epithelial cancer such as breast, bladder, renal, neck gastric etc. cancer [14].

In this study, AuNPs were first electrodeposed on the surface on Au electrode followed by their functionalization with cysteamine to form a self-assembly monolayer (SAM). Protein G was then immobilized to cysteamine SAM and used to bind Fc region of specific anti-EGFR antibody. Finally affinity reaction with EGFR antigen was evaluated by means of electrochemical impedance spectroscopy (EIS) using $[Fe(CN)_6]^{3-/4-}$ as redox

probe. AuNPs showed an increase of electroactive area of the electrode by a factor of 3, allowing the detection of EGFR with good sensibility and reproducibility both in PBS buffer either in human plasma.

AuNPs-based label free immunosensor was also applied for the detection of CA125;

Au nanostructures were first electrodeposed on the surface of a microchip (composed by a layer of SiO_2 covered by Au and by another layer of SiO_2 with a circular aperture of 5 μm) and after functionalized with cystamine in order to form a SAM.

Cystamine residues were coupled with glutaraldehyde and with anti-CA125 antibody.

Affinity reaction with antigen was evaluated analysing the reduction of $[Fe(CN)_6)^{3-/4-}$ oxidation current due to the formation of a layer of protein that block the electron transfer from the solution to the surface of the chip. This sensor allowed the detection of CA125 in serum an blood with good detection limit and reproducibility [125].

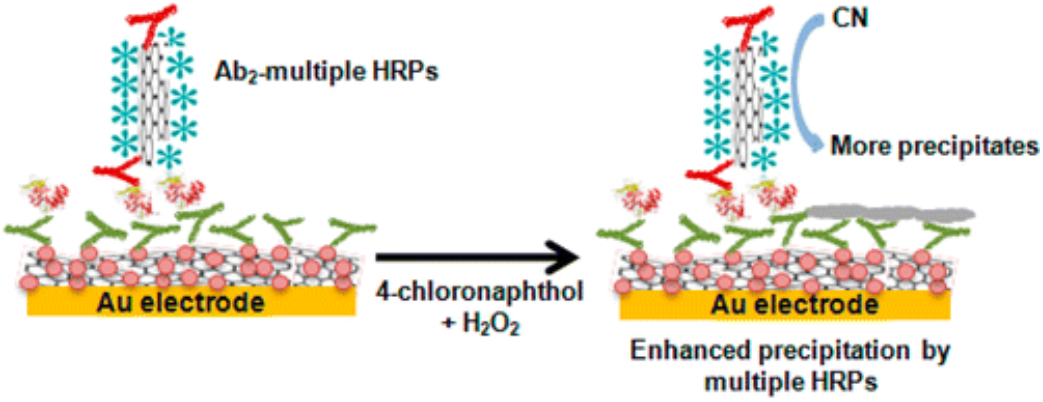

Figure 1.8. Representation of AuNPs/MWCNTs/Au immunosensor for detection of PSA antigen through multiple-HRP/MWCNTs label strategy [126].

Another assay, involved the immobilization of AuNPs on thiolated MWCNTs-modified Au electrode. This assay was presented in form of ELISA sandwich assay in which AuNPs/MWCNTs/Au-modified electrodes were incubated with anti-PSA primary antibody, PSA antigen, and anti-PSA secondary attached to the surface of HRP-modified MWCNTs. The amplified detection was achieved by the enhanced precipitation of 4-chloro-1-naphthol using a higher number of horseradish peroxidase (HRP) molecules immobilized on MWCNTs, coupled with an higher number of primary Ab bound on the surface of Au electrodes [126].

A recent strategy for simultaneous determination of three liver cancer biomarkers (alpha-fetoprotein – AFP –, alpha-fetoprotein variant – AFP-L3 –, and abnormal prothrombin –

APT –) based on three redox labels was reported by Li *et al.*[127]. AuNPs functionalized with CNTs were used as carriers to immobilize redox probes labelled (ferrocene, 2,2'-bipyridine-4,4'-dicarboxylic acid and thionine) antibodies and to amplify the signals. Affinity reaction detection was achieved by the analysis of the different electrochemical behaviour of the labels by means of differential pulse voltammetry (DPV).

Mani *et al.* [128] reported the development of a densely packed gold nanoparticles platform combined with a multiple-enzyme labelled detection antibody-magnetic bead bioconjugate for the analysis of PSA cancer biomarker in serum samples.

AuNPs-glutathione colloid was adsorbed layer-by-layer through electrostatic interaction on a layer of cationic poly diallyldimethyl ammonium chloride (PDDA), deposited on a pyrolytic graphite electrode.

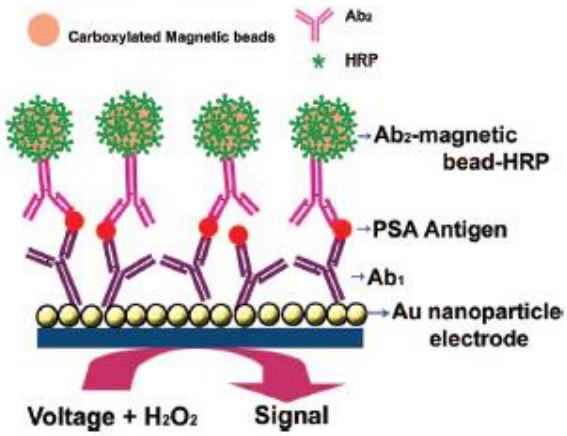

Figure 1.9. AuNPs-based immunosensor for detection of PSA in serum, cell lysate and human serum of cancer patients [128].

Anti-PSA Ab was immobilized to the AuNPs-modified electrode via amidization (using EDAC/NHS solution) and then casein was used to block free Ab binding site on the electrode surface. After the incubation with PSA, the assay was completed adding the anti-PSA secondary antibody conjugated with HRP-modified magnetic particles. This complex enhanced the catalytic reduction of H_2O_2 and thus PSA concentration was evaluated by amperometric measurements. This approach allowed the detection of PSA in serum sample with a very low detection limit (0.5 pg mL^{-1}) and was also successfully applied for the measurement of PSA in cell lysates and human serum of cancer patients.

AuNPs/PDDA-modified pencil graphite electrode was later applied for the determination of human interleukin-6 (IL-6) cancer biomarker in serum [129].

The assay was based on a sandwich format in which GSH-AuNPs were deposed as in the previous reported work. Anti-IL-6 antibody was then bound to the sensor surface and bovine serum albumin (BSA) was used to reduce the non-specific binding of other proteins. The sandwich was completed by the incubation with a biotinylated secondary Ab and with streptavidin-HRP. Also in this approach, the amperometric measurements of the reduction of H_2O_2 were used to determinate the concentration of IL-6.

Moreover, authors compared the performance of AuNPs- and MWCNTs-based assay showing that AuNPs-based biosensor provided a better results and a lower detection limits for the measurements of IL-6 cancer biomarker.

Finally, Chikkaveeraiah *et al.* [130] utilized coupled this assay with microfluidic system using an 8-electrode screen-printed carbon array.

Another microfluidic system (based on the development of a sandwich assay using AuNPs functionalized with HRP-labelled secondary Ab) for the detection of alpha-fetoprotein was recently developed by Zhang *et al.* [131].

Zhong *et al.* [132] developed an immunosensor for the detection of CEA cancer biomarker based on AuNPs enwrapped graphene nanocomposites. Initially, AuNPs and were electrodeposed (applying a constant potential) on the surface of Prussian Blue-modified glassy carbon electrode and then functionalized with primary anti-CEA Abs and BSA. After the reaction with the antigen, the sandwich assay was completed by incubation with HRP-labelled secondary anti-CEA antibodies immobilized on the surface of multi-AuNPs shell assembled on a chitosan-protected graphene nanocore.

The sandwich complex allowed the signal amplification on CEA detection promoting the electron transfer from HRP(Fe^{3+}) to HRP(Fe^{2+}) and allowing the reduction of H_2O_2 in water solution.

This immunosensor was successfully applied for the determination of CEA biomarker in serum obtained from cancer patients with good correlation with reference method. Potentiometric immunosensor for total PSA detection was reported by Wang *et al.* [133]. The biosensor was assembled by the immobilization of a first layer of AuNPs on PVC electrode. Poly(amidoamine) G4 dendrimer was the deposed between this and another layer of AuNPs.

Anti-total PSA Ab was finally absorbed on the surface of the second layer of AuNPs. The detection of t-PSA concentration was evaluated analysing the variation of the electric potential of the electrode surface (without application of current) before and after the Ab-

Ag interaction. The developed immunosensor showed good precision, stability and reproducibility and consistent results with reference ELISA test.

Catalytic deposition of silver on AuNPs coupled with anodic stripping analysis was also exploited for the detection of cancer biomarkers.

Lin *et al.* [134] developed a sandwich assay for the detection of CEA (Carcinoembryonic Antigen) cancer biomarker using AuNPs-modified detection anti-CEA antibody.

The immunosensor was assembled by covalent immobilization of capture anti-CEA Ab on the surface of chitosan-modified graphene-coated glassy carbon electrode followed by the addition of BSA and by the incubation with CEA antigen.

AuNPs-modified poly(styrene-*co*-acrylic acid) beads were functionalized with anti-CEA detection Ab and finally deposed to the sensor to complete the sandwich assay.

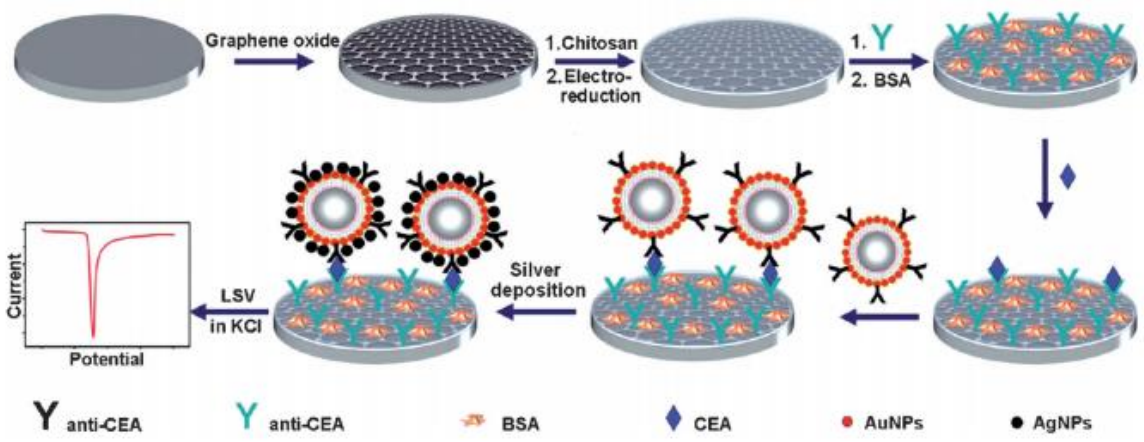

Figure 1.10. Schematic representation of silver-enhancement based immunosensor for CEA cancer biomarker detection [134].

The anchored AuNPs induced the catalytically deposition of silver allowing the formation of AgNPs-coated AuNPs.

Compared with AuNPs (detectable by stripping analysis in HCl), silver nanoparticles (AgNPs) can be oxidized at more negative potential with a relatively sharp peak, which is preferred to overcome the interference of reducing species and improving the detection precision and sensitivity. Immunoreaction was evaluated analysing the stripping current of silver obtained using linear sweep voltammetry technique.

Similar approach was developed by Hong Min and co-worker [135]. In this study electrochemical stripping analysis of AgNPs-coated AuNPs was used to detect

Concavalin A (Con A) and can be used to monitor glycan-leticin interaction and cancer related glycans.

The assay was presented in sandwich format in which Con A was specifically bound to mannose self-assembly monolayer formed on the surface of a gold electrode. The sensor was the incubated with mannose-coated gold nanoparticles to complete the sandwich. Silver deposition on AuNPs was then performed using silver staining solution. AgNPs were the dissolved in HNO_3 solution and the resulting silver ions electrochemically deposed to the electrode surface by the application of specific potential. Finally deposited silver was stripped by means of anodic stripping voltammetry. Stripping silver current was used to determinate the concentration of Con A protein.

Aptamers were also used, instead of antibodies, in gold-nanostructured electrochemical biosensors for the detection of cancer biomarkers.

Liu *et al.* [136] described the development of a sensitive aptasensor for the detection of prostate specific antigen (PSA) based on the signal amplification of biotin-avidin system using AuNPs-modified graphite electrode.

In particular graphite electrode was covered with AuNPs-modified graphite mesoporous nanoparticles (GMCs) prepared by linkage between 1,6-hexanedithiol-functionalized GMCs and AuNPs *via* Au-S binding. Streptavidin was the attached to AuNPs/GMCs-modified electrode to immobilize a larger amount of biotinylated anti-PSA aptamer. Affinity reaction with PSA cancer biomarkers was then evaluated using hexacyanoferrate redox probe and differential pulse voltammetry technique. An increase of PSA concentration led to a decrease of redox probe current allowing the construction of a calibration curve.

The developed aptasensor was successfully applied to the determination of PSA concentration in serum samples showing high specificity, good stability and reproducibility.

Label-free aptasensor based on AuNPs-modified Au electrode for the determination of HER2 cancer biomarker was reported by Chun *et al.* [137].

A thin layer of AuNPs were electrodeposed on the surface of gold electrode using 10 mM $HAuCl_4$ solution prepared in 0.5 M H_2SO_4 and applying a potential of -0.2 V (*vs.* Ag/AgCl reference electrode) for 20 seconds. Electrodeposed AuNPs were then functionalized with 3-mercaptopropionic acid followed by the attachment of ssDNA-NH_2

anti-HER2 aptamer *via* EDAC/NHS chemistry. Free surface of the sensor was finally blocked with BSA.

Evaluation of affinity reaction was carried out by electrochemical impedance spectroscopy using $[Fe(CN)_6]^{3-/4-}$ as redox probe. The proposed aptasensor showed fast HER2 detection with no reported cross reactivity in other species present in human serum (such as glucose, IgG, DNA and RNA). Furthermore, the aptasensors could be regenerated using acid solution (pH 4).

Label-free approach was also used to detect MUC1 cancer biomarker. Florea and co-worker [138] reported the development of two aptasensors based on the immobilization of thiolated anti-MUC1 aptamer of AuNPs-modified graphite and gold screen printed electrodes.

In the first strategy, AuNPs were electrodeposed on the surface of graphite screen-printed electrode followed by the covalent immobilization of SH-modified anti-MUC1 aptamer and by the formation of a self-assembly monolayer with 6-mercapto-1-hexanol (MCH). After the interaction with the antigen electrochemical impedance spectroscopy measurements (using $[Fe(CN)_6]^{3-/4}$ as redox probe) were performed to construct the calibration curve.

In the second approach, AuNPs were electrodeposed on the surface of gold screen-printed electrodes. AuNPs were then functionalized with MCH and methylene-blue (MB), used as redox probe. The interaction between aptamer and MUC1 antigen caused a decrease in MB redox current due to the reduction of the amount of intercalated MB present in the immobilized aptamers.

Recently, an electrochemical aptamer biosensor based on an enzyme–gold nanoparticles dual label for the detection of MUC1 antigen was developed [139].

In particular, AuNPs were functionalized with a hairpin oligonucleotide (HO) anti-MUC1 (modified with thiol at the 5′-end and biotin at the 3′-end), with HPR enzyme and deoxyadenosine triphosphate (dATP).

In the absence of MUC1, the immobilised hairpin aptamer was in a “closed” state, which shielded biotin from being captured by the streptavidin-modified electrode. In contrast, in the presence of MUC1, the HO was disrupted, and the biotin was captured by the streptavidin molecules immobilized on the transducer. In this case, redox behaviour of 2,3-diaminophenazine (DAP), catalytically produced by HRP in presence of o-

phenylenediamine and H_2O_2, was used to determinate the concentration of MUC1 cancer biomarker.

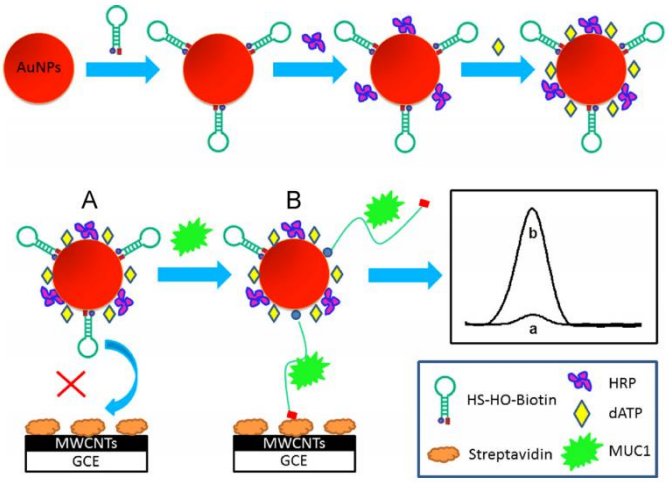

Figure 1.11. Schematic diagram regarding MUC1 detection with AuNPs-modified anti-MUC1 HO-aptamer. (A) In the absence of MUC1, the biotin was shielded and thus inaccessible to the streptavidin immobilized on the transducer. (B) Upon target binding, the disruption of the stem-loop makes the biotin exposed and easily captured by the streptavidin-modified electrode [139].

Because platelet-derived growth factor (PDGF) possess two epitopes that can bind selectively by two aptamers, an AuNPs-based aptamers sandwich assay was reported [140]. Thiolated anti-PDGF aptamer was first immobilized on gold electrode *via* Au-S link followed by the formation of mixed SAM with 6-mercapto-1-hexanol. Parallel, AuNPs were synthesized by citrate reduction method and covered with thiolated anti-PDGF aptamer. After the formation of sandwich between Au electrode/anti-PDGF aptamer and AuNPs-modified anti-PDGF aptamer, $[Ru(NH_3)_5Cl]^{2+}$ was added to the sensor. $[Ru(NH_3)_5Cl]^{2+}$ molecules were immobilized onto the surface of the above sandwich structure and the analysis of its redox behaviour allowed the detection on PDGF antigen.

Aptamer sandwich based assay for the determination of CEA biomarker was also reported [141].

In this approach, CEA antigen was sandwiched between a capture aptamer (immobilized on a gold electrode) and a detection aptamer immobilize on AuNPs modified with 6-ferrocenyl hexanethiol. The presence of the antigen allowed the formation of the sandwich and CEA concentration was directly correlated with the redox behaviour of 6-ferrocenyl hexanethiol redox probe.

4.2. Magnetic nanoparticles (MNPs)-based biosensors for cancer biomarkers detection

Magnetic beads were used as powerful and versatile tool in a variety of analytical and biotechnology applications.

Magnetic particles were generally synthetized by co-precipitation of Fe (II) and Fe (III) aqueous salts by the addition of a base resulting in the formation of solid magnetic iron oxide such as magnetite (Fe_3O_4) and maghemite (γ-Fe_2O_3).

The selection of synthesis parameters (such as the type of salts, Fe (II) and Fe (III) ratio, pH, ionic strength) allowed the formation of magnetic particles with different shapes, sizes and compositions.

Furthermore the synthesis conducted using organic polymers (including cellulose, polystyrene and polyacrylic derivatives) led to the functionalization with different functional groups (i.e. amine, carboxylic acid, aldehyde, thiol, epoxy, hydroxyl, streptavidin, protein A and G, albumin, biotin) which conferred a proper biocompatibility and allowed the modification with biological molecules of interest (such as antibodies, DNA, RNA, aptamers etc.).

These coated magnetic particles are commercially available in nano- and micrometric dimensions [142, 143].

Magnetic particles with high magnetic susceptibilities were currently used for sensors and biosensors development because they offer benefits such as a large surface area and easy immobilization of proteins, DNA, enzymes and antibodies.

Moreover, because the immobilization of bioreceptors molecules directly on the electrode surface presents some problems (such as shielding of the surface by bioreceptors that cause hindrance in electron transfer reducing the analytical signals) magnetic particles were used as solid support to perform bioreceptor – analyte affinity reaction.

In this case, because the modified beads were in suspension, the probability that bioreceptor met the magnetic beads or that bioreceptor-modified magnetic beads met the analyte in very high.

Furthermore, the matrix effect was minimized due to the improved washing and separation steps and for this reason the working electrode surface was easily accessible by redox probe since it diffused onto the bare electrode surface. These properties allowed a

greater increase of sensibility and a reduction of the time for the development of the assay [144, 145].

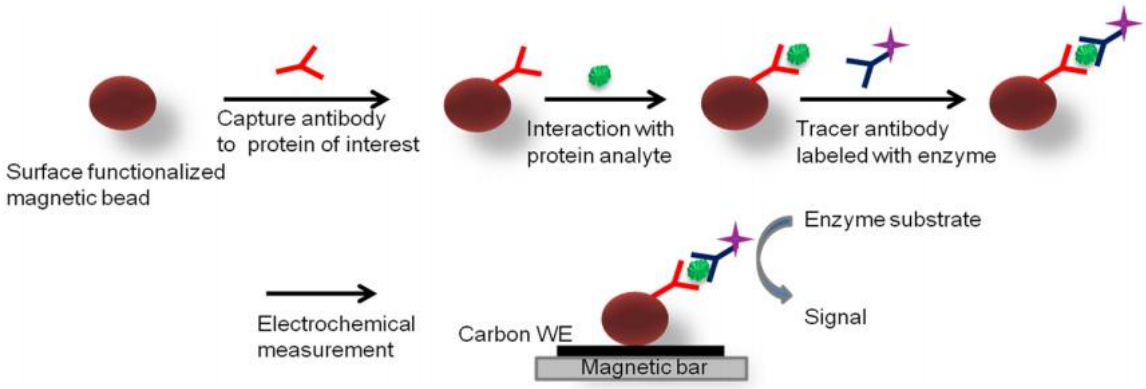

Figure 1.12. General representation of magnetic beads-based assay for protein of interest detection [146].

Generically procedure for the realization of a magnetic beads-based sandwich assay coupled with electrochemical determination, consists in the functionalization of magnetic beads with bioreceptor (in aqueous suspension) followed by the application of a magnetic field in order to collect the particles allowing the removal of unbound biomolecules. After the affinity reaction with antigen and with the detection probe, the modified particles were placed on the surface of bare working electrode (transducer) and finally electrochemical analysis of redox probe was carried out.

This strategy was extensively applied for the detection of cancer biomarkers using sandwich-based assay and employing different types of capture and detection probe.

Sakar *et al.* [147] reported the development of an electrochemical sandwich immunoassay for the detection of free PSA (f-PSA) using magnetic beads as solid support.

In particular, anti-PSA antibody was covalently bound to the surface of polyurethane-coated magnetic beads followed by several washing steps (using magnetic particles concentrator) in order to remove the unbound molecules. Subsequently affinity reaction with PSA, washing steps, functionalization with anti-PSA secondary HRP-labelled antibody and final washing steps were carried out to realize the sandwich assay. Modified-particles were then collect on the surface of the working electrode of screen-printed cells and the amperometric determination of hydrogen peroxide (produced by HRP in presence of TMB) was related to the concentration of f-PSA. This assay was also

applied successfully for the determination of f-PSA in human serum samples allowing the use for clinical analysis.

Similar approach was later reported by Zani and co-worker in which PSA antigen was detected using protein G-coated magnetic beads as solid support for the immobilization of anti-PSA capture probe. The assay was then performed adding PSA antigen, capture anti-PSA antibody and a tertiary alkaline phosphatase-labelled antibody which bound selectively the capture Ab.

The transducer used for the assay development was constituted by screen-printed 8-sensor arrays (based on 8 graphite screen-printed working electrodes each one with its own silver pseudo-reference electrode and graphite counter electrode). The analysis of the redox behaviour of alpha-naphthol (produced by alkaline phosphatase in presence of alpha-naphthyl phosphate as substrate) allowed the development of calibration curve for PSA detection.

The authors also integrated this magnetic-bead based assay in a commercially available microfluidic system (GRAVI-Cell, DyagnoSwiss, Monthey, CH) in which GRAVI-Chip (composed by 8 microchannel with integrate gold microelectrodes) that allowed the real-time monitoring of the kinetic enzyme-label reaction. With this approach PSA concentration was detected in serum sample with good sensibility and reproducibility [148].

The same research group also exploited magnetic beads-based sandwich assay for the determination of HER2 cancer biomarker in buffered and in serum samples obtained for cancer patients [149].

Biosensor for the detection of CEA biomarker using anti-CEA antibody-modified-magnetic beads coupled with a flow-injection electrochemical device was reported by Pan *et al.* [150]. The immunosensor was developed by immobilizing anti-CEA antibody on the surface of epoxysilane-modified core–shell magnetic Fe_3O_4/SiO_2 nanoparticles.

The analytical cycle (including the immobilization of bionanoparticles, the antigen–antibody interaction, and sensor regeneration) was carried out using a flow-injection electrochemical system. Difference in transfer charge resistance before and after Ab-Ag interaction were evaluated by means of electrochemical impedance spectroscopy (EIS) using 10 mM $[Fe(CN)_6]^{3-/4-}$ solution prepared in phosphate buffer saline (PBS) pH 7.4. This procedure was also applied for the detection of CEA antigen in human serum samples. Core–shell–shell $CoFe_2O_4$–MPS/AuNPs composites were also developed and

used for the determination of alpha-1-fetoprotein by potentiometric measurements in human serum [151].

In-flow multiplexed immunoassay for simultaneous electrochemical determination of carcinoembryonic (CEA) and alpha-fetoprotein (AFP) in biological fluids was developed by Tang *et al*. [152].

The immunoassay was based on biofunctionalized magnetic graphene nanosheets (MGO), used as immunosensing probes, and multifunctional nanogold hollow microspheres, used (GHS) as distinguishable signal tags. The probes were fabricated by means of co-immobilization of primary anti-CEA and anti-AFP antibodies on the surface of magnetic nanoparticle-coated graphene nanosheets. Reverse-micelle method was then used for the synthesis of distinguishable signal tags by the encapsulation of horseradish peroxide (HRP) thionine (conjugated with anti-CEA detection probe) and HRP-ferrocene (conjugate with anti-AFP detection probe) into nanogold hollow microspheres.

The detection procedure of CEA and AFP cancer biomarkers was based on the catalytic reduction of H_2O_2 at the various peak potentials in the presence of the corresponding mediators. The developed immunosensor enabled the simultaneous detection of AFP and CEA with very low detection limit for both analyte (1.0 pg mL^{-1}). The proposed immunosensor was also evaluated for the analysis of clinical serum specimens, obtaining a good correlation between the reference methods.

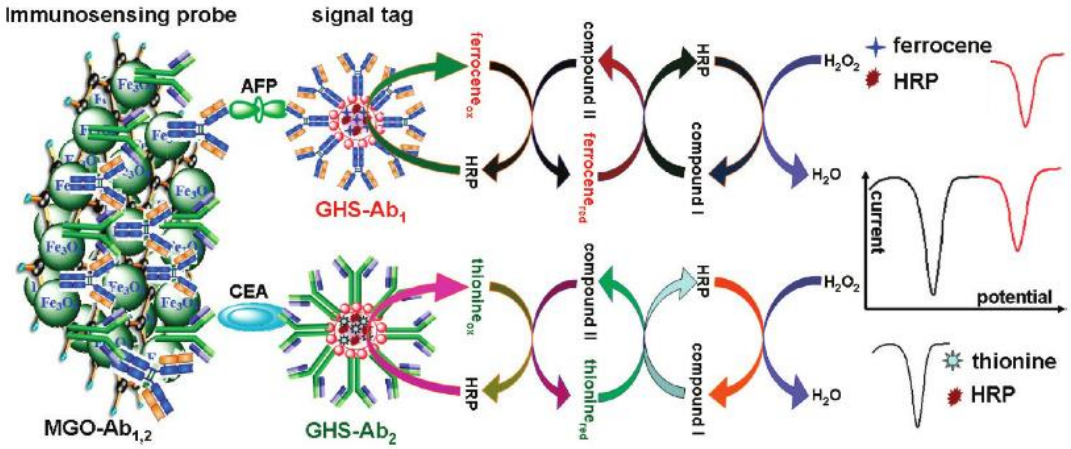

Figure 1.13. Immunosensor development for simultaneous detection of CEA and AFP cancer biomarker by graphene-modified magnetic beads [152].

Magnetic beads-coated bioreceptor molecules were also coupled with AuNPs or used as label.

Munge *et al.* [153] developed a nanostructured immunosensor for detection of interleukin-8 in attomolar range based on glutathione-coated AuNPs deposed on the sensor surface and using anti-PSA detection antibody immobilized on HRP-loaded magnetic cluster (achieved by taking the advantage of interactions between streptavidin-coated magnetic beads and biotinylated HRP). This strategy gave a LOD value for the detection of IL-8 30000-fold lower than that of the conventional ELISA and about 1000-fold lower than that of commercial beads-based protein assays.

Another approach, involved the use of magnetic bead as immobilization platform for the capture of the bioreceptor (in this case pseudorabies virus, PRV), followed by the interaction with analytes of interest (PVR antibody) ad by the addition of AuNPs-coated detection anti-PVR antibody.

Functionalized beads were then collected on the surface of magnetic glass carbon electrode (MGCE) and the oxidation current of AuNPs (at 1.3 V *vs.* saturated calomel reference electrode, SCE) obtained by DPV measurements was used to the development of the calibration curve for the detection of PVR antibody in buffered and real samples solutions [154].

Electrochemical immunosensor for carcinoembryonic antigen based on nanosilver-coated magnetic beads and gold-graphene nanolabels for detection of CEA cancer biomarker was also reported [155].

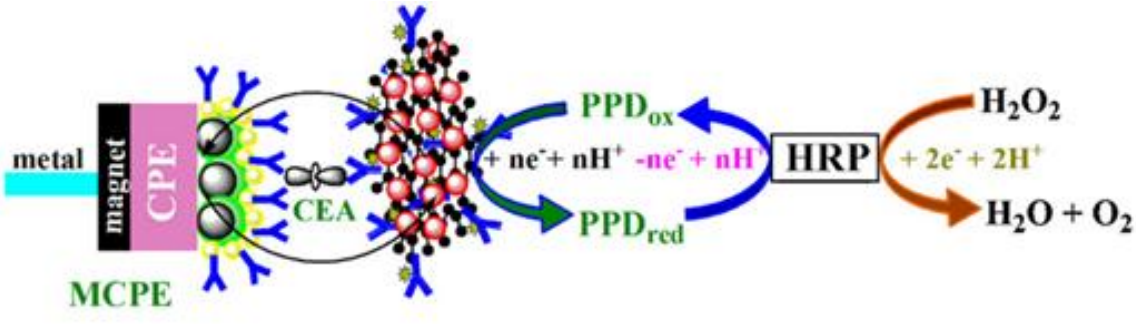

Figure 1.14. Schematic representation of nanosilver-coated magnetic beads and gold-graphene nanolabels-based electrochemical immunoassay for CEA detection [155].

In this study, magnetic Fe_3O_4 beads were first immobilized on the surface of magnetic carbon paste electrode (MCPE) and then functionalized with o-phenylenediamine polymer (PPD), obtained by cyclic voltammetry electropolymerization of o-phenylenediamine. Subsequently, in order to increase the number of bioreceptor

molecules, colloidal silver nanoparticles (AgNPs) were immobilized on the surface of PDD-modified MCPE.

CEA antigen was then incubated with the sensor and the sandwich assay completed by the addition of anti-CEA detection probe labelled with HRP conjugated to AuNPs-modified graphene oxide. Calibration curve was constructed by means of DPV measurements analysing the PDD-mediated reduction H_2O_2.

The developed immunosensor showed a detection limit of 1 pg mL^{-1} and a good comparison with ELISA reference method.

In another approach CEA cancer biomarker was detected using nanogold coated-magnetic particles. First, magnetic particles were prepared by reduction of Fe^{3+} and Fe^{2+} salts in presence of NH_3 at pH 9, followed by the deposition of Au layer [156].

Au/Fe_3O_4 particles were then functionalized several time with AuNPs by addition of thiourea (in order to obtain a multilayer of nanogolds) and modified with anti-CEA bioreceptor.

Detection of cancer biomarker was achieved by competitive methods using CEA and HRP-labelled CEA antigen.

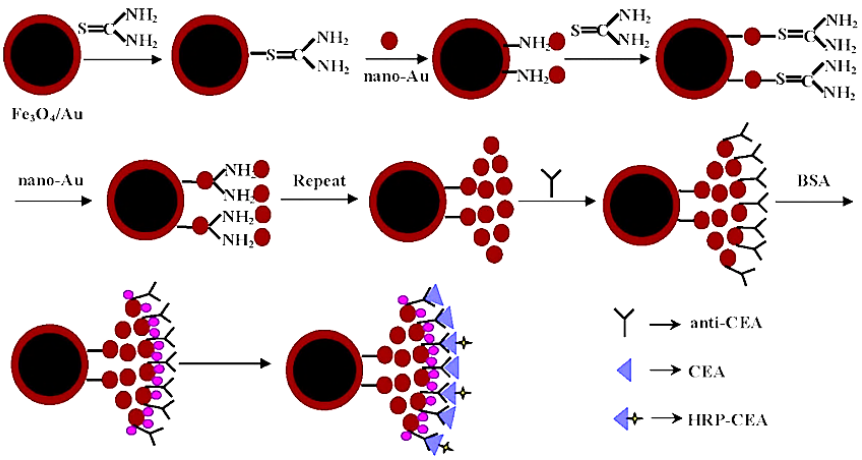

Figure 1.15. Biosensor development for CEA cancer biomarker detection using AuNPs/Au/Fe_3O_4 particles [156].

An interesting electrochemical immunoassay for detection of AFP protein was developed by Ding *et al.* [157].

The immunoassay was based on bio-bar-code amplification which possesses the Polymerase Chain Reaction (PCR)-like sensitivity without a need of enzymatic amplification. AFP was captured between streptavidin-coated magnetic beads and AuNPs-modified with detection probe and with CdS nanoparticles modified DNA probe.

Once the sandwich is formed, the CdS particles were dissolved in HNO_3 acid with the production of Cd^{2+} ions finally determined by anodic stripping voltammetry (ASV) technique.

With this approach, a linear dose-response curve in the concentration range of AFP from 0.02 to 3.5 ng mL^{-1} (limit of detection 9.6 pg mL^{-1}) was obtained.

A nanoparticles-based electrochemical immunoassay for the detection of CA125 was also reported [158].

CA125 protein was sandwiched between anti-CA125 antibody-modified magnetic beads and HRP-labelled anti-CA125 secondary antibody-modified silica nanoparticles. Moreover, in order to increase the electron communication between the immobilized HRP and the electrode, silica nanoparticles were coated with thionine redox mediator.

Analysis of electrochemical behaviour of H_2O_2 was used to construct the CA125 calibration curve.

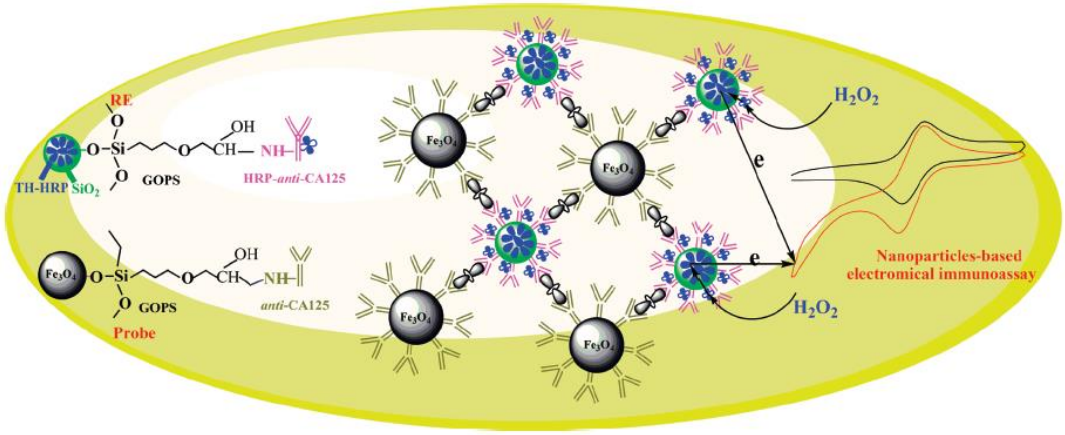

Figure 1.16. CA125 immunosensors development based on magnetic and thionine-modified beads[158].

DNA aptamer-modified magnetic beads were applied in particular for the detection of thrombin biomarker.

Centi *et al.* [159] reported the development of a sandwich aptamer assay for detection of thrombin. The assay was constructed using streptavidin-modified magnetic beads for the immobilization of the primary biotinylated aptamer followed by the affinity reaction with thrombin and by the functionalization with a secondary biotinylated aptamer and with streptavidin-alkaline phosphatase. The detection of the product generated by the enzymatic reaction was achieved by differential pulse voltammetry (DPV).

The biosensors showed good sensitivity and selectivity both in buffered solution either on thrombin-spiked serum and plasma samples. Almost the same authors further

demonstrated the detection of thrombin using aptamer-modified magnetic beads by different approaches (such as indirect and direct competitive assays) and by the detection of thrombin reaction product [160].

Similar assay for detection of thrombin using aptamer-modified magnetic beads was reported by Wand and co-worker [161]. Briefly, streptavidin-coated magnetic beads were used as support to perform the sandwich between thrombin and a capture biotinylated aptamer and detection aptamer immobilized on the surface of ferrocenylhexanethiol loaded silica nanocapsules (FeSH/SiNCs). After the addition of a base in the functionalized-magnetic beads dispersion FcSH residues were released in solution and subsequently deposed on the surface of a gold electrode. DPV measurements were then used to determinate the peak current related to the FeSH residues present on the surface of the electrode.

The peak current of released FcSH had a good linear relationship with the thrombin concentration in the range of 0.1 – 5 nM in buffered solution; this method has been also used to detect thrombin in human serum albumin with minimum background interference.

CHAPTER 2

1. Electrochemical techniques

1.1. Cyclic voltammetry

Cyclic voltammetry (CV) is one of the most widely applied electrochemical techniques for the determination of the thermodynamics or kinetic parameters of redox processes. Moreover CV is also used for the characterization of electrode surface as well a rapid location of redox potentials of electroactive species and the analysis of the effect of the media on the redox processes.

CV measurements were performed applying a triangular potential waveform (Figure 2.1 A) to the working electrode (in an unstirred solution) and analysing the corresponding current variations. Depending on the requested information, single or multiple cycles can be performed.

The results were reported in a characteristic potential *vs*. current plot called voltammograms (Figure 2.1 B).

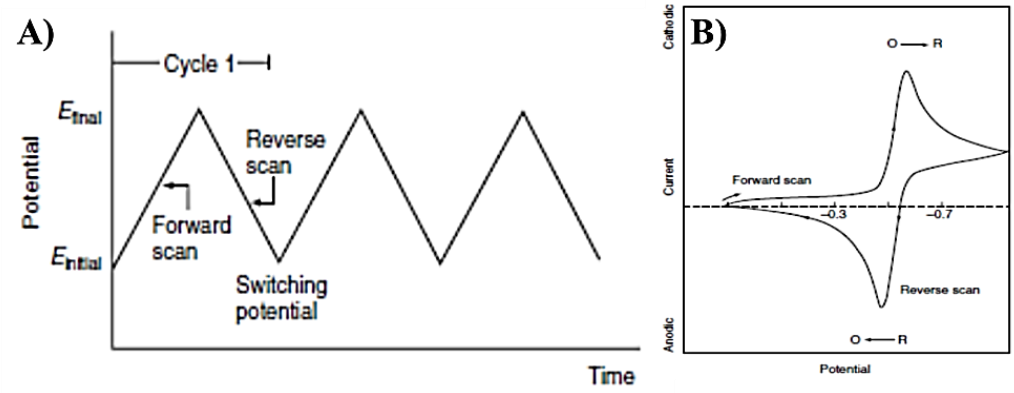

Figure 2.1. A) Potential-time waveform applied in a typical CV experiment. B) Voltammogram obtained for a reversible redox process [7].

The analysis of voltammograms allows the determination of cathodic peak potential (E_{pc}, related to the process Ox + ne^- → Red), anodic peak potential (E_{pa}, related to the process Red → Ox + ne^-) and the correspondent cathodic and anodic peak currents (respectively i_{pc} and i_{pa}).

These parameters can be used for the characterization of the reversibility of the redox process and for the comparison with Nernstian system behaviour.

In particular for a Nernstian system, the ratio between i_{pc} and i_{pa} should be equal to 1, while at 25 °C the difference between anodic and cathodic peak potential ($\Delta_p = E_{pa} - E_{pc}$) should be 0.059/n, where *n* in the number of the electron involved in the half-reaction.
Other important information can be retrieved using Randles-Sevcik equation that, at 25 °C for a reversible system, has the form of:

$$i_p = (2.69 \text{ x } 10^5) n^{3/2} A D^{1/2} C \upsilon^{1/2}$$

in which i_p is the peak current, *n* the number of the electrons, *A* the electrode area (in cm^2), *C* the concentration (in mol/cm^3), *D* the diffusion coefficient (in cm^2/s) and ν the potential scan rate (in V/s). With this equation is possible to calculate on of the parameters (i.e. the electroactive electrode area, *A*) if the others are known.

1.2. Differential pulse voltammetry

In differential pulse voltammetry a fixed magnitude pulse (superimposed on a linear potential ramp) was applied to the working electrode of an electrochemical cell (Figure 2.2. A). The current was then sampled twice: just before the pulse application (1, Figure 2.2 A) and just later in the pulse life (generally after about 40 ms, at 2, Figure 2.2 B).
The difference between these two collected currents ($\Delta i = i_2 - i_1$) was plotted *vs.* the potential obtaining a voltammogram spectrum constituted by a peak: peak height is directly proportional to the concentration of the analyte while its position (redox potential) is related to the difference species.
The main advantage of DPV technique (but also of all pulse techniques) consists in the increase of signal-to-noise ratio, due to the reduction of background current (obtained by taking the difference between the sampled currents) and to the faster decay of capacitive current respect to faradic current.
High sensibility and low detection limit was thus achieved in comparison with others not-pulsed measurements. Moreover this peak-shaped response allows the determination of species with little differences in its redox potential (about 50 mV) providing for instance, the use of DPV measurements in the analysis of metals by anodic stripping voltammetry technique (ASV) [7, 162, 163].

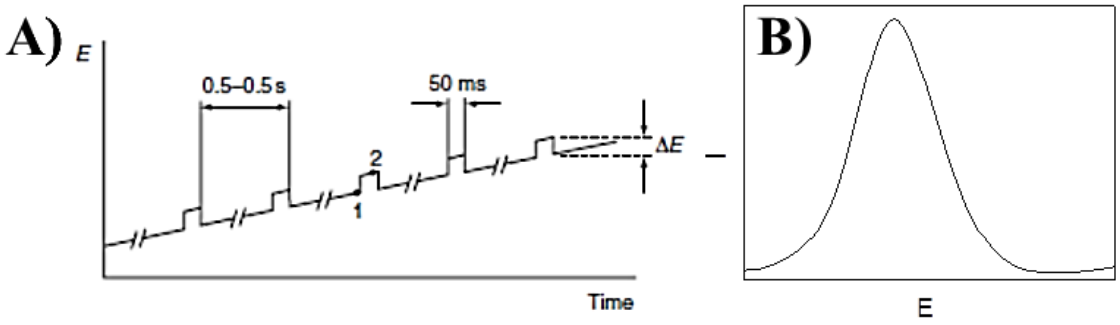

Figure 2.2. A) Potential-time waveform applied in a typical DPV experiment. B) Peak-shape voltammogram obtained DPV experiment [7].

1.3. Electrochemical impedance spectroscopy

Impedance spectroscopy is a powerful method of analysing the complex electrical resistance of a system and is sensitive to surface phenomena and changes of bulk properties.

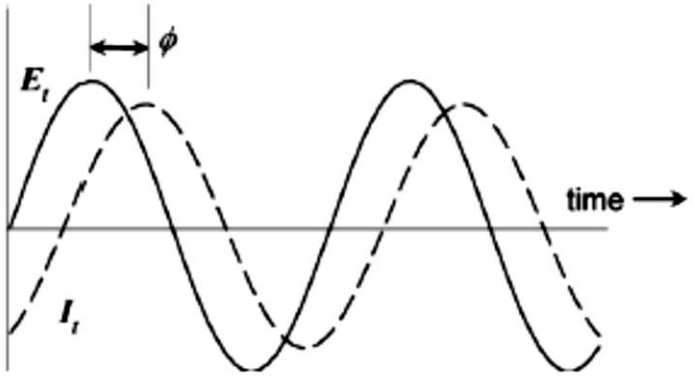

Figure 2.3. Sinusoidal applied AC potential (E_t, solid line) and sinusoidal AC current response (I_t, dotted line) in a generically EIS experiment [164].

The impedance *Z* of a system was determined by the application of an AC voltage perturbation (superimposing an applied DC voltage), for potentiostatic mode, or by the application of an AC current perturbation (superimposing an applied DC current), for galvanostatic mode. In both procedures the AC voltage or AC current amplitudes were adjusted in a proper way.

Then, the analysis of the AC current response (potentiostatic mode) or of the AC voltage response (galvanostatic mode) was achieved.

The rate between the AC voltage-time function and the resulting AC current-time response (shifted in phase) allow the determination of *Z* value by the following equation:

$$Z = \frac{E(t)}{I(t)} = \frac{E_0 \sin(2\pi\upsilon t)}{I_0 \sin(2\pi\upsilon t + \phi)}$$

where *E(t)* and *I(t)* are respectively the potential and the current in a time, E_0 and I_0 are respectively the potential and the current at zero point, ν the frequency, *t* the time and ϕ the phase shift between the voltage- and the current-time functions.

Since the impedance is a complex value (because the current and the potential differ both in phase either in amplitude) its value can be represent by the modulus |Z| and the phase shift ϕ or in a different way, by the real part Z_r (or Z') and the imaginary part Z_i (or –Z'') of the impedance.

Thus, the results of an impedance measurements can be represented by the Bode plot (in which log|Z| and ϕ are plotted *vs.* log ν) or by the Nyquist plot (in which Z_r values are plotted *vs.* Z_i values).

In electrochemical impedance spectroscopy (EIS) experiments, equivalent circuits were used to approximate the experimental results with ideal impedance elements (ohmic resistance – R –, capacitance – C –, constant phase element – CPE –, Warbug impedance – W –) arranged in series and/or in parallel.

When an electrolyte is in contact with an electrolyte, one of the most used equivalent circuits is the so-called Randles circuit (Figure 3.4 A).

Randles circuit includes the solution resistance R_s (depending by the ion concentration and the electrochemical cell geometry), the charge transfer resistance R_{ct} (representing the current flow produced by redox reaction at the interface), the double layer capacitance C_{dl} (resulting from the charge being stored in the double layer ant the interface) and the Warbug impedance W (due to the diffusion from the bulk solution to the interface) elements.

If non-Faradic processes were evaluated, Randles equivalent circuit can be simplified omitting the Warbug element (Figure 3.4 B).

Generally, in biosensor application, the bioreceptor was immobilized on the electrode surface and the affinity reaction with the analyte was further detected. The use of EIS, in this case, allows the monitoring of each phase of the assembly of the biosensor (immobilization of the bioreceptor, self-assembly monolayer formation etc.) and provides the detection of the affinity reaction in a label-free way, namely without the use of label

agents (enzymes, fluorophores etc.) which could affect the properties of biorecognition process.

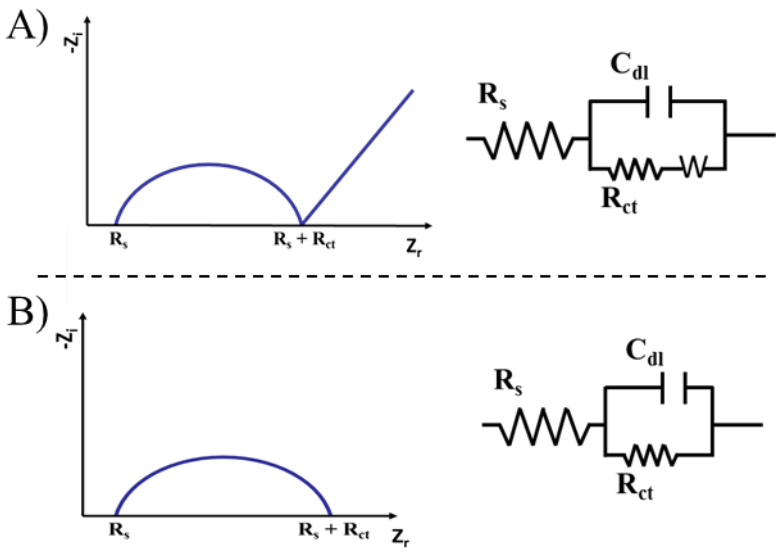

Figure 2.4. Nyquist plots and equivalent circuits for: A) Faradic EIS experiments, B) Non-Faradic EIS experiment. Legend: R_s: solution resistance, R_{ct}: charge transfer resistance, C_{dl}: double layer capacitance, W: Warbug impedance.

Moreover, the absence of a label step reduces the time and the costs necessary for the completion of the bioassay. In this approach, a redox probe (such as $[Fe(CN)_6]^{3-/4-}$) and DC potential (constant for all the time of the measurement) was applied to control the process that occur onto the electrode surface. Charge transfer resistance (R_{ct}) and Δ charge transfer resistance (ΔR_{ct}) were taken as analytical signal.

In fact, when a bioreceptor (such as antibody, DNA probe, etc.) was immobilized on the surface of the electrode, an increase of R_{ct} value was observed due to the presence of a layer of molecules which reduce the electron transfer from the redox probe solution to the electrode surface (generally because steric hindrance of electrostatic repulsions).

Furthermore, because affinity reaction between the bioreceptor and the antigen increases the formation of a non-conductive layer, a proportional increase of R_{ct} values respect to the increase of analyte concentration was detected [164, 165].

References

[1] Thevenot DR, Toth K, Durst RA, Wilson GS. Electrochemical biosensors: recommended definitions and classification. Biosens Bioelectron 2001; 16:121-31.

[2] Ronkainen NJ, Halsall HB, Heineman WR. Electrochemical biosensors. Chem Soc Rev 2010; 39:1747-63.

[3] Borisov SM, Wolfbeis OS. Optical Biosensors. Chem Rev 2008; 108:423-61.

[4] Lucarelli F, Tombelli S, Minunni M, Marrazza G, Mascini M. Electrochemical and piezoelectric DNA biosensors for hybridisation detection. Anal Chim Acta 2008; 609:139-59.

[5] Ramanathan K, Danielsson B. Principles and applications of thermal biosensors. Biosensors and Bioelectronics 2001; 16:417-23.

[6] Llandro J, Palfreyman JJ, Ionescu A, Barnes CHW. Magnetic biosensor technologies for medical applications: a review. Med Biol Eng Comput 2010; 48:977-98.

[7] Wang J, Analytical electrochemistry: Wiley. com, 2006.

[8] Daniels JS, Pourmand N. Label-Free Impedance Biosensors: Opportunities and Challenges. Electroanal 2007; 19:1239-57.

[9] Li J, Li S, Yang CF. Electrochemical Biosensors for Cancer Biomarker Detection. Electroanal 2012; 24:2213-29.

[10] Tothill IE. Biosensors for cancer markers diagnosis. Seminars in Cell & Developmental Biology 2009; 20:55-62.

[11] Soper SA, Brown K, Ellington A, et al. Point-of-care biosensor systems for cancer diagnostics/prognostics. Biosensors and Bioelectronics 2006; 21:1932-42.

[12] Laschi S, Tombelli S, Palchetti I, Mascini M, Marrazza G, New Affinity Biosensors as Diagnostic Tools for Tumour Marker Analysis. In: Baldini F, D'Amico A, Di Natale C, et al., editors. Sensors: Springer New York, 2014: 19-23.

[13] Konforte D, Diamandis EP. Is Early Detection of Cancer with Circulating Biomarkers Feasible? Clin Chem 2013; 59:35-7.

[14] Ludwig JA, Weinstein JN. Biomarkers in cancer staging, prognosis and treatment selection. Nat Rev Cancer 2005; 5:845-56.

[15] Sharma S. Tumor markers in clinical practice: General principles and guidelines. Indian journal of medical and paediatric oncology : official journal of Indian Society of Medical & Paediatric Oncology 2009; 30:1-8.

[16] Dhanasekaran SM, Barrette TR, Ghosh D, et al. Delineation of prognostic biomarkers in prostate cancer. Nature 2001; 412:822-6.

[17] Markman M. Limitations to the use of the CA-125 antigen level in ovarian cancer. Curr Oncol Rep 2003; 5:263-4.

[18] Gutman S, Kessler LG. The US Food and Drug Administration perspective on cancer biomarker development. Nat Rev Cancer 2006; 6:565-71.

[19] Mishra A, Verma M. Cancer Biomarkers: Are We Ready for the Prime Time? Cancers 2010; 2:190-208.

[20] Diehl F, Schmidt K, Choti MA, et al. Circulating mutant DNA to assess tumor dynamics. Nature medicine 2008; 14:985-90.

[21] Majewski IJ, Bernards R. Taming the dragon: genomic biomarkers to individualize the treatment of cancer. Nature medicine 2011; 17:304-12.

[22] Brooks JD. Translational genomics: The challenge of developing cancer biomarkers. Genome Res 2012; 22:183-7.

[23] Diamandis EP. Mass Spectrometry as a diagnostic and a cancer biomarker discovery tool - Opportunities and potential limitations. Mol Cell Proteomics 2004; 3:367-78.

[24] Hanash SM, Pitteri SJ, Faca VM. Mining the plasma proteome for cancer biomarkers. Nature 2008; 452:571-9.

[25] Liang SF, Xu ZZ, Xu XJ, Zhao X, Huang CH, Wei YQ. Quantitative Proteomics for Cancer Biomarker Discovery. Comb Chem High T Scr 2012; 15:221-31.
[26] Sawyers CL. The cancer biomarker problem. Nature 2008; 452:548-52.
[27] Srinivas PR, Verma M, Zhao YM, Srivastava S. Proteomics for cancer biomarker discovery. Clin Chem 2002; 48:1160-9.
[28] Tainsky MA. Genomic and proteomic biomarkers for cancer: A multitude of opportunities. Bba-Rev Cancer 2009; 1796:176-93.
[29] Chauhan SC, Kumar D, Jaggi M. Mucins in ovarian cancer diagnosis and therapy. Journal of ovarian research 2009; 2:21.
[30] Hollingsworth MA, Swanson BJ. Mucins in cancer: protection and control of the cell surface. Nat Rev Cancer 2004; 4:45-60.
[31] Singh AP, Senapati S, Ponnusamy MP, et al. Clinical potential of mucins in diagnosis, prognosis, and therapy of ovarian cancer. The lancet oncology 2008; 9:1076-85.
[32] Bast RC, Jr., Feeney M, Lazarus H, Nadler LM, Colvin RB, Knapp RC. Reactivity of a monoclonal antibody with human ovarian carcinoma. J Clin Invest 1981; 68:1331-7.
[33] Davis HM, Zurawski VR, Jr., Bast RC, Jr., Klug TL. Characterization of the CA 125 antigen associated with human epithelial ovarian carcinomas. Cancer Res 1986; 46:6143-8.
[34] Goodell CA, Belisle JA, Gubbels JA, et al. Characterization of the tumor marker muc16 (ca125) expressed by murine ovarian tumor cell lines and identification of a panel of cross-reactive monoclonal antibodies. Journal of ovarian research 2009; 2:8.
[35] Duffy MJ, Bonfrer JM, Kulpa J, et al. CA125 in ovarian cancer: European Group on Tumor Markers guidelines for clinical use. International journal of gynecological cancer : official journal of the International Gynecological Cancer Society 2005; 15:679-91.
[36] Moss EL, Hollingworth J, Reynolds TM. The role of CA125 in clinical practice. Journal of clinical pathology 2005; 58:308-12.
[37] Zaretsky JZ, Barnea I, Aylon Y, Gorivodsky M, Wreschner DH, Keydar I. MUC1 gene overexpressed in breast cancer: structure and transcriptional activity of the MUC1 promoter and role of estrogen receptor alpha (ERalpha) in regulation of the MUC1 gene expression. Molecular cancer 2006; 5:57.
[38] Lotzniker M, Pavesi F, Scarabelli M, Vadacca G, Franchi M, Moratti R. Tumour associated antigens CA 15.3 and CA 125 in ovarian cancer. The International journal of biological markers 1991; 6:115-21.
[39] Kim HS, Park YH, Park MJ, et al. Clinical significance of a serum CA15-3 surge and the usefulness of CA15-3 kinetics in monitoring chemotherapy response in patients with metastatic breast cancer. Breast cancer research and treatment 2009; 118:89-97.
[40] Depres-Brummer P, Itzhaki M, Bakker PJ, Hoek FJ, Veenhof KH, de Wit R. The usefulness of CA15.3, mucin-like carcinoma-associated antigen and carcinoembryonic antigen in determining the clinical course in patients with metastatic breast cancer. Journal of cancer research and clinical oncology 1995; 121:419-22.
[41] Deng J, Wang L, Chen H, et al. The role of tumour-associated MUC1 in epithelial ovarian cancer metastasis and progression. Cancer metastasis reviews 2013.
[42] Zaczek A, Brandt B, Bielawski KP. The diverse signaling network of EGFR, HER2, HER3 and HER4 tyrosine kinase receptors and the consequences for therapeutic approaches. Histology and histopathology 2005; 20:1005-15.
[43] Cho HS, Mason K, Ramyar KX, et al. Structure of the extracellular region of HER2 alone and in complex with the Herceptin Fab. Nature 2003; 421:756-60.
[44] Rubin I, Yarden Y. The basic biology of HER2. Annals of oncology : official journal of the European Society for Medical Oncology / ESMO 2001; 12 Suppl 1:S3-8.
[45] Gutierrez C, Schiff R. HER2: biology, detection, and clinical implications. Archives of pathology & laboratory medicine 2011; 135:55-62.

[46] Tai W, Mahato R, Cheng K. The role of HER2 in cancer therapy and targeted drug delivery. Journal of controlled release : official journal of the Controlled Release Society 2010; 146:264-75.
[47] Steffensen KD, Waldstrom M, Brandslund I, Jakobsen A. Prognostic impact of prechemotherapy serum levels of HER2, CA125, and HE4 in ovarian cancer patients. International journal of gynecological cancer : official journal of the International Gynecological Cancer Society 2011; 21:1040-7.
[48] Pils D, Pinter A, Reibenwein J, et al. In ovarian cancer the prognostic influence of HER2/neu is not dependent on the CXCR4/SDF-1 signalling pathway. British journal of cancer 2007; 96:485-91.
[49] Lyttle DJ, Fraser KM, Fleming SB, Mercer AA, Robinson AJ. Homologs of vascular endothelial growth factor are encoded by the poxvirus orf virus. Journal of virology 1994; 68:84-92.
[50] Tokunaga Y, Yamazaki Y, Morita T. Specific distribution of VEGF-F in Viperinae snake venoms: isolation and characterization of a VGEF-F from the venom of Daboia russelli siamensis. Archives of biochemistry and biophysics 2005; 439:241-7.
[51] Yamazaki Y, Matsunaga Y, Tokunaga Y, Obayashi S, Saito M, Morita T. Snake venom Vascular Endothelial Growth Factors (VEGF-Fs) exclusively vary their structures and functions among species. The Journal of biological chemistry 2009; 284:9885-91.
[52] Ferrara N, Gerber HP, LeCouter J. The biology of VEGF and its receptors. Nature medicine 2003; 9:669-76.
[53] Muller YA, Christinger HW, Keyt BA, de Vos AM. The crystal structure of vascular endothelial growth factor (VEGF) refined to 1.93 Å resolution: multiple copy flexibility and receptor binding. Structure 1997; 5:1325-38.
[54] Ferrara N. Vascular endothelial growth factor: basic science and clinical progress. Endocrine reviews 2004; 25:581-611.
[55] Bussolino F, Mantovani A, Persico G. Molecular mechanisms of blood vessel formation. Trends in biochemical sciences 1997; 22:251-6.
[56] Carmeliet P, Ferreira V, Breier G, et al. Abnormal blood vessel development and lethality in embryos lacking a single VEGF allele. Nature 1996; 380:435-9.
[57] Ferrara N, Carver-Moore K, Chen H, et al. Heterozygous embryonic lethality induced by targeted inactivation of the VEGF gene. Nature 1996; 380:439-42.
[58] Carmeliet P, Jain RK. Angiogenesis in cancer and other diseases. Nature 2000; 407:249-57.
[59] Carmeliet P. VEGF as a key mediator of angiogenesis in cancer. Oncology 2005; 69:4-10.
[60] Li L, Wang L, Zhang W, et al. Correlation of serum VEGF levels with clinical stage, therapy efficacy, tumor metastasis and patient survival in ovarian cancer. Anticancer research 2004; 24:1973-9.
[61] Barak V, Pe'er J, Kalickman I, Frenkel S. VEGF as a Biomarker for Metastatic Uveal Melanoma in Humans. Curr Eye Res 2011; 36:386-90.
[62] Harris LJ, Larson SB, Hasel KW, Day J, Greenwood A, McPherson A. The three-dimensional structure of an intact monoclonal antibody for canine lymphoma. Nature 1992; 360:369-72.
[63] Weiner LM, Surana R, Wang S. Monoclonal antibodies: versatile platforms for cancer immunotherapy. Nature reviews Immunology 2010; 10:317-27.
[64] Mian IS, Bradwell AR, Olson AJ. Structure, function and properties of antibody binding sites. Journal of molecular biology 1991; 217:133-51.
[65] Leenaars M, Hendriksen CF. Critical steps in the production of polyclonal and monoclonal antibodies: evaluation and recommendations. ILAR journal / National Research Council, Institute of Laboratory Animal Resources 2005; 46:269-79.

[66] Lipman NS, Jackson LR, Trudel LJ, Weis-Garcia F. Monoclonal versus polyclonal antibodies: distinguishing characteristics, applications, and information resources. ILAR journal / National Research Council, Institute of Laboratory Animal Resources 2005; 46:258-68.
[67] Toulmé J-J, Daguer J-P, Dausse E, Aptamers: Ligands For All Reasons. Aptamers in Bioanalysis: John Wiley & Sons, Inc., 2008: 1-30.
[68] Ellington AD, Szostak JW. In vitro selection of RNA molecules that bind specific ligands. Nature 1990; 346:818-22.
[69] Tuerk C, Gold L. Systematic evolution of ligands by exponential enrichment: RNA ligands to bacteriophage T4 DNA polymerase. Science 1990; 249:505-10.
[70] Song S, Wang L, Li J, Fan C, Zhao J. Aptamer-based biosensors. TrAC Trends in Analytical Chemistry 2008; 27:108-17.
[71] Binz HK, Amstutz P, Pluckthun A. Engineering novel binding proteins from nonimmunoglobulin domains. Nature biotechnology 2005; 23:1257-68.
[72] Gebauer M, Skerra A. Engineered protein scaffolds as next-generation antibody therapeutics. Curr Opin Chem Biol 2009; 13:245-55.
[73] Skerra A. Alternative non-antibody scaffolds for molecular recognition. Curr Opin Biotech 2007; 18:295-304.
[74] Lee SB, Hassan M, Fisher R, et al. Affibody molecules for in vivo characterization of HER2-positive tumors by near-infrared imaging. Clinical Cancer Research 2008; 14:3840-9.
[75] Orlova A, Magnusson M, Eriksson TLJ, et al. Tumor Imaging using a picomolar affinity HER2 binding affibody molecule. Cancer Res 2006; 66:4339-48.
[76] Tolmachev V, Orlova A, Nilsson FY, Feldwisch J, Wennborg A, Abrahmsen L. Affibody molecules: potential for in vivo imaging of molecular targets for cancer therapy. Expert Opin Biol Th 2007; 7:555-68.
[77] Tolmachev V, Orlova A, Pehrson R, et al. Radionuclide therapy of HER2-positive microxenografts using a 177Lu-labeled HER2-specific Affibody molecule. Cancer Res 2007; 67:2773-82.
[78] Nygren PA. Alternative binding proteins: affibody binding proteins developed from a small three-helix bundle scaffold. The FEBS journal 2008; 275:2668-76.
[79] Harris M, Tombelli S, Marrazza G, Turner AP, Affibodies as an alternative to antibodies in biosensors for cancer markers. In: Higson S, editor. Biosensors for medical applications: Woodhead Publishing Limited, 2012: 217-32.
[80] Boisselier E, Astruc D. Gold nanoparticles in nanomedicine: preparations, imaging, diagnostics, therapies and toxicity. Chem Soc Rev 2009; 38:1759-82.
[81] El-Sayed IH, Huang X, El-Sayed MA. Selective laser photo-thermal therapy of epithelial carcinoma using anti-EGFR antibody conjugated gold nanoparticles. Cancer Letters 2006; 239:129-35.
[82] Giljohann DA, Seferos DS, Daniel WL, Massich MD, Patel PC, Mirkin CA. Gold Nanoparticles for Biology and Medicine. Angewandte Chemie International Edition 2010; 49:3280-94.
[83] Huang XH, Jain PK, El-Sayed IH, El-Sayed MA. Plasmonic photothermal therapy (PPTT) using gold nanoparticles. Laser Med Sci 2008; 23:217-28.
[84] Ghosh P, Han G, De M, Kim CK, Rotello VM. Gold nanoparticles in delivery applications. Advanced drug delivery reviews 2008; 60:1307-15.
[85] Mody VV, Siwale R, Singh A, Mody HR. Introduction to metallic nanoparticles. Journal of pharmacy & bioallied sciences 2010; 2:282-9.
[86] Faraday M. The Bakerian Lecture: Experimental Relations of Gold (and Other Metals) to Light. Philosophical Transactions of the Royal Society of London 1857; 147:145-81.
[87] Freestone I, Meeks N, Sax M, Higgitt C. The Lycurgus Cup - A Roman nanotechnology. Gold Bull 2007; 40:270-7.

[88] Ghosh SK, Pal T. Interparticle coupling effect on the surface plasmon resonance of gold nanoparticles: From theory to applications. Chem Rev 2007; 107:4797-862.
[89] Nehl CL, Hafner JH. Shape-dependent plasmon resonances of gold nanoparticles. Journal of Materials Chemistry 2008; 18:2415-9.
[90] Orendorff CJ, Sau TK, Murphy CJ. Shape-Dependent Plasmon-Resonant Gold Nanoparticles. Small 2006; 2:636-9.
[91] Turkevich J, Stevenson PC, Hillier J. A study of the nucleation and growth processes in the synthesis of colloidal gold. Discussions of the Faraday Society 1951; 11:55-75.
[92] Frens G. Controlled nucleation for the regulation of the particle size in monodisperse gold suspensions. Nature 1973; 241:20-2.
[93] Brown KR, Natan MJ. Hydroxylamine seeding of colloidal Au nanoparticles in solution and on surfaces. Langmuir 1998; 14:726-8.
[94] Jana NR, Gearheart L, Murphy CJ. Seed-mediated growth approach for shape-controlled synthesis of spheroidal and rod-like gold nanoparticles using a surfactant template. Advanced Materials 2001; 13:1389.
[95] Johnson CJ, Dujardin E, Davis SA, Murphy CJ, Mann S. Growth and form of gold nanorods prepared by seed-mediated, surfactant-directed synthesis. Journal of Materials Chemistry 2002; 12:1765-70.
[96] Murphy CJ, Jana NR. Controlling the aspect ratio of inorganic nanorods and nanowires. Advanced Materials 2002; 14:80.
[97] Nikoobakht B, El-Sayed MA. Preparation and growth mechanism of gold nanorods (NRs) using seed-mediated growth method. Chemistry of Materials 2003; 15:1957-62.
[98] Daniel MC, Astruc D. Gold nanoparticles: Assembly, supramolecular chemistry, quantum-size-related properties, and applications toward biology, catalysis, and nanotechnology. Chem Rev 2004; 104:293-346.
[99] Campbell FW, Compton RG. The use of nanoparticles in electroanalysis: an updated review. Anal Bioanal Chem 2010; 396:241-59.
[100] Elshafey R, Tavares AC, Siaj M, Zourob M. Electrochemical impedance immunosensor based on gold nanoparticles–protein G for the detection of cancer marker epidermal growth factor receptor in human plasma and brain tissue. Biosensors and Bioelectronics 2013; 50:143-9.
[101] Rathod D, Warren S, Keane K, Egan DA, Dempsey E. Evaluation of a modified carbon micromesh electrode as a new substrate for electrochemical immunosensing. Anal Methods-Uk 2011; 3:799-805.
[102] Takahashi Y, Tatsuma T. Electrodeposition of thermally stable gold and silver nanoparticle ensembles through a thin alumina nanomask. Nanoscale 2010; 2:1494-9.
[103] Finot MO, McDermott MT. Characterization of n-alkanethiolate monolayers adsorbed to electrochemically deposited gold nanocrystals on glassy carbon electrodes. J Electroanal Chem 2000; 488:125-32.
[104] Dai XA, Compton RG. Direct electrodeposition of gold nanoparticles onto indium tin oxide film coated glass: Application to the detection of arsenic(III). Anal Sci 2006; 22:567-70.
[105] Li F, Yang LM, Zhao C, Du ZF. Electroactive gold nanoparticles/polyaniline/polydopamine hybrid composite in neutral solution as high-performance sensing platform. Anal Methods-Uk 2011; 3:1601-6.
[106] Luo X-L, Xu J-J, Zhang Q, Yang G-J, Chen H-Y. Electrochemically deposited chitosan hydrogel for horseradish peroxidase immobilization through gold nanoparticles self-assembly. Biosensors and Bioelectronics 2005; 21:190-6.
[107] Luo X-L, Xu J-J, Du Y, Chen H-Y. A glucose biosensor based on chitosan–glucose oxidase–gold nanoparticles biocomposite formed by one-step electrodeposition. Analytical Biochemistry 2004; 334:284-9.

[108] Qiu J-D, Liang R-P, Wang R, Fan L-X, Chen Y-W, Xia X-H. A label-free amperometric immunosensor based on biocompatible conductive redox chitosan-ferrocene/gold nanoparticles matrix. Biosensors and Bioelectronics 2009; 25:852-7.
[109] Saberi RS, Shahrokhian S, Marrazza G. Amplified Electrochemical DNA Sensor Based on Polyaniline Film and Gold Nanoparticles. Electroanal 2013; 25:1373-80.
[110] Hsiao Y-P, Su W-Y, Cheng J-R, Cheng S-H. Electrochemical determination of cysteine based on conducting polymers/gold nanoparticles hybrid nanocomposites. Electrochim Acta 2011; 56:6887-95.
[111] Mazeiko V, Kausaite-Minkstimiene A, Ramanaviciene A, Balevicius Z, Ramanavicius A. Gold nanoparticle and conducting polymer-polyaniline-based nanocomposites for glucose biosensor design. Sensors and Actuators B: Chemical 2013; 189:187-93.
[112] Xiao Y, Patolsky F, Katz E, Hainfeld JF, Willner I. "Plugging into enzymes": Nanowiring of redox enzymes by a gold nanoparticle. Science 2003; 299:1877-81.
[113] Cui RJ, Huang HP, Yin ZZ, Gao D, Zhu JJ. Horseradish peroxidase-functionalized gold nanoparticle label for amplified immunoanalysis based on gold nanoparticles/carbon nanotubes hybrids modified biosensor. Biosens Bioelectron 2008; 23:1666-73.
[114] Nagatani N, Tanaka R, Yuhi T, et al. Gold nanoparticle-based novel enhancement method for the development of highly sensitive immunochromatographic test strips. Sci Technol Adv Mat 2006; 7:270-5.
[115] Preechakasedkit P, Pinwattana K, Dungchai W, et al. Development of a one-step immunochromatographic strip test using gold nanoparticles for the rapid detection of Salmonella typhi in human serum. Biosens Bioelectron 2012; 31:562-6.
[116] Castaneda MT, Alegret S, Merkoci A. Electrochemical sensing of DNA using gold nanoparticles. Electroanal 2007; 19:743-53.
[117] Wang J, Polsky R, Xu DK. Silver-enhanced colloidal gold electrochemical stripping detection of DNA hybridization. Langmuir 2001; 17:5739-41.
[118] Kim SK, Cho H, Jeong J, Kwon JN, Jung Y, Chung BH. Label-free and naked eye detection of PNA/DNA hybridization using enhancement of gold nanoparticles. Chem Commun 2010; 46:3315-7.
[119] Lei KF, Butt YKC. Colorimetric immunoassay chip based on gold nanoparticles and gold enhancement. Microfluid Nanofluid 2010; 8:131-7.
[120] Morris RE, Ciraolo GM, Saelinger CB. Gold Enhancement of Gold-Labeled Probes - Gold-Intensified Staining Technique (Gist). J Histochem Cytochem 1991; 39:1585-91.
[121] de la Escosura-Muñiz A, Sánchez-Espinel C, Díaz-Freitas Bn, González-Fernández Af, Maltez-da Costa M, Merkoçi A. Rapid Identification and Quantification of Tumor Cells Using an Electrocatalytic Method Based on Gold Nanoparticles. Anal Chem 2009; 81:10268-74.
[122] Ambrosi A, Airo F, Merkoci A. Enhanced gold nanoparticle based ELISA for a breast cancer biomarker. Anal Chem 2010; 82:1151-6.
[123] Zhou F, Yuan L, Wang H, Li D, Chen H. Gold Nanoparticle Layer: A Promising Platform for Ultra-Sensitive Cancer Detection. Langmuir 2011.
[124] Zhou F, Wang MM, Yuan L, Cheng ZP, Wu ZQ, Chen H. Sensitive sandwich ELISA based on a gold nanoparticle layer for cancer detection. Analyst 2012; 137:1779-84.
[125] Das J, Kelley SO. Protein Detection Using Arrayed Microsensor Chips: Tuning Sensor Footprint to Achieve Ultrasensitive Readout of CA-125 in Serum and Whole Blood. Anal Chem 2011; 83:1167-72.
[126] Akter R, Rahman MA, Rhee CK. Amplified Electrochemical Detection of a Cancer Biomarker by Enhanced Precipitation Using Horseradish Peroxidase Attached on Carbon Nanotubes. Anal Chem 2012; 84:6407-15.

[127] Li Y, Zhong ZY, Chai YQ, et al. Simultaneous electrochemical immunoassay of three liver cancer biomarkers using distinguishable redox probes as signal tags and gold nanoparticles coated carbon nanotubes as signal enhancers. Chem Commun 2012; 48:537-9.
[128] Mani V, Chikkaveeraiah BV, Patel V, Gutkind JS, Rusling JF. Ultrasensitive Immunosensor for Cancer Biomarker Proteins Using Gold Nanoparticle Film Electrodes and Multienzyme-Particle Amplification. Acs Nano 2009; 3:585-94.
[129] Munge BS, Krause CE, Malhotra R, Patel V, Silvio Gutkind J, Rusling JF. Electrochemical immunosensors for interleukin-6. Comparison of carbon nanotube forest and gold nanoparticle platforms. Electrochem Commun 2009; 11:1009-12.
[130] Chikkaveeraiah BV, Mani V, Patel V, Gutkind JS, Rusling JF. Microfluidic electrochemical immunoarray for ultrasensitive detection of two cancer biomarker proteins in serum. Biosens Bioelectron 2011; 26:4477-83.
[131] Zhang H, Liu L, Fu X, Zhu Z. Microfluidic beads-based immunosensor for sensitive detection of cancer biomarker proteins using multienzyme-nanoparticle amplification and quantum dotslabels. Biosensors and Bioelectronics 2013; 42:23-30.
[132] Zhong Z, Wu W, Wang D, et al. Nanogold-enwrapped graphene nanocomposites as trace labels for sensitivity enhancement of electrochemical immunosensors in clinical immunoassays: Carcinoembryonic antigen as a model. Biosensors and Bioelectronics 2010; 25:2379-83.
[133] Wang XL, Tao GH, Meng YH. Double-Layer Nanogold and Poly(amidoamine) Dendrimer-Functionalized PVC Membrane Electrode for Enhanced Electrochemical Immunoassay of Total Prostate Specific Antigen. Electroanal 2009; 21:2109-15.
[134] Lin DJ, Wu J, Wang M, Yan F, Ju HX. Triple Signal Amplification of Graphene Film, Polybead Carried Gold Nanoparticles as Tracing Tag and Silver Deposition for Ultrasensitive Electrochemical Immunosensing. Anal Chem 2012; 84:3662-8.
[135] Min IH, Choi L, Ahn KS, et al. Electrochemical determination of carbohydrate-binding proteins using carbohydrate-stabilized gold nanoparticles and silver enhancement. Biosens Bioelectron 2010; 26:1326-31.
[136] Liu B, Lu LS, Hua EH, Jiang ST, Xie GM. Detection of the human prostate-specific antigen using an aptasensor with gold nanoparticles encapsulated by graphitized mesoporous carbon. Microchim Acta 2012; 178:163-70.
[137] Chun L, Kim S-E, Cho M, et al. Electrochemical detection of HER2 using single stranded DNA aptamer modified gold nanoparticles electrode. Sensors and Actuators B: Chemical 2013; 186:446-50.
[138] Florea A, Taleat Z, Cristea C, Mazloum-Ardakani M, Săndulescu R. Label free MUC1 aptasensors based on electrodeposition of gold nanoparticles on screen printed electrodes. Electrochem Commun 2013; 33:127-30.
[139] Hu R, Wen W, Wang Q, et al. Novel electrochemical aptamer biosensor based on an enzyme–gold nanoparticle dual label for the ultrasensitive detection of epithelial tumour marker MUC1. Biosensors and Bioelectronics 2014; 53:384-9.
[140] Wang J, Meng W, Zheng X, Liu S, Li G. Combination of aptamer with gold nanoparticles for electrochemical signal amplification: Application to sensitive detection of platelet-derived growth factor. Biosensors and Bioelectronics 2009; 24:1598-602.
[141] Shu H, Wen W, Xiong H, Zhang X, Wang S. Novel electrochemical aptamer biosensor based on gold nanoparticles signal amplification for the detection of carcinoembryonic antigen. Electrochem Commun 2013; 37:15-9.
[142] Aguilar-Arteaga K, Rodriguez JA, Barrado E. Magnetic solids in analytical chemistry: A review. Anal Chim Acta 2010; 674:157-65.
[143] Gupta AK, Gupta M. Synthesis and surface engineering of iron oxide nanoparticles for biomedical applications. Biomaterials 2005; 26:3995-4021.

[144] Centi S, Laschi S, Mascini M. Improvement of analytical performances of a disposable electrochemical immunosensor by using magnetic beads. Talanta 2007; 73:394-9.
[145] Paleček E, Fojta M. Magnetic beads as versatile tools for electrochemical DNA and protein biosensing. Talanta 2007; 74:276-90.
[146] Chikkaveeraiah BV, Bhirde AA, Morgan NY, Eden HS, Chen X. Electrochemical immunosensors for detection of cancer protein biomarkers. Acs Nano 2012; 6:6546-61.
[147] Sarkar P, Ghosh D, Bhattacharyay D, Setford SJ, Turner APF. Electrochemical immunoassay for free prostate specific antigen (f-PSA) using magnetic beads. Electroanal 2008; 20:1414-20.
[148] Zani A, Laschi S, Mascini M, Marrazza G. A New Electrochemical Multiplexed Assay for PSA Cancer Marker Detection. Electroanal 2011; 23:91-9.
[149] Al-Khafaji QAM, Harris M, Tombelli S, et al. An Electrochemical Immunoassay for HER2 Detection. Electroanal 2012; 24:735-42.
[150] Pan J, Yang QW. Antibody-functionalized magnetic nanoparticles for the detection of carcinoembryonic antigen using a flow-injection electrochemical device. Anal Bioanal Chem 2007; 388:279-86.
[151] Wang L, Gan XX. Antibody-functionalized magnetic nanoparticles for electrochemical immunoassay of alpha-1-fetoprotein in human serum. Microchim Acta 2009; 164:231-7.
[152] Tang J, Tang D, Niessner R, Chen G, Knopp D. Magneto-Controlled Graphene Immunosensing Platform for Simultaneous Multiplexed Electrochemical Immunoassay Using Distinguishable Signal Tags. Anal Chem 2011; 83:5407-14.
[153] Munge BS, Coffey AL, Doucette JM, et al. Nanostructured Immunosensor for Attomolar Detection of Cancer Biomarker Interleukin-8 Using Massively Labeled Superparamagnetic Particles. Angew Chem Int Edit 2011; 50:7915-8.
[154] Li F, Zhou R, Zhao K, Chen H, Hu Y. Magnetic beads-based electrochemical immunosensor for detection of pseudorabies virus antibody in swine serum. Talanta 2011; 87:302-6.
[155] Chen H, Tang D, Zhang B, Liu B, Cui Y, Chen G. Electrochemical immunosensor for carcinoembryonic antigen based on nanosilver-coated magnetic beads and gold-graphene nanolabels. Talanta 2012; 91:95-102.
[156] Li J, Gao H, Chen Z, Wei X, Yang CF. An electrochemical immunosensor for carcinoembryonic antigen enhanced by self-assembled nanogold coatings on magnetic particles. Anal Chim Acta 2010; 665:98-104.
[157] Ding C, Zhang Q, Zhang S. An electrochemical immunoassay for protein based on bio bar code method. Biosensors and Bioelectronics 2009; 24:2434-40.
[158] Tang D, Su B, Tang J, Ren J, Chen G. Nanoparticle-Based Sandwich Electrochemical Immunoassay for Carbohydrate Antigen 125 with Signal Enhancement Using Enzyme-Coated Nanometer-Sized Enzyme-Doped Silica Beads. Anal Chem 2010; 82:1527-34.
[159] Centi S, Tombelli S, Minunni M, Mascini M. Aptamer-based detection of plasma proteins by an electrochemical assay coupled to magnetic beads. Anal Chem 2007; 79:1466-73.
[160] Centi S, Messina G, Tombelli S, Palchetti I, Mascini M. Different approaches for the detection of thrombin by an electrochemical aptamer-based assay coupled to magnetic beads. Biosensors and Bioelectronics 2008; 23:1602-9.
[161] Wang Y, He X, Wang K, Ni X, Su J, Chen Z. Electrochemical detection of thrombin based on aptamer and ferrocenylhexanethiol loaded silica nanocapsules. Biosensors and Bioelectronics 2011; 26:3536-41.
[162] Skoog DA, Holler FJ, Nieman TA. Principles of instrumental analysis. 1998.
[163] Skoog DA, West DM, Holler FJ. Fundamentals of analytical chemistry. 1988.
[164] ErtuğruL HD, Uygun ZO, Impedimetric Biosensors for Label-Free and Enzymless Detection, 2013.

[165] Lisdat F, Schafer D. The use of electrochemical impedance spectroscopy for biosensing. Anal Bioanal Chem 2008; 391:1555-67.

CHAPTER 3

New label free CA125 detection based on gold nanostructured screen-printed electrodes

A. Ravalli [a], G. Pilon dos Santos [b], M. Ferroni [c], G. Faglia [d] H. Yamanaka [b], G. Marrazza [a]

[a] Department of Chemistry "Ugo Schiff", University of Florence, Via della Lastruccia 3, 50019 Sesto Fiorentino, Florence, Italy

[b] Department of Analytical Chemistry, São Paulo State University (UNESP), Rua Prof. Francisco Degni, 14800-900, Araraquara/SP, Brazil

[c] SENSOR Laboratory - Department of Physics and Chemistry, University of Brescia, and CNR-IDASC. Via Valotti 9, 25133 Brescia, Italy

Corresponding author: tel.: +39 055-4573320
E-mail address: giovanna.marrazza@unifi.it

Abstract

This paper describes the optimisation and the analytical performances of a label-free impedimetric immunosensor for the detection of tumour marker CA125 based on gold nanoparticles modified graphite screen-printed electrode. Experimental conditions of each step for the developed immunosensor were studied and optimised. The immunosensor response varied linearly (R^2 = 0.996) with antigen concentration between 0 and 100 U mL^{-1}. The estimated detection limit was 6.7 U mL^{-1}. The electrochemical immunosensor allowed unambiguous identification of CA125, while no significant non-specific signal was detected in the case of all negative controls. The analytical usefulness of the impedimetric immunosensor was finally demonstrated analysing serum samples.

Keywords: tumour marker, CA125, impedimetric immunosensor, gold nanoparticles, screen-printed electrode

1. Introduction

Biomarkers, informative signals derived from the body, are used in clinical practice to indicate the diagnosis, prognosis, or status of a specific disease or to guide therapy. More recently, some biomarkers from the field of oncology have been used as tumour marker in different pathologies [1, 2]. In tumorous process, increased levels of tumour markers in human serum are significantly associated in patients with certain tumour or carcinoma. Many markers are still going through evaluation to improve their specificity and sensitivity in the context of their clinical use [3].

Being the detection of tumour marker levels in serum important for early diagnosis of cancer, many efforts have been made to develop and improve immunoassays [4-8] for the detection of novel biomarkers with the aim of making portable and affordable devices. Immunosensors combine the high sensitivity of sensors and the high specificity of immunoreactions and can simultaneously monitor the progress of immunoreactions on sensor surfaces in real time. Despite many advances in this field, new approaches that can improve the simplicity, selectivity and sensitivity of clinical immunoassay have been reported [9].

In clinical assays, the methods of tumour markers detection in serum include radiation immunological assays (RIAs), time-resolved fluorescence, chemiluminescence, etc. These conventional techniques have some disadvantages, such as being environmentally unfriendly, time-consuming, having poor precision, and experience difficulty in realising automation. In some methods, the cost of specific instruments and reagents limit their wide application in clinical laboratories.

Therefore, there is an urgent requirement for the development of a new immunoassay method with low-cost, high speed and real-time control in large-scale disease screening [10, 11].

Compared with conventional immunoassay techniques, electrochemical immunosensors are of great interest because they are specific, simple and can have the reduction in size, cost and time of analysis. An immunological system was tested for CA125, a useful tumour marker with a threshold value of 35 U mL^{-1}, high levels of which have been found in ovarian cancer [12, 13]. CA125 is a mucin-like glycoprotein, greater than 200 kDa, which was first detected over 30 years ago using the OC125 monoclonal antibody [14],

providing the basis for assays to detect and monitor the progression of epithelial ovarian cancer.

The development of a radioimmunoassay for the antigen showed that serum CA125 levels are elevated in about 80% of patients with epithelial ovarian cancer but in less than 1% of healthy women. Numerous studies since that time have confirmed the usefulness of CA125 levels in monitoring the progress of patients with epithelial ovarian cancer [15].

This antigen is also elevated in other cancers including endometrial, lung, breast and gastrointestinal [16]. Due to the importance of an early diagnosis of cancer, various electrochemical immunosensors for the detection of CA125 tumour marker have been reported [17-20].

Different impedimetric immunosensors are reported in literature because they are a sensitive technique for label-free detection of antigen–antibody binding [21-25].

The principle is based on the change in interfacial property between the electrode surface and solution when an antibody immobilized onto electrode surface reacts with an antigen to form a complex. The formation of a layer of protein produces an increase or a decrease of the resistance charge transfer (dependent on pH and ionic strength of the mediator and on the isoelectric point of the protein) that is taken as analytical signal to determinate the concentration of the antigen.

A wide variety of nanomaterial, especially nanoparticles with different properties have found broad application in affinity biosensors [7, 26, 27]. Among the nanomaterial, gold has a special role. The increasing of the area/volume relationship and consequently the attached biocomponent on the nanostructured surface improves the sensor response. In addition, gold surface can be easily modified by thiol-ended molecules, which makes then suitable for many different biological assemblies [28].

Many synthetic procedures can be found in the literature in order to control the size, monodispersion, morphology and surface chemistry of gold nanoparticles (AuNPs). Immobilisation of biomolecules with nanoparticles can effectively increase the stability and maintain the activity of biomolecules, and it can be a good option for biomolecular immobilisation. Furthermore, gold nanoparticles (AuNPs) permit direct electron transfer between redox proteins and bulk electrode materials, thus allowing electrochemical sensing to be performed with no need for electron transfer mediators [29].

In this work, a label-free impedimetric immunosensor for the detection of tumour marker CA125 was reported. The immunoassay is based on self-assembled monolayer (SAM) of

electrodeposited gold nanostructures onto graphite screen-printed electrodes (GSPEs) with subsequent monoclonal antibody anti-CA125 (mAb-CA125) immobilisation. Each step of the developed immunosensor was successfully characterised using cyclic voltammetry (CV) and electrochemical impedance spectroscopy (EIS). The performance of the immunoassay in terms of sensitivity, reproducibility and selectivity has been also studied. Finally, the immunosensor response in serum samples was also tested.

2. Materials and Methods

2.1 Chemicals

Tetrachloroauric (III) acid ($HAuCl_4$), 6-mercapto-1-hexanol (MCH), 11-mercaptoundecanoic acid (MUDA), potassium chloride, sodium chloride, IgG from rabbit serum (rIgG) and human serum from AB plasma sample were obtained from Sigma-Aldrich (Milan, Italy).

1-Ethyl-3-(3'-dimethylaminopropyl) carbodiimide (EDAC) was purchased from Calbiochem (Milan, Italy) and N-hydroxysuccinimide (NHS) was obtained from Fluka (Milan, Italy). Di-sodium hydrogen phosphate (Na_2HPO_4), sodium dihydrogenphosphate dehydrate ($NaH_2PO_4 \cdot 2H_2O$), sulphuric acid, potassium ferrocyanide ($K_4[Fe(CN)_6]$) and potassium ferricyanide ($K_3[Fe(CN)_6]$) were purchased from Merck (Milan, Italy). Ethanol was obtained from CarloErba Reagents (Milan, Italy).

Monoclonal mouse IgG anti-CA125 antibody (Ab-CA125) and CA125 were obtained respectively from Novus Biologicals (Cambridge, UK) and Acris-Antibodies GmbH (Herford, Germany). PBS buffer: phosphate buffer solution 0.1 M pH 7.4 containing sodium chloride 0.1 M. Human prostate-specific antigen (PSA) (Acris-Antibodies GmbH, Herford, Germany) was used as aspecific control.

All chemicals were used as received without any further purification. Milli-Q water was used throughout this work.

2.2 Instrumentations

Electrochemical experiments were performed in a digital potentiostat/galvanostat AUTOLAB PGSTAT 30(2)/FRA2 controlled with the General Purpose Electrochemical System (GPES) and Frequency Response Analyzer (FRA2) 4.9 software (Eco Chemie,

Utrecht, The Netherlands). The immunosensor was assembled using screen-printed cells, comprising of a graphite working electrode (2.5 mm in diameter) and counter graphite electrode and a pseudo-silver reference [6].

The screen-printed cells were produced in house on a DEK 248 screen-printing machine (DEK, Weymouth, UK). The printing was performed on a polyester film (Autostat CT5) from Autotype (Milan, Italy) using the polymeric inks (Electrodag PF-410 (silver)) and (Electrodag 423 SS (graphite)), which were purchased from Acheson (Milan, Italy). Vinylfast 36–100 was used as the insulting ink and was obtained from Argon (Lodi, Italy).

2.3 Electrochemical measurements

2.3.1 Electrochemical impedance spectroscopy (EIS) measurements

Faradic impedance measurements were carried out in the presence of 0.01 M $[Fe(CN)_6]^{3-/4-}$ redox probe (equimolecular mixture in 0.1M KCl or in 0.1 M PBS buffer pH 7.4).

A voltage of 10 mV in amplitude (peak-to-peak), within the frequency range 100 kHz – 10 mHz, was superimposed to the applied bias potential.

The DC potential was set up to +0.13V, the formal potential of $[Fe(CN)_6]^{3-/4-}$ redox probe.

Experimental spectra, presented in the form complex plane diagrams (i.e. Nyquist plot), were fitted with proper equivalent circuits (Figure 3.1) using the facilities of the FRA2 4.9.004 (EcoChemie) software.

Both charge transfer resistance (Rct) and Δ charge transfer resistance (ΔRct) values were taken as analytical signals.

All potentials were referred to the silver screen-printed pseudo-reference electrode; the experiments were carried out at room temperature (25°C).

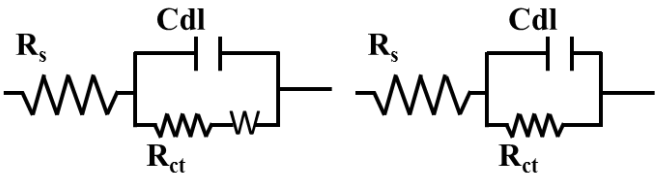

Figure 3.1. Randles equivalent circuit used to fit EIS spectra (R_s: electrolyte resistance, C_{dl}: double layer capacitance, R_{ct}: charge transfer resistance, W: Warburg impedance).

2.3.2 Cyclic Voltammetry measurements

Electrodeposition of gold nanoparticles (AuNPs) onto graphite screen-printed electrodes (GSPEs) was obtained by cyclic voltammetry in the range 0 and +1.3 V *vs.* screen-printed silver pseudo-reference using $HAuCl_4$ solution in 0.5 M H_2SO_4 solution.

Cyclic voltammetry measurements for surface characterization in a range of potential between -0.6 and +0.8 V *vs.* screen-printed silver pseudo-reference in the presence of 0.01 M $[Fe(CN)_6]^{3-/4-}$ (equimolecular mixture in KCl 0.1 M) were carried out.

Cyclic voltammetry measurements for surface characterization in a range of potential between 0 and +1.3 V *vs*. screen-printed silver pseudo-reference in the presence of 0.5 M H_2SO_4 solution were carried out.

2.4 Scanning Electron Microscopy (SEM) characterization

SEM analysis was carried out by field-emission LEO 1525 microscope (Zeiss, Germany) equipped with In-Lens detector and with an Ultra FEG-SEM (Zeiss, Germany) mounted with an EsB detector for secondary-electrons imaging.

The samples were fixed onto conventional stub, without any preliminary pre-treatments.

2.5 Scheme of the immunoassay

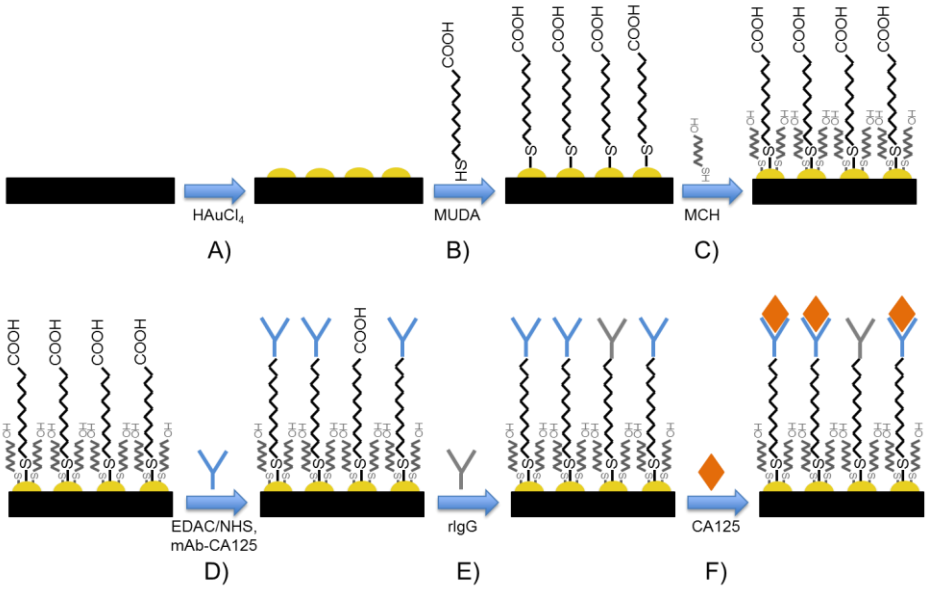

Figure 3.2. Scheme of AuNPs-based label-free immunosensor for CA125 detection: A) electrodeposition of AuNPs on GSPEs, B) Functionalization of gold nanoparticles with MUDA, C) Mixed SAM formation with MCH, D) activation of –COOH groups with EDAC/NHS and mAb-CA125 immobilisation, E) blocking step with rIgG, F) Ab-Ag affinity reaction.

In this work, a label-free impedimetric immunosensor for CA125 was developed and the steps are illustrated in Figure 3.2.

2.5.1 Electrodepositing of gold nanoparticles (AuNPs) on graphite screen-printed electrodes (GSPEs)

Electrodepositing of AuNPs on graphite screen-printed electrodes (GSPEs) was carried out by cyclic voltammetry (CV) between the range potential of -0.2 and +1.6 V *vs.* screen-printed silver pseudo-reference, 25 cycles, at scan rate 0.1 V s^{-1}, in a 0.0006 M $HAuCl_4$ solution containing sulphuric acid 0.5 M [30]. After, the modified electrodes were rinsed with Milli-Q water in order to remove the free ions from the GSPEs surface.

2.5.2 Mixed self-assembly monolayer (SAM) formation

The nanostructured AuNPs/GSPEs was modified with 0.001 M MUDA, prepared in a mixture of 1:3 (v/v) of ethanol and water for 3 hours at 25 °C in a wet chamber. Mixed SAM formation was then carried out incubating the electrode surface with 10 μL of 0.001 M MCH solution (prepared in a mixture of 4:1 in volume of ethanol and water), for 30 minutes at 25 ºC. After each modification steps, the electrodes were rinsed with Milli-Q water.

2.5.3 Antibody immobilization

The antibody immobilisation was based on preliminary formation of a SAM of a reactive thiol followed by carbodiimide coupling with amino groups of mAb-CA125 antibody.
In order to react with the amino groups of antibody, the carboxyl groups of MUDA need to be activated.
With the addition of EDAC and NHS, carboxyl groups were converted into active esters, which lead a formation of an amide bond between the amino groups of antibody and the activated carboxyl group of MUDA. Thus, 5 μL of a solution containing 0.2 M EDAC and 0.05 M NHS, prepared in 0.1 M PBS buffer solution pH 7.4, together with 24 mg L^{-1} of mAb-CA125 antibody was placed on the nanostructured working electrode and incubated for 30 minutes at 25 ºC. In order to limit the nonspecific interaction between the assay reagents and the unreacted carboxyl groups eventually present, after the mAb-CA125 antibody immobilisation, a blocking step was introduced. A 10 mg L^{-1} rIgG

solution, prepared in 0.1 M PBS buffer solution pH 7.4, was placed onto the sensor surface and incubated for 30 minutes at 25 ºC.
After each step, the sensors were rinsed with 0.1 M PBS buffer solution pH 7.4.

2.5.4 Affinity reaction

To perform the calibration curve, the immunosensor with different concentrations of CA125 protein for 30 minutes at 25 °C was incubated. The sensors were then rinsed with 0.1 M PBS buffer solution pH 7.4. Finally EIS spectra were recorded in the conditions described above.
The control experiments were performed using prostate specific antigen (PSA). PSA is a glycoprotein (such as CA125) mainly related to prostate cancer, with a clinical cut-off of 4 μg L^{-1}. Its level increases in presence of ovarian cancer and in patients with lymphoma in the serum, such as CA125 level, as reported in literature [31] and [32].
In our work we used a concentration of aspecific protein of 50 and 100 mg L^{-1} to test the selectivity of the receptor and to calculate the amount of background signal not caused by the immunocomplex at 0 concentration of CA125 protein.

2.5.5 Serum samples analysis

Preliminary experiments for the determination of CA125 protein in serum samples were also performed.
The immunosensor response was tested in 1/10 diluted (in PBS 0.1 M, pH 7.4) filtered (0.45 μm) serum sample with standard addition of CA125 protein, in the same condition used for the determination of CA125 calibration curve described above.
Control experiments were performed with diluted serum sample spiked with 100 mg L^{-1} of PSA.

3. Results and Discussion

The immunosensor was optimised with respect to several parameters such as gold electrodepositing, antibody immobilisation and blocking agent. In this work, cyclic voltammetry and EIS spectra were employed to characterise for studying the interface properties of surface-modified electrodes.

3.1 Optimization of experimental conditions

Graphite screen-printed electrodes (GSPEs) were modified by electrodeposition of gold nanoparticles using cyclic voltammetry.

First, in order to optimise the electrodeposition process different experimental parameters were considered. These included the effect of concentration of $HAuCl_4$, the number of cycles and scan rate of cyclic voltammetry

The concentration of $HAuCl_4$ and the number of cycles for the nucleation of gold nanoparticles on the electrode surface play an important role for the morphology, size and uniformity of electrodeposed particles [33, 34]. Figure 3.3 shows the influence of these variables by analysing the electron transfer resistance values R_{ct} obtained by EIS experiments.

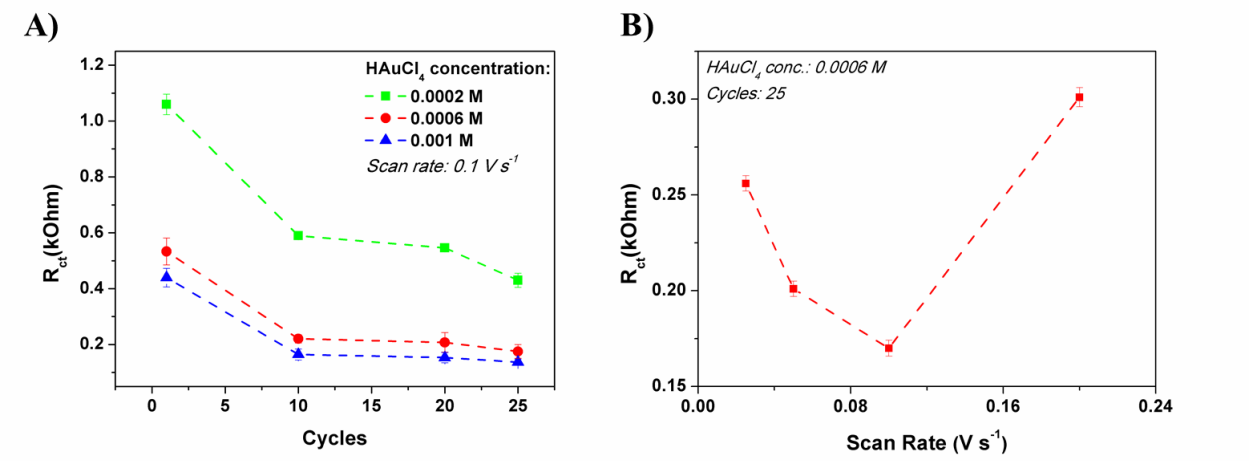

Figure 3.3. A) R_{ct} as function of number of cycles (1, 10, 20, 50) using different concentrations of $HAuCl_4$: (■) 0.0002, (●) 0.0006 and (▲) 0.001 M; scan Rate: 0.1 V s^{-1}. B) R_{ct} as function of scan rate (0.025, 0.05, 0.1, 0.2 V s^{-1}) using 0.0006 M and 25 cycles. EIS measurements were performed in 0.01 M $[Fe(CN)_6]^{3-/4-}$ equimolecular mixture in 0.1 M KCl; each point was repeated at least 3 times using different gold nanostructured screen-printed graphite electrodes (AuNPs/GSPEs).

The effect of number of cycles was tested at 1, 10, 20 and 25, and the concentration of $HAuCl_4$ at 0.0002, 0.0006 and 0.001 M. It can be seen that an increase in both variables lead lower R_{ct}, implying that a high surface area of GSPEs is coated with gold nanoparticles (Figure 3.3 A). No significant differences in R_{ct} values starting from a concentration 0.001 M or 0.0006 M of $HAuCl_4$ and using 25 cycles for the electrodeposited process were obtained. Thus, 0.0006 M of $HAuCl_4$ and 25 cycles were used in the following experiments.

The effect of scan rate on the nucleation of gold nanoparticles was evaluated at 0.025, 0.05, 0.1 and 0.2 V s^{-1} using a 0.0006 M $HAuCl_4$ solution and 25 cycles. These variables can influence mainly in the size and shape of AuNPs [35]. The lowest R_{ct} value was achieved when a scan rate of 0.1 V s^{-1} was applied, being this rate selected for optimal electrodeposition parameter. The R_{ct} obtained for each scan rate is presented in Figure 3.3 B.

The electrochemical impedance (EIS) spectra of AuNPs-modified GSPEs by using optimised conditions for the nucleation of particles in a 0.01 M $[Fe(CN)_6]^{3-/4-}$ equimolecular mixture in 0.1 M KCl were obtained (Figure 3.4).

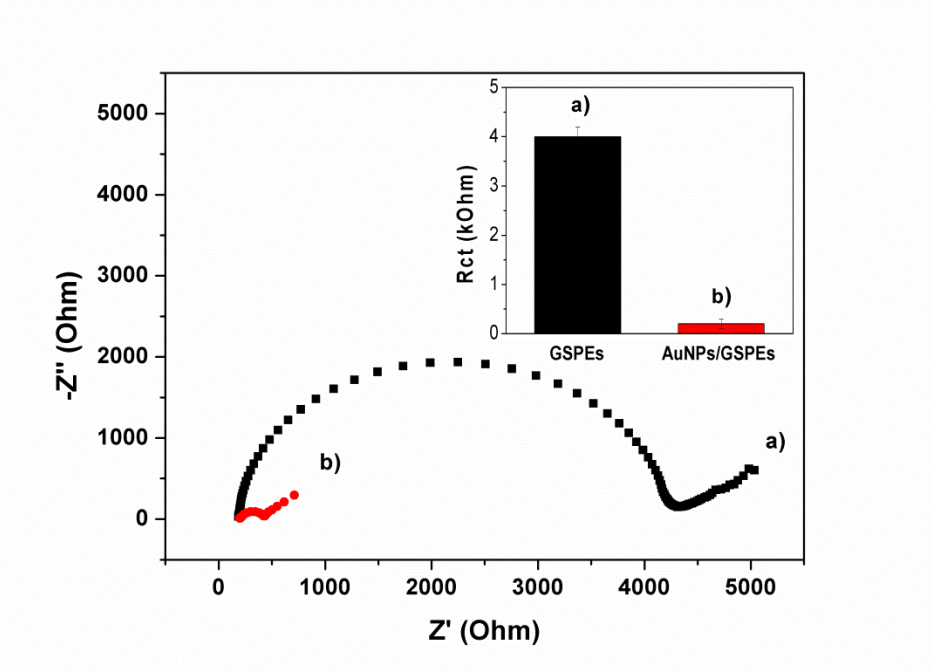

Figure 3.4. Nyquist plot of 0.01 M $[Fe(CN)_6]^{3-/4-}$ equimolecular mixture in 0.1 M KCl solution for the bare (■, curve a) and AuNPs modified GSPEs (•, curve b) obtained using 0.0006 M $HAuCl_4$, 25 cycles and scan rate 0.1 V s^{-1}. Inset: average and standard deviation respect to the R_{ct} for bare graphite screen-printed electrodes (Bare GSPEs) and for gold nanostructured graphite screen-printed electrodes (AuNPs/GSPEs). The measurements were repeated at least 3 times using different GSPEs.

Gold nanostructured GSPEs presented a significant difference of the electron transfer resistance (R_{ct}) in comparison with bare GSPEs. When the GSPEs were modified with AuNPs, the R_{ct} has decreased significantly from 4.0 ± 0.2 to 0.2 ± 0.1 kOhm.

This demonstrated that the gold nanoparticles make the electron transfer easier. Cyclic voltammetry measurements in acid solutions have been used for the identification of some features related to the process of formation and reduction of oxide films on noble

metals [36]. Therefore, the obtained gold nanostructured-GSPEs were then studied by cyclic voltammetry experiments. Voltammograms were obtained for the bare and gold nanostructured GSPEs in 0.5 M H_2SO_4 solution, between the range potential of 0 and +1.3 V *vs.* screen-printed silver pseudo-reference at a scan rate of 0.1 V s^{-1} (Figure 3.5 A). It can be seen that the bare electrode shows only a background charging current of graphite, contributed by the double layer charging and surface faradic reactions involving surface oxide groups [37], while AuNPs modified GSPEs present peaks around +1.1 V due to the formation of gold oxide and its correspondent reduction around +0.7 V, which is in accordance to the inherent feature of a gold electrode surface.

Moreover, in order to characterise the electrochemical performance of the electrode, the CV measurements of bare and gold nanostructured GSPEs in 0.01 M $[Fe(CN)_6]^{3-/4-}$ 0.1 M KCl solution were carried out. The voltammogram of gold nanoparticles-modified GSPEs displays higher and narrow peaks of redox couple in comparison with unmodified GSPE; this effect is due to the large resistance of the graphite surface (Figure 3.5 B).

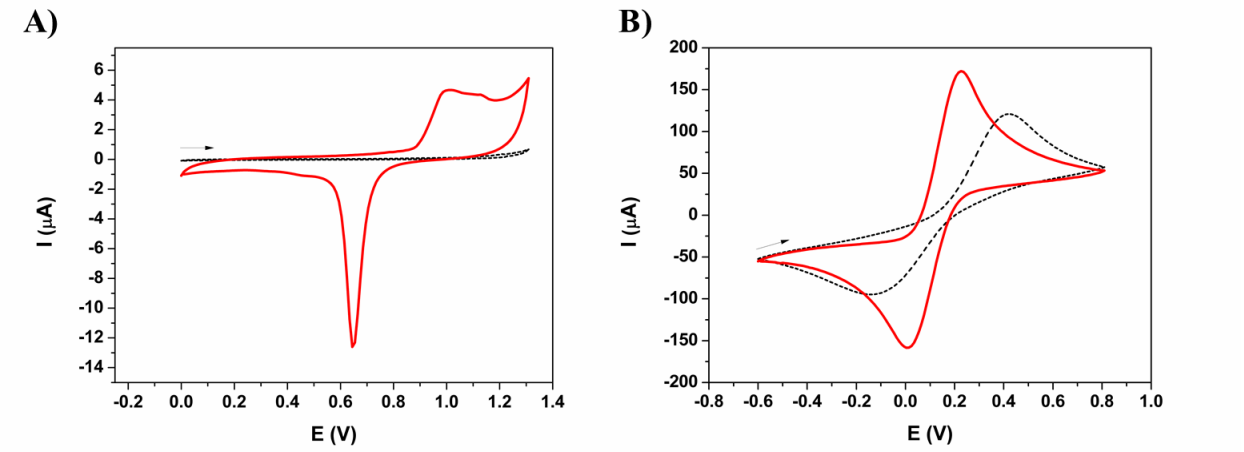

Figure 3.5. A) Cyclic voltammograms obtained in 0.5 M H_2SO_4 solution for the bare GSPEs (- -) and AuNPs/GSPEs (—). B) Cyclic voltammograms obtained in 0.01 M $[Fe(CN)_6]^{3-/4-}$ 0.1 M KCl solution for the bare GSPEs (- -) and GSPEs modified with AuNPs (—).

3.2 SEM analysis

SEM technique was used in first to verify the presence of AuNPs on the surface of GSPEs and then to find the optimal electrodepositing parameters.

SEM images of graphite electrodes show the presence of amorphous micro and macrostructures randomly distributes over the entire electrode surface. It is also possible notice the presence of pores and holes of various shapes and dimensions.

Electrodeposition performed in optimised condition, provides the formation of evenly distributed gold nanostructures (Figure 3.6 A) with dimensions between 40 – 100 nm. To confirm the presence of AuNPs on the electrode surface (in order to highlight the difference in composition) an analysis with SEM-EsB detector was also performed (Figure 3.6 B). The image clearly shows the presence of AuNPs well distributed over the entire electrode surface.

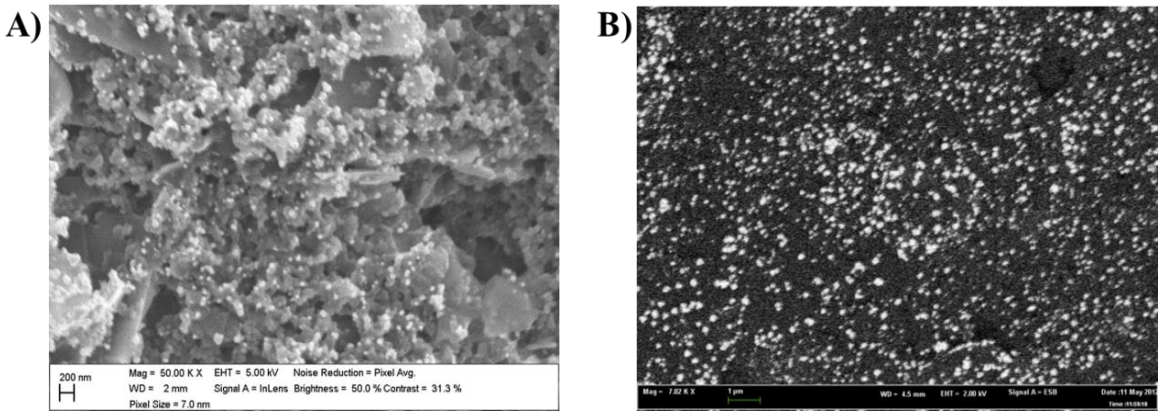

Figure 3.6. SEM image of AuNPs electrodeposed onto graphite screen-printed electrodes prepared in optimised experimental conditions (0.0006 M $HAuCl_4$, 25 cycles 0.1 V s^{-1}), using different detectors: A) In-Lens and B) EsB detector.

3.3 Immunosensor development

Due to the importance of MUDA (as a precursor for further modifications on Au surface and for the opportunity to replace the acid end group by other functionalized groups quite easy), this system have been studied by EIS measurements for the formation of a well-ordered monolayer.

The optimisation of the conditions for the modification of gold nanostructured GSPEs with 0.001 M MUDA was done in different incubation times: 3, 6, 9 and 12 hours. EIS results are: R_{ct} (3 hours) = 2.9 ± 0.2 kOhm, R_{ct} (6 hours) = 2.9 ± 0.2 kOhm, R_{ct} (9 hours) = 2.9 ± 0.2 kOhm, R_{ct} (12 hours) = 2.7 ± 0.1 kOhm. There are no significant differences between R_{ct} at all the times studied in these conditions. Thus, for the next experiments an incubation time of 3 hours was used.

The change of electrode behaviour after each assembly steps can be characterised by impedance measurements in the presence of $[Fe(CN)_6]^{3-/4-}$ redox probe. Figure 3.7 shows the comparison of R_{ct} for gold nanostructured GSPEs and after MUDA chemisorption.

It can be seen a significant enhancement in R_{ct} (from 0.2 to 2.9 kOhm) after MUDA attachment.

This may be due to the insulating MUDA layer that perhaps hinders diffusion of ions toward the electrode surface resulting in increased value of R_{ct}.

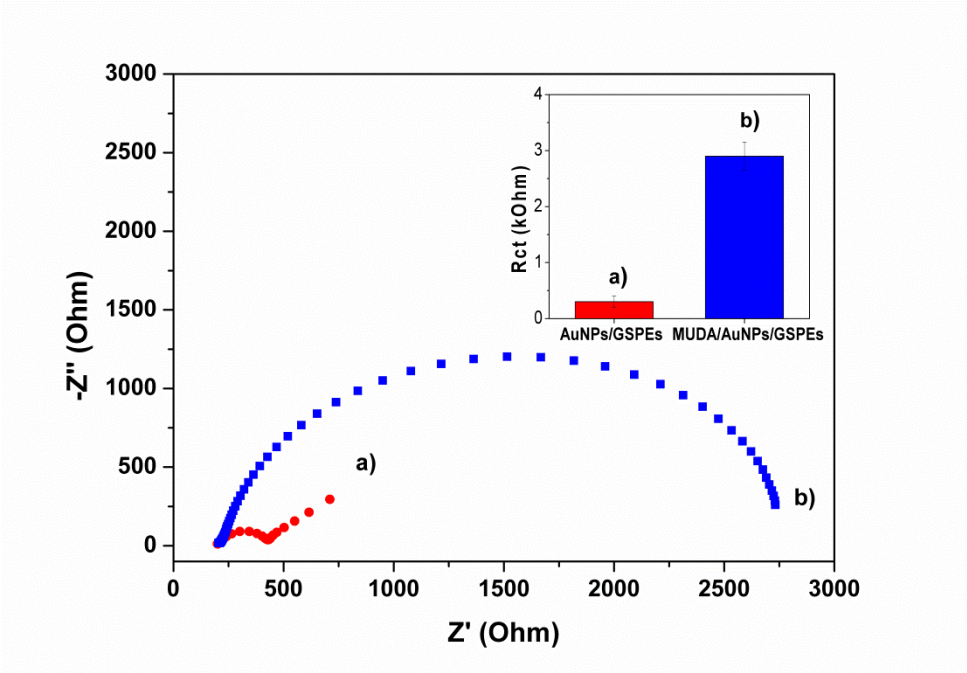

Figure 3.7. Nyquist plot of AuNPs-modified GSPEs (•, curve a) and after the MUDA chemisorption (■, curve b) obtained in 0.01 M $[Fe(CN)_6]^{3-/4-}$ equimolecular mixture in 0.1 M KCl. Inset: average and standard deviation respect to the R_{ct} for gold nanostructured graphite screen-printed electrodes (AuNPs/GSPEs) and after the MUDA chemisorption (MUDA/AuNPs/GSPEs). The measurements were repeated at least 3 times using different GSPEs.

EIS measurements were also used to characterize the other steps (mixed SAM formation with MCH, mAb-CA125 immobilization, rIgG blocking step) involved in the assembly of the immunosensor. It can be seen that in each assembly the R_{ct} increases over the previous step, except in the case of blocking the sites not attached with the mAb-CA125 with rIgG. It implies that a conductive layer (rIgG) is assembled on the electrode surface resulting in accelerate electron transfer between rIgG and the mAb-CA125 modified electrode [38]. The R_{ct} values for each assembly steps are presented in Table 3.1.

The immunosensor performance on the detection of CA125 at different concentration useful for clinical applications, was evaluated analysing the change in R_{ct} values obtained by electrochemical impedance spectroscopy after the affinity reaction using 0.01 M $[Fe(CN)_6]^{3-/4-}$ 0.1 M PBS pH 7.4 buffer solution.

The calibration curve (Figure 3.8 A) for the detection of CA125 was conducted under optimised conditions. It can be seen a proportional increase of R_{ct} with antigen concentration, which may be attributed to more CA125 molecules binding to the immobilized antibodies, providing a kinetic barrier for the electron transfer.

Table 3.1. Sensor surface characterisation of the single steps of the immunoassay performed in 0.01 M $[Fe(CN)_6]^{3-/4-}$ equimolecular mixture solution in KCl 0.1 M, PBS 0.1 M, pH 7.4. Each measurement was repeated at least 3 times using different screen-printed electrodes. Legend: A) AuNPs electrodeposed on GSPEs, B) Functionalization of gold nanostructured graphite screen-printed electrodes with MUDA, C) mixed SAM formation with MCH; D) immobilisation of mAb-CA125, E) blocking step with rIgG, F) affinity reaction with 30 U mL^{-1} CA125 solution.

EIS electrode surface characterisation	**R_{ct} (kΩ)**
A) AuNPs/GSPEs	0.2 ± 0.1
B) MUDA/AuNPs/GSPEs	3.5 ± 0.2
C) MCH/MUDA/AuNPs/GSPEs	4.0 ± 0.3
EIS immunosensor characterisation	**R_{ct} (kΩ)**
D) mAb-CA125-MCH/MUDA/AuNPs/GSPEs	4.9 ± 0.2
E) rIgG/mAb-CA125/MCH/MUDA/AuNPs/GSPEs	3.32 ± 0.02
F) CA125/rIgG/mAb-CA125/MCH/MUDA/AuNPs/GSPEs	3.58 ± 0.07

A linear relationship between the change in R_{ct} and concentration of antigen was obtained in the range of 0 and 100 U mL^{-1}. The linear regression from the calibration curve, ΔRct = 4.51E-4 + 0.009 x [CA125], has a correlation coefficient of 0.996 with limit of detection (LOD) of 6.7 U mL^{-1} (calculated as: LOD = $3S_{blank}$/Slope).

In order to evaluate the selectivity of the immunoassay, the effect of prostate-specific antigen (PSA), as non-specific antigen, was studied. As can be observed in Figure 3.8 A inset, a very similar R_ct value compared to the blank was achieved. This result confirms that the observed relative change in impedance is originated from the specific monoclonal Ab-CA125/CA125 interactions, showing that this good selectivity is appropriate to apply the immunosensor for the detection of CA125.

The reproducibility of the immunosensor was analysed by the relative standard deviation (RSD) in three different electrodes for each concentration of antigen. The RSD for 30 U mL^{-1} was 2%. Thus, the proposed assay presents a good reproducibility, providing a convenient platform for CA125 detection.

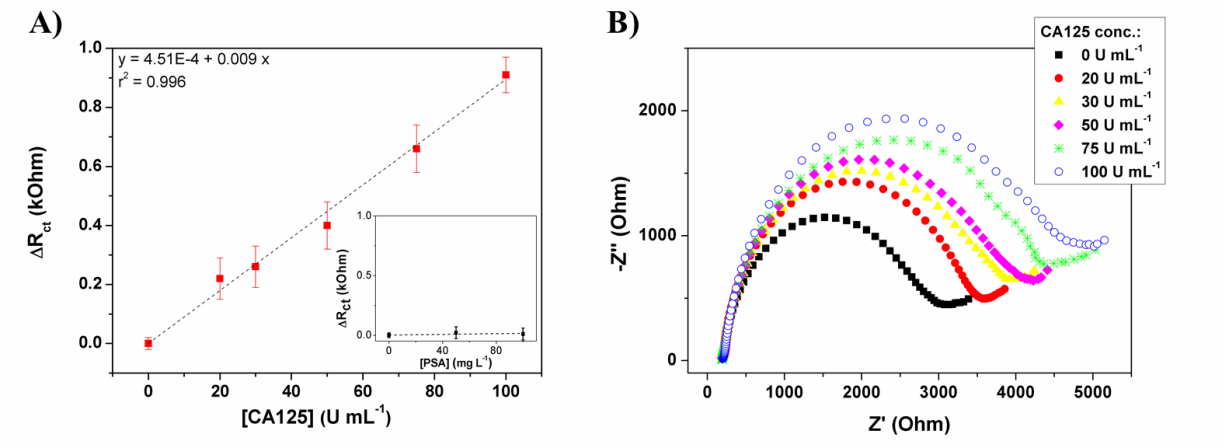

Figure 3.8. A) Calibration curve for CA125 antigen. Inset: aspecific calibration curve with PSA (0, 50, 100 mg L^{-1}). B) Nyquist plot of mAb-CA125-CA125 interaction. EIS measurements were obtained using 0.01 M $[Fe(CN)_6]^{3-/4-}$ equimolecular mixture prepared in 0.1 M PBS pH 7.4. Each concentration was repeated at least 3 times using different gold nanostructured graphite screen-printed electrodes.

Once verified the suitability of the immunosensor to detect CA125 in standard solutions, experiments on serum samples were carried out.

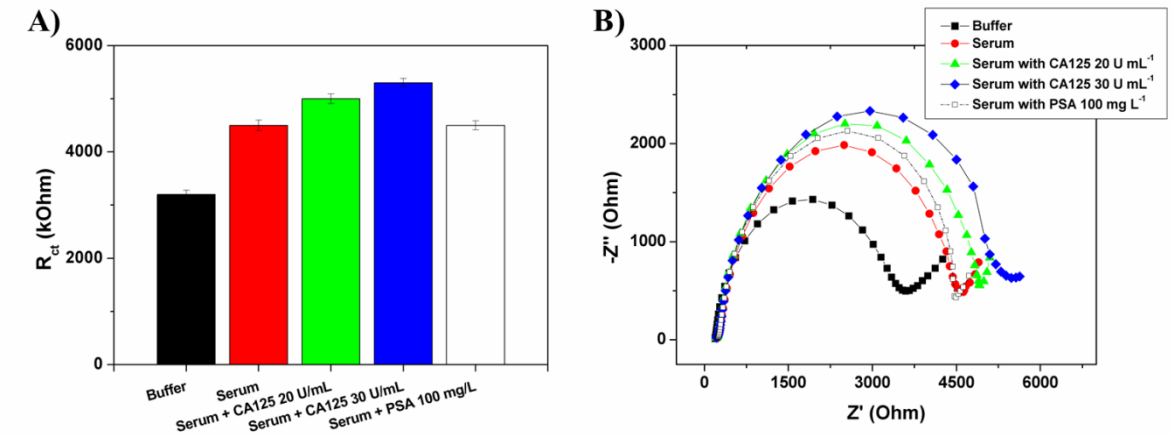

Figure 3.9. A) Average and standard deviation respect to the R_{ct} for the immunosensor response in buffer, serum and serum samples spiked with CA125 (20 and 30 U mL^{-1}) and PSA (aspecific control, 100 mg L^{-1}) obtained in 0.01 M $[Fe(CN)_6]^{3-/4-}$. B) Nyquist plot of the immunosensor response in buffer, serum and serum samples spiked with CA125 (20 and 30 U mL^{-1}) and PSA (aspecific control, 100 mg L^{-1}) obtained in 0.01 M $[Fe(CN)_6]^{3-/4-}$ equimolecular mixture in PBS 0.1 M pH 7.4. The measurements were repeated at least 3 times using different GSPEs.

Experiments concerned commercial serum spiked with CA125 at a known concentration. CA125 was added to commercially available serum after filtration and dilution 1/10 in 0.1 M PBS buffer solution pH 7.4. Results are reported in Figure 3.9. Increase of R_{ct} was obtained with spiked serum samples.

Although the concentration of PSA (100 mg L^{-1}) is 20 time higher respect the clinical cut-off value used to determinate the presence of cancer, the R_{ct} signal of serum sample spiked with PSA is comparable with the signal of serum sample.

Thus, the increase of signal of serum sample respect to the signal detected in buffer is related to the aspecific adsorption of the matrix protein on the electrode surface and can be considered as background noise.

4. Conclusions

A label-free electrochemical immunosensor based on gold nanostructured screen-printed graphite electrode for the detection of the tumour marker CA125 was developed. A good linear relationship between the electron transfer resistance and CA125 concentration in the range of 0-100 U mL^{-1} with a LOD of 6.7 was obtained.

The sensitivity achieved was adequate for the analysis of serum samples, since 35 U mL^{-1} was defined as the appropriate cut-off between normal and elevated serum CA125 protein levels. The immunoassay was also tested on serum samples, yielding promising results for use with real samples. The method can be expanded for detecting other tumour markers and has the potential for reliable diagnosis of cancer and other diseases.

Acknowledgments

This work was supported by project BIOMIMIC, no. FP7-PEOPLE-IRSES-2008-230849, by the Ministero dell'Istruzione, dell'Università e della Ricerca PRIN 2009, "Nanomaterial-based biosensors for rapid cancer biomarker detection" and Regione Toscana (NANO-TREAT project) Pasqualantonio Pingue (SCUOLA NORMALE SUPERIORE).

Giampiero Pallocca and Alessio Lombardo (ASSING SpA) are gratefully acknowledged for providing the ZEISS UltraPlus microscope at Laboratorio NEST for EsB imaging.

References:

[1] Ullah MF, Aatif M. The footprints of cancer development: Cancer biomarkers. Cancer treatment reviews 2009; 35:193-200.
[2] Yilmaz MB, Nikolaou M, Solal AC. Tumour biomarkers in heart failure: is there a role for CA-125? Eur J Heart Fail 2011; 13:579-83.
[3] Tothill IE. Biosensors for cancer markers diagnosis. Seminars in Cell & Developmental Biology 2009; 20:55-62.
[4] Al-Khafaji QAM, Harris M, Tombelli S, et al. An Electrochemical Immunoassay for HER2 Detection. Electroanal 2012; 24:735-42.
[5] Fu X-H. Electrochemical Immunoassay for Carbohydrate Antigen-125 Based on Polythionine and Gold Hollow Microspheres Modified Glassy Carbon Electrodes. Electroanal 2007; 19:1831-9.
[6] Rasooly A, Jacobson J. Development of biosensors for cancer clinical testing. Biosensors and Bioelectronics 2006; 21:1851-8.
[7] Vinicius Foguel M, Pilon dos Santos G, Aparecido Pupim Ferreira A, Yamanaka H, Vicente Benedetti A. Amperometric Immunosensor for Chagas' Disease Using Gold CD-R Transducer. Electroanal 2011; 23:2555-61.
[8] Zani A, Laschi S, Mascini M, Marrazza G. A New Electrochemical Multiplexed Assay for PSA Cancer Marker Detection. Electroanal 2011; 23:91-9.
[9] Ray S, Chandra H, Srivastava S. Nanotechniques in proteomics: Current status, promises and challenges. Biosensors and Bioelectronics 2010; 25:2389-401.
[10] Chen H, Jiang C, Yu C, Zhang S, Liu B, Kong J. Protein chips and nanomaterials for application in tumor marker immunoassays. Biosensors and Bioelectronics 2009; 24:3399-411.
[11] D'Orazio P. Biosensors in clinical chemistry — 2011 update. Clin Chim Acta 2011; 412:1749-61.
[12] Fu X-H. Poly(amidoamine) Dendrimer-Functionalized Magnetic Beads as an Immunosensing Probe for Electrochemical Immunoassay for Carbohydrate Antigen-125 in Human Serum. Anal Lett 2010; 43:455-65.
[13] Wu L, Yan F, Ju H. An amperometric immunosensor for separation-free immunoassay of CA125 based on its covalent immobilization coupled with thionine on carbon nanofiber. Journal of immunological methods 2007; 322:12-9.
[14] Bast RC, Jr., Feeney M, Lazarus H, Nadler LM, Colvin RB, Knapp RC. Reactivity of a monoclonal antibody with human ovarian carcinoma. The Journal of Clinical Investigation 1981; 68:1331-7.
[15] Yin BWT, Lloyd KO. Molecular Cloning of the CA125 Ovarian Cancer Antigen: IDENTIFICATION AS A NEW MUCIN, MUC16. Journal of Biological Chemistry 2001; 276:27371-5.
[16] Sjövall K, Nilsson B, Einhorn N. The Significance of Serum CA 125 Elevation in Malignant and Nonmalignant Diseases. Gynecologic oncology 2002; 85:175-8.
[17] Chen S, Yuan R, Chai Y, Min L, Li W, Xu Y. Electrochemical sensing platform based on tris(2,2′-bipyridyl)cobalt(III) and multiwall carbon nanotubes–Nafion composite for immunoassay of carcinoma antigen-125. Electrochim Acta 2009; 54:7242-7.
[18] Das J, Kelley SO. Protein Detection Using Arrayed Microsensor Chips: Tuning Sensor Footprint to Achieve Ultrasensitive Readout of CA-125 in Serum and Whole Blood. Anal Chem 2011; 83:1167-72.

[19] Tang D, Yuan R, Chai Y. Electrochemical immuno-bioanalysis for carcinoma antigen 125 based on thionine and gold nanoparticles-modified carbon paste interface. Anal Chim Acta 2006; 564:158-65.
[20] Wu J, Zhang Z, Fu Z, Ju H. A disposable two-throughput electrochemical immunosensor chip for simultaneous multianalyte determination of tumor markers. Biosensors and Bioelectronics 2007; 23:114-20.
[21] Chullasat K, Kanatharana P, Limbut W, Numnuam A, Thavarungkul P. Ultra trace analysis of small molecule by label-free impedimetric immunosensor using multilayer modified electrode. Biosensors and Bioelectronics 2011; 26:4571-8.
[22] Ciani I, Schulze H, Corrigan DK, et al. Development of immunosensors for direct detection of three wound infection biomarkers at point of care using electrochemical impedance spectroscopy. Biosensors and Bioelectronics 2012; 31:413-8.
[23] Fang X, Han M, Lu G, Tu W, Dai Z. Electrochemiluminescence of CdSe quantum dots for highly sensitive competitive immunosensing. Sensors and Actuators B: Chemical 2012; 168:271-6.
[24] Ferreira AAP, Fugivara CS, Barrozo S, Suegama PH, Yamanaka H, Benedetti AV. Electrochemical and spectroscopic characterization of screen-printed gold-based electrodes modified with self-assembled monolayers and Tc85 protein. J Electroanal Chem 2009; 634:111-22.
[25] Lucarelli F, Marrazza G, Mascini M. Enzyme-based impedimetric detection of PCR products using oligonucleotide-modified screen-printed gold electrodes. Biosensors and Bioelectronics 2005; 20:2001-9.
[26] Berti F, Eisenkolbl C, Minocci D, et al. Cannabinoid receptor gene detection by electrochemical genosensor. J Electroanal Chem 2011; 656:55-60.
[27] Berti F, Lozzi L, Palchetti I, Santucci S, Marrazza G. Aligned carbon nanotube thin films for DNA electrochemical sensing. Electrochim Acta 2009; 54:5035-41.
[28] Pingarrón JM, Yáñez-Sedeño P, González-Cortés A. Gold nanoparticle-based electrochemical biosensors. Electrochim Acta 2008; 53:5848-66.
[29] Vidotti M, Carvalhal RF, Mendes RK, Ferreira DCM, Kubota LT. Biosensors based on gold nanostructures. Journal of the Brazilian Chemical Society 2011; 22:3-20.
[30] Rathod D, Warren S, Keane K, Egan DA, Dempsey E. Evaluation of a modified carbon micromesh electrode as a new substrate for electrochemical immunosensing. Anal Methods-Uk 2011; 3:799-805.
[31] Yu H, Diamandis EP, Levesque M, Asa SL, Monne M, Croce CM. Expression of the prostate-specific antigen gene by a primary ovarian carcinoma. Cancer Res 1995; 55:1603-6.
[32] Wiernik P. Serum CA125 and PSA concentrations in patients with lymphoma. Clinical advances in hematology & oncology: H&O 2008; 6:527.
[33] Huang L, Wang M, Zhang Y, Guo Z, Sun J, Gu N. Synthesis of Gold Nanotadpoles by a Temperature-Reducing Seed Approach and the Dielectrophoretic Manipulation. The Journal of Physical Chemistry C 2007; 111:16154-60.
[34] Zhao Y, Wu Y, Zhang Y, et al. Electrocatalytic Behavior and Amperometric Detection of Morphine on ITO Electrode Modified with Directly Electrodeposited Gold Nanoparticles. Electroanal 2009; 21:939-43.
[35] Shulga O, Kirchhoff JR. An acetylcholinesterase enzyme electrode stabilized by an electrodeposited gold nanoparticle layer. Electrochem Commun 2007; 9:935-40.
[36] Angerstein-Kozlowska H, Conway BE, Barnett B, Mozota J. The role of ion adsorption in surface oxide formation and reduction at noble metals: General features of

the surface process. Journal of Electroanalytical Chemistry and Interfacial Electrochemistry 1979; 100:417-46.
[37] Gun G, Tsionsky M, Lev O. Voltammetric studies of composite ceramic carbon working electrodes. Anal Chim Acta 1994; 294:261-70.
[38] Ansari AA, Kaushik A, Solanki PR, Malhotra BD. Nanostructured zinc oxide platform for mycotoxin detection. Bioelectrochemistry 2010; 77:75-81.

CHAPTER 4

CA125 Immunosensor based on poly-anthranilic acid modified screen-printed electrodes

Zahra Taleat [a], Andrea Ravalli [b], Mohammad Mazloum-Ardakani [a], Giovanna Marrazza [*,b]

[a] Department of Chemistry, Faculty of Science, Yazd University, Yazd, 89195-741, Iran

[b] Department of Chemistry ''Ugo Schiff'', University of Florence, Via della Lastruccia 3, 50019 Sesto Fiorentino (Fi), Italy

tel.: +39 0554573320; fax: +39 0554573396
*e-mail: giovanna.marrazza@unifi.it

Received: August 3, 2012
Accepted: September 26, 2012
Published online: November 13, 2012

Abstract

In this paper, two simple and sensitive approaches for CA125 detection are presented by using antibody immobilized on poly-anthranilic acid modified graphite screen printed electrodes. The first proposed approach is a label free impedimetric immunosensor.

The immunoassay is based on poly-anthranilic acid (PAA) modified graphite screen-printed electrodes with subsequent covalently monoclonal antibody anti-CA125 immobilization. The modified screen-printed electrodes are used to capture the protein from the sample solutions. A curve calibration by electrochemical impedance spectroscopy (EIS) was obtained.

The second approach is based on a sandwich format. The monoclonal anti-CA125 antibody (mAb-CA125) immobilized on poly anthranilic acid modified graphite screen-printed electrodes is used to capture the protein from the sample solution. The sandwich assay is then performed by adding secondary anti-CA125 antibody (pAb-CA125) labelled with gold nanoparticles (AuNPs).

The antibody-AuNPs captured onto immunosensor surface induced the silver deposition from a silver enhancer solution. The deposited AgNPs could be measured by anodic stripping analysis (ASV) in acid solution. A curve calibration by ASV was obtained.

The experimental conditions were examined and were optimized using electrochemical impedance spectroscopy. The performance of both immunosensors in terms of sensitivity, reproducibility and selectivity were studied.

Keywords: Poly-anthranilic acid, CA125 biomarker, Gold nanoparticles, Silver enhancement, Screen-printed electrode

DOI: 10.1002/elan.201200425

1. Introduction

Recently, electrochemical immunoassays have shown their considerable importance in the field of clinical analysis for early cancer screening and diagnosis. This is due to their higher analytical efficiency as well as the unique advantages of electrochemical biosensors including low cost, high sensitivity and good portability [1, 2]. The aim of the present work is the investigation of screening devices for the detection of the cancer antigen 125 (CA125) based on poly-anthranilic acid (PAA) modified graphite screen-printed electrodes (GSPEs).

In clinical analysis, the cancer antigen 125 (CA125) is one of the most important cancer biomarkers, which found on the surface of many ovarian cancer cells. Normal blood levels are usually less than 35 U mL^{-1} (units per milliliter). More than 90% of women have high levels of CA125 when the cancer is advanced. CA125 levels are also elevated in about half of women whose cancer has not spread outside of the ovary. If the CA125 level is increased at the time of diagnosis, changes in the CA125 level can be used to lead cancer patients to the most appropriate therapeutic approach [3]. Various immunoassays have been proposed in the literature for the determination of CA125 using different detection techniques such as nanowire transistors [4, 5], enzyme-labelled beads [6], micro-nanoarrays [7] and microfluidic immunoarrays [8] and recently, an imprinted polymer on three-dimensional gold nanoelectrode ensembles [9].

In this study, we aimed to develop a low cost, sensitive and easy to use immunosensor for CA125 biomarker by poly anthranilic acid (PAA) modified graphite screen-printed electrodes. The conductive polymers are the most suitable materials to immobilize the bioreceptors for efficient biosensor developing. Among them, poly-aniline and its derivatives have been the focus of much interest for the immobilization of proteins [10-12], because of their unique reversible proton dopability, excellent redox behaviour, environmental stability, and variable electrical conductivity, low cost and easy synthesis. Poly-anthranilic acid (PAA), a carboxylated aniline based polymer capable of self-doping, is of interest as a soluble derivative of poly-aniline.

The carboxylic acid groups of the electro-synthesized polymer for covalently antibody immobilization can be used. Copolymers of aniline and amino benzoic acids have been synthesized by chemical [13, 14] and electrochemical routes [15, 16]. For example, a SPR immunosensor based on an electro-polymerized PAA film was constructed for the

electrochemically controlled detection of human IgG [15]. Preechaworapun and co-workers have used an electropolymerized poly-anthranilic acid-modified boron-doped diamond electrode as an amperometric immunosensor [17].

These types of electrochemical immunosensors have demonstrated to gather useful analytical characteristics such high sensitivity, rapid response and easiness of use to measure biomarker proteins for early detection and monitoring of cancers [18].

In this paper, two simple and sensitive approaches for CA125 detection are presented.

The first proposed approach is a label-free impedimetric immunosensor. Impedance measurement is a sensitive technique for label-free detection of antigen–antibody binding. The principle is based on the change in interfacial property between the electrode surface and solution when an antibody attached to an electrode surface reacts with an antigen to form a complex. One way to enhance the response of a label free immunosensor is to increase the amount of an immobilized antibody on the electrode so that a larger immunological complex can occur, and therefore produce a larger signal. The covalently monoclonal anti-CA125 antibody (mAb-CA125) was immobilized on poly-anthranilic acid (PAA) modified graphite screen-printed electrodes. After the incubation of immunosensor with different concentrations of CA125 protein, a curve calibration by using electrochemical impedance spectroscopy (EIS) was performed.

In order to improve the performances of the immunosensing, a second approach is developed by using sandwich polyclonal rabbit anti-CA125 antibody-functionalized gold nanoparticles (pAb-CA125/AuNPs) bioconjugates along with silver deposition. The application of gold nanoparticles as labels in biosensors is very common lately. They have been applied in ultrasensitive detection of DNA hybridization, protein– protein interactions, and carbohydrate – protein interactions [19-21]. As reported in literature [22-24], a signal amplification based on silver staining on the gold nanoparticles, offers a distinct enhancement of the immunoreaction response, comparing with conventional electrochemical immunosensors.

The sandwich assay is performed after the antigen was captured from the sample solution by adding secondary polyclonal rabbit anti-CA125 antibody-functionalized gold nanoparticles (pAb-CA125/AuNPs). The antibody-functionalized AuNPs captured onto immunosensor surface induced the silver deposition from a silver enhancer solution. The deposited AgNPs could be directly measured by anodic stripping analysis in acid solution. A high sensitivity with a detection limit of 2 U mL^{-1} of human CA125 protein

was achieved. This level of detection could be attributed to the sensitive electrochemical determination of silver ions and to the catalytic precipitation of a large number of silver ions on the gold nanoparticles- labelled antibody.

The performance of the immunosensors in terms of sensitivity, reproducibility and selectivity has been studied.

Because of the simple, specific and sensitive nature of this methodology, the immunosensors developed may find potential use in serum-based protein diagnostics.

2. Experimental

2.1 Chemicals

Anthranilic acid, 1-ethyl-3-(3'-dimethylaminopropyl)carbodiimide hydrochloride (EDC), bovine serum albumin (BSA), ethanolamine (EA), magnesium chloride, sodium citrate, tetrachloroauric (III) acid ($HAuCl_4$), tris(hydroxymethyl) aminomethane hydrochloride (TRIS), silver enhancer solution (equal volumes of solutions A and B) and 2.5% sodium thiosulfate pentahydrate from a Silver Enhancer Kit were purchased from Sigma-Aldrich (Milan, Italy). Potassium chloride, sodium dihydrogen phosphate, disodium hydrogen phosphate, potassium ferrocyanide ($K_4[Fe(CN)_6]$) potassium ferricyanide ($K_3[Fe(CN)_6]$), acetic acid, sodium hydroxide, 2-(N-morpholino) ethanesulfonic acid (MES) and sulfuric acid were obtained from Merck (Milan, Italy); N-hydroxysuccinimide (NHS) was obtained from Fluka (Milan, Italy).

The immunologic reagents mouse monoclonal CA125 antibody (mAb-CA125), human CA125 protein, and rabbit polyclonal CA125 antibody (pAb-CA125) were obtained from Novus Biologicals (Cambridge, UK); prostate specific antigen (PSA, Acris-Antibodies GmbH, Herford, Germany) was used as aspecific control. All the solutions were prepared using MilliQ grade water.

2.2 Apparatus and electrochemical measurements

Electrochemical experiments were performed with an AUTOLAB PGSTAT 30(2) digital potentiostat/galvanostat with a GPES 4.9004 software package (EcoChemie, Netherlands). Graphite screen-printed cell consists of graphite working electrode (GSPE), a graphite counter electrode and a silver pseudo-reference electrode. Materials and procedures to screen-print the transducers are described in [1].

All the functionalization steps involved in the assembly of the immunosensor were performed using 8 mL of the appropriate solution deposited on the graphite screen-printed working electrode surface in order to prevent the fouling of counter and reference screen-printed electrodes.

UV-Vis spectra of AuNPs were acquired with a Cary 100 Bio spectrophotometer (Varian, USA) between 400 and 900 nm using glass cuvette with a of 1 cm path length.

The electropolymerization was performed by cyclic voltammetry (CV) between the 0 and +1.0 V *vs.* Ag/AgCl pseudo reference with a scan rate of 0.05 V s^{-1}.

Impedance measurements were carried out in the presence of 0.01 M $[Fe(CN)_6]^{3-/4-}$ redox probe prepared in 0.01 M TRIS buffer, pH 7.4 with NaCl 0.1 M. A voltage of 0.01 V in amplitude (peak-to-peak), within the frequency range 100 kHz–100 mHz, was superimposed to the applied bias potential. The dc potential was set up to +0.13 V, the formal potential of $[Fe(CN)_6]^{3-/4-}$ redox probe.

Experimental spectra, presented in the form of complex plane diagrams (i.e., Nyquist plots), were fitted with proper equivalent circuits using the facilities of the FRA2 software 4.9004 (EcoChemie). Both charge transfer resistance and Δ charge transfer resistance values were taken as analytical signals.

Anodic stripping voltammetry (ASV) experiments were carried out first applying a potential of -0.2 V for 180 s to accumulate the dissolved silver and then, differential pulse stripping voltammetry was performed from -0.3 to +0.5 V using a scan rate of 0.05 V s^{-1}, modulation time 0.05 s; interval time 0.15 s; step potential 0.005 V; modulation amplitude 0.07 V.

2.3 Immunosensor development

2.3.1 Electropolymerization of anthranilic acid (AA)

The electropolymerization was performed using a solution of 0.05 M anthranilic acid monomer (AA) in 1 M H_2SO_4, 0.1 M KCl on a graphite screen-printed electrode (GSPE) with an applied potential ranging from 0 to +1.0 V at a scan rate of 0.05 V s^{-1} for 15 cycles.

The poly-anthranilic acid modified screen-printed electrodes (PAA/GSPEs) were then rinsed with distilled water to remove the excess monomer. PAA-modified GSPEs were then characterized by EIS measurements.

2.3.2 Primary antibody anti-CA125 (mAb-CA125) immobilization on poly-anthranilic acid modified graphite screen-printed electrodes (PAA-GSPEs)

8 µL of 0.1 M MES buffer solution (pH 5.5) containing 0.4 M of EDC and 0.2 M of NHS solution were placed on the working electrode surface of the poly-anthranilic acid modified screen-printed electrodes (PAA/GSPE) to activate the carboxylic acid groups of the PAA film. Then, the sensors were washed with water and subsequently incubated for 60 minutes at 25 °C in 8 µL of 30 mg L^{-1} mouse monoclonal anti-CA125 antibody (mAb-CA125) solution in 0.1 M PBS buffer (pH 7.4).

The antibody was immobilized onto the PAA/GSPEs through the formation of covalent bonds between carboxylic acid groups of the polymer and amine groups of the antibody. The immunosensors (mAb-CA125/PAA/GSPEs) were then rinsed thoroughly with the PBS buffer to remove the weakly adsorbed antibodies and then in order to deactivate the free COOH groups, 8 µL of a 0.01 M ethanolamine (EA) solution was drop cast onto each mAb-CA125/PAA/GSPEs and incubated for 15 min. Then, they were washed 3 times with 0.1 M PBS buffer.

2.3.3 Label-free immunosensor

The immunosensors (mAb-CA125/PAA/GSPEs) were incubated with 8 µL with CA125 protein at various concentrations (0, 10, 20, 30, 40, 50 U mL^{-1}), prepared in 0.1 M PBS buffer, for 60 minutes at 25 °C. Then, the electrodes were washed 3 times with 0.01 M TRIS buffer, pH 7.4 and finally EIS measurements were carried out in the conditions described above.

2.3.4 Immunosensor based on gold nanoparticle-silver enhancement

2.3.4.1 Preparation of secondary antibody anti-CA125 (pAb-CA125) gold nanoparticle conjugates

Gold nanoparticles (AuNPs) were prepared according to protocol of the literature [25]. In brief, 1.75 mL of 1% sodium citrate solution was added into 50 mL boiling solution of 0.025 M $HAuCl_4$ prepared in water, which result in a change in solution colour from yellow to bright red. Boiling was continued for 15 min, followed by continued stirring until the solution reached room temperature. Then the colloidal solution was stored at 4

°C. UV-Vis spectra of prepared AuNPs shows a peak cantered at 520 nm with an ABS value of 1.67 (Figure 4.1).

In according with reference [26], the synthesis produces AuNPs with a diameter of 16 nm and with a concentration of 6.2 10^{-9} M.

Polyclonal rabbit anti-CA125 antibody (pAb–CA125)-gold nanoparticle conjugates (pAb–CA125/AuNPs-) were prepared following the procedure reported in [27]. First, 1 mL of colloidal AuNPs (adjusted to pH 9.0 with 0.01 M NaOH) was mixed with 100 mL of 100 mg L^{-1} pAb–CA125 for 20 min at 25 °C under continuous stirring. The antibody was absorbed onto the surface of AuNPs through a combination of ionic and hydrophobic interactions. After, 100 mL of 1 mg L^{-1} solution of BSA was added to the AuNPs- pAb–CA125 conjugated in order to block the uncovered AuNPs surface (minimizing the aspecific adsorptions) and then, the mixture solution was purified by centrifugation at 11300 rpm for 20 min. Finally, the supernatant was discarded and the resulting AuNPs-labelled pAb–CA125 were resuspended in water and stored at 4 °C.

The concentration of gold nanolabels was calculated to be 6.0 10^{-9} M using the same procedure described above. This stock solution was diluted 2 times with 0.1 M PBS buffer (pH 7.4) for every use in immunosensor procedure.

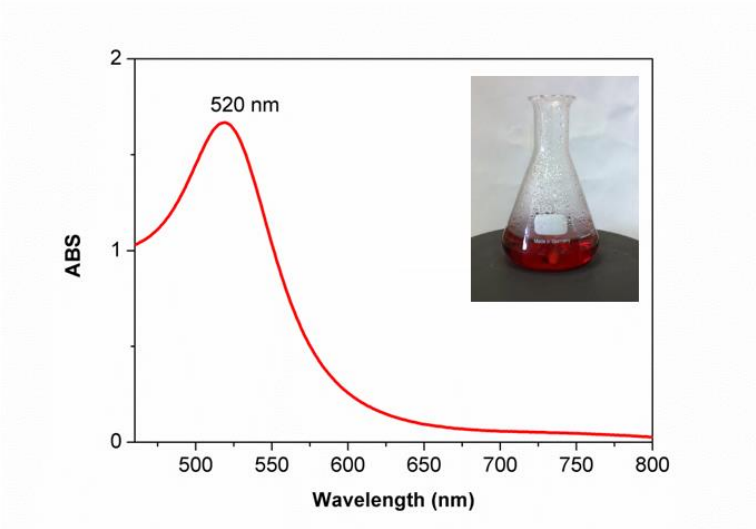

Figure 4.1. UV-Vis spectra of AuNPs colloidal solution obtained by citrate reduction method. Inset: bright red colour of AuNPs (16 nm) colloidal solution synthesized by citrate reduction method.

2.3.4.2 Silver enhancement detection

The immunosensors were first incubated with 8 mL with CA125 protein at various concentrations (0, 5, 10, 15, 20, 25 U mL^{-1}), prepared in 0.1 M PBS buffer, for 60 min. at

25 °C. After 3 washing steps with PBS buffer solution, the immunosensor was incubated with 8 mL of AuNPs-pAb-CA125 conjugate for 60 minutes at 25 °C and afterward washed 3 times with MilliQ water.

Then, 10 mL of silver enhancement buffer (mixture of the two solutions from the Silver Enhancer Kit in a 1:1 volume ratio prepared just prior to use) was added on the immunosensor and incubated in the dark for optimum deposition time of 8 min. Next, in accordance with the instruction of the producer, $Na_2S_2O_3$ solution was placed on the working electrode surface for 2 minutes. Finally, washing steps were performed 3 times with MilliQ water.

The deposited silver was dissolved by 50 ml of 1 M HNO_3, 0.1 M KCl for 5 min and then quantified by differential pulse anodic stripping voltammetry (ASV) as reported above.

3. Results and discussion

The two different approaches for CA125 detection are shown in Figure 4.2:

Route A) label-free immunosensor;

Route B) sandwich assay with gold nanoparticle silver enhancement.

Briefly, the protocol involves the following steps:

(a) modification of GSPEs with poly-anthranilic acid (PAA) through electropolymerization of anthranilic acid monomer (AA); (b) activation of COOH groups using EDC/NHS (c) followed by immobilization of mAb-CA125 primary antibody on the PAA-modified GSPEs; (d) blocking of the active sites with ethanolamine (EA); (e) affinity reaction with CA125 protein.

The immunosensor prepared in this way were then used for both approaches.

Route A: Label-free detection of CA125 by EIS measurements using 0.01 M $[Fe(CN)_6]^{3-/4-}$ prepared in TRIS 0.01 M pH 7.4 as redox probe.

Route B: (f) addition of secondary anti-CA125 antibodies-functionalized gold nanoparticles (pAb-CA125/AuNPs); (g) catalytic precipitation of silver onto the gold nanoparticles label using the silver enhancer solution; (h) silver dissolution in 1 M HNO_3; (i) ASV measurement of the silver dissolved.

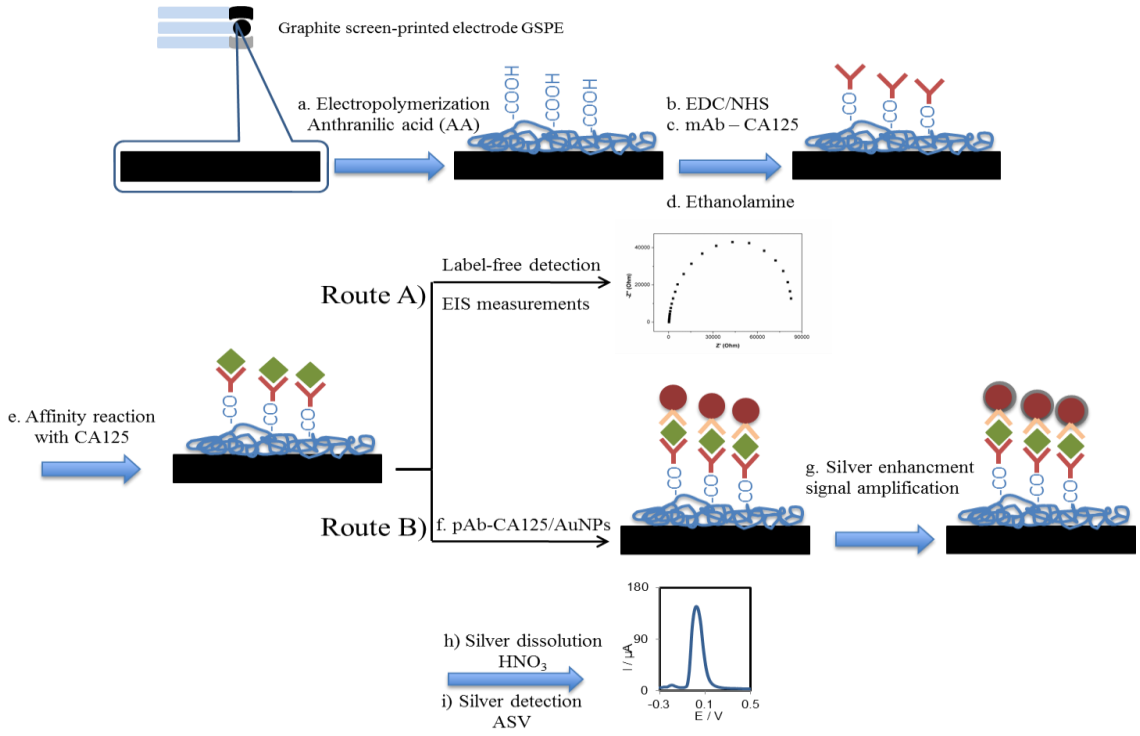

Figure 4.2. Scheme of the immunosensors: electropolymerization of anthranilic acid (AA) (a), activation of polymer (b), mAb-CA125 immobilization on the modified GSPEs surface (c), COOH-free sites blocking with ethanolamine (d), incubation with CA125 protein (e). Route A) EIS measurements for CA125 label-free detection.
Route B) reaction with pAb-CA125/AuNPs conjugate (f), silver enhancement (g) dissolution of silver nanoparticles in HNO_3 1M (h) ASV for silver detection (i).

3.1 Characterization of poly-anthranilic acid (PAA)-modified GSPEs

The electropolymerization of anthranilic acid (AA) onto graphite-screen printed electrodes (GSPEs) was performed using a solution of 0.05 M anthranilic acid monomer in 1 M H_2SO_4, 0.1 M KCl on a graphite screen-printed electrode (GSPE) with an applied potential ranging from 0 to +1.0 V at a scan rate of 0.05 V s^{-1} for 15 cycles.

The poly-anthranilic acid modified screen-printed electrodes (PAA/GSPEs) were then rinsed with distilled water to remove the excess monomer.

Electropolymerization spectrum of anthranilic acid on the GSPEs surface by cyclic voltammetry is reported in Figure 4.3 A and B.

Figure 4.3 A shows the voltammograms of bare graphite screen-printed electrodes (a) and 15th cycle of 50 mM anthranilic acid solution (b) with potential scanning from 0 to +1 V. These CV pattern are consistent with the previous studies of electropolymerization of PAA on electrode surface, which showed the redox peak of PAA film appearing between two redox peaks of polyaniline [15, 28].

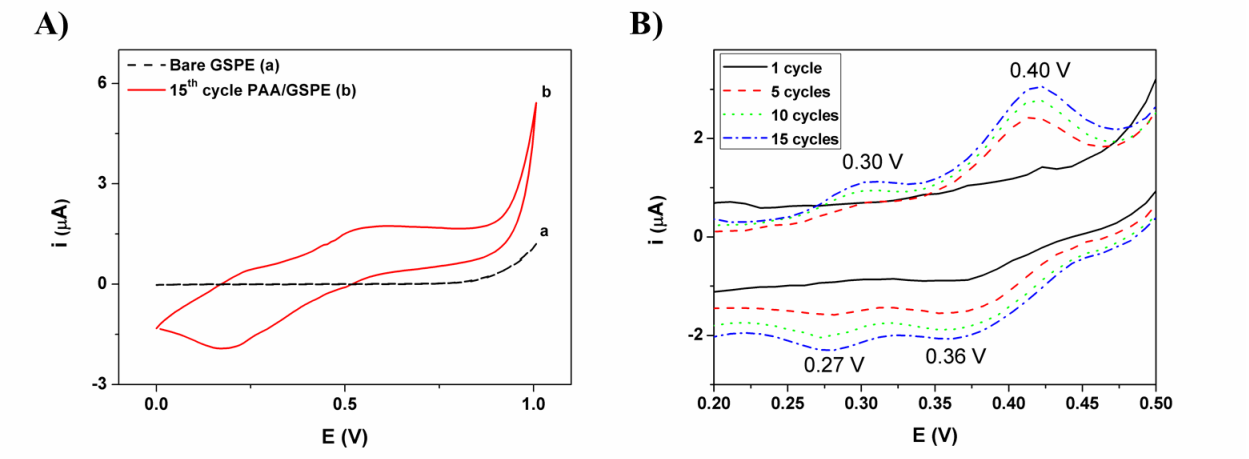

Figure 4.3. Cyclic voltammograms of anthranilic acid electropolimerization. A) Cyclic voltammograms: bare graphite screen-printed electrode (GSPE, curve a); 15th cycle of poly-anthranilic acid modified graphite screen-printed electrode (curve b, PAA/GSPE) in 1 M H_2SO_4, 0.1 M KCl solution. The scan rate was 0.05 mV s^{-1}. B) Magnification of 1, 5, 10, 15 cycles obtained using 0.05 M anthranilic acid (AA) in 1 M H_2SO_4, 0.1 M KCl solution, and with a scan rate of 0.05 mV s^{-1}.

3.2 Optimization of EIS measurements and polymerization conditions

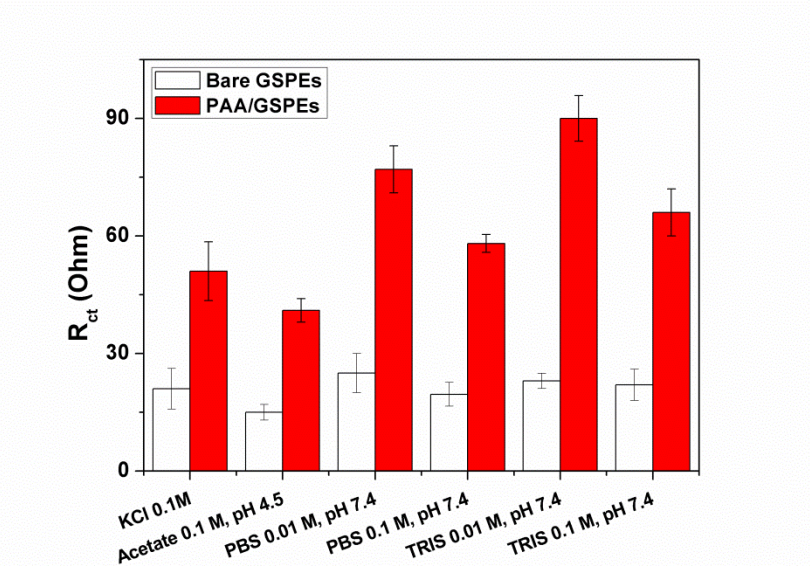

Figure 4.4. R_{ct} responses of bare graphite screen-printed electrodes (GSPEs) and poly-anthranilic acid modified graphite screen-printed electrodes (PAA/GSPEs) using 0.01 M $[Fe(CN)_6]^{3-/4-}$ redox probe prepared in different buffered solutions. Each point was repeated at least 3 times using different graphite screen-printed electrodes. The polymerization was carried out using 50 mM AA by cyclic voltammetry.

First, experiments were performed for optimizing the EIS measurements of PAA-modified GSPEs.

EIS measurements were carried out using $[Fe(CN)_6]^{3-/4-}$ redox probe prepared in different solutions: 0.1 M KCl; 0.1 M acetate buffer pH 4.5; 0.01 M and 0.1 M PBS pH 7.4; 0.01 M and 0.1 M TRIS pH 7.4. The results obtained showed a higher signal ratio between

bare GSPE and PAA-modified GSPE when redox probe was prepared in 0.01 M TRIS pH 7.4 (Figure 4.4). The effect is due to different composition and ionic strength of the buffer solution as reported in literature [29]. Therefore, the following EIS measurements were performed using $[Fe(CN)_6]^{3-/4-}$ redox probe prepared in 0.01 M TRIS buffer, pH 7.4.

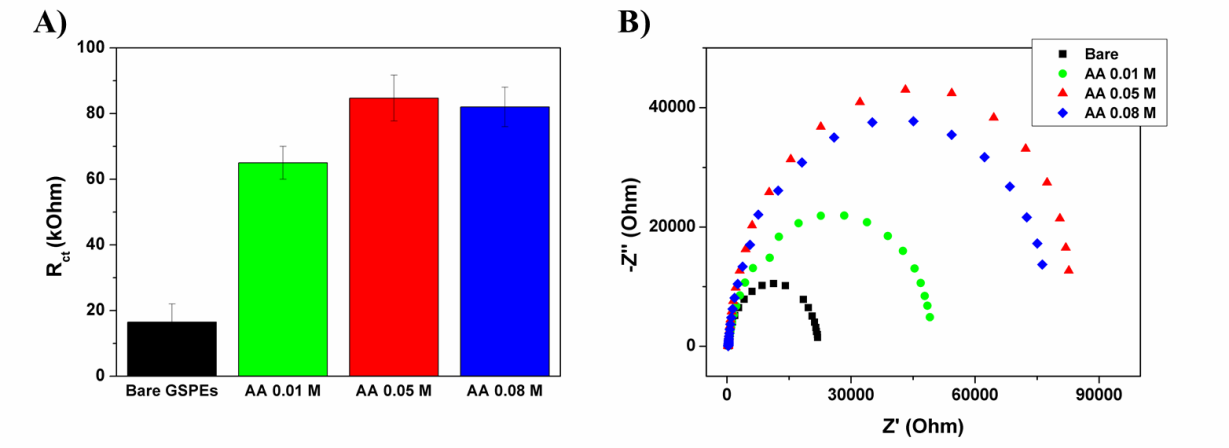

Figure 4.5. Optimization of acid anthranilic acid (AA) concentration for electropolymerization. A) R_{ct} measurements of PAA/GSPEs prepared starting from different monomer concentrations (0.01, 0.05, 0.08 mM), using 15 cycles and a scan rate of 0.05 V s^{-1}. B) Nyquist plot of bare GSPE (■) and of PAA-modified GSPEs using different AA concentrations: 0.01 M (●), 0.05 M (▲), 0.08 M (◆). Electrochemical impedance spectra were performed in 0.01 M $[Fe(CN)_6]^{3-/4-}$ in 0.01 M TRIS (pH 7.4). Each point was repeated at least 3 times using different screen-printed graphite electrodes.

In order to optimise the electropolimerization process different experimental parameters were considered (including monomer concentration, 0.01, 0.05, 0.08 M and number of CV cycles, 1, 5, 10, 15). Optimization of anthranilic acid concentration and cycles of electropolymerization were performed with EIS technique measuring the changes in charge-transfer resistance (R_{ct}) values.

As the monomer concentration increases from 0.01 to 0.05 M, the electron transfer resistance increases respectively from 65.4 ± 5.4 to 84.7 ± 7.2 kOhm (Figure 4.5). No significant change in R_{ct} was observed increasing the anthranilic acid concentration up to 80 mM (R_{ct} = 82.5±6.5 kOhm). Thus, 50 mM of anthranilic acid solution was selected as optimal monomer concentration.

Optimization of the number of electropolimerization cycles is shown in Figure 4.6.

EIS results show that the PAA-modified GSPEs obtained using 10 and 15 cycles for electropolymerization, exhibit similar values for R_{ct} (respectively, 83.5 ± 5.0 and 84.7 ± 5.3 kOhm); so, 15 cycles was chosen as the optimized value. In this condition, the electrode surface is completely covered with PAA film.

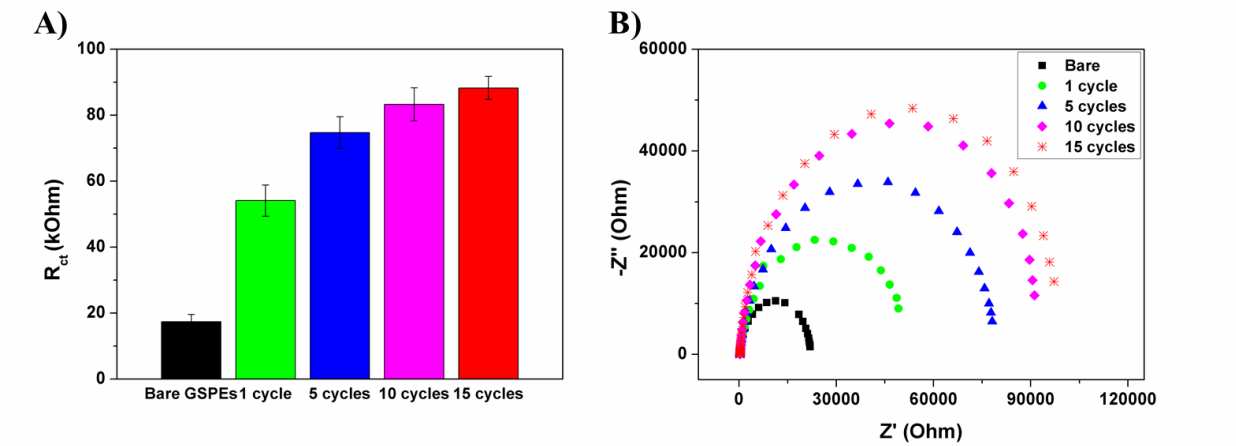

Figure 4.6. Optimization of electropolymerization cycles. A) R_{ct} measurements of poly-anthranilic acid modified graphite screen-printed electrodes (PAA/GSPEs) prepared starting from AA 50 mM, with a scan rate of 50 mV s^{-1}, using different cycles (1, 5, 10, 15). B) Nyquist plot of bare GSPE (■) and of poly-anthranilic acid modified graphite screen-printed electrodes (PAA/GSPEs) using different polymerization cycles: 1 (●), 5 (▲), 10 (◆) and 15 (✳). Electrochemical impedance spectra were performed in 0.01 M $[Fe(CN)_6]^{3-/4-}$ in 0.01 M TRIS (pH 7.4). Each point was repeated at least 3 times using different screen-printed graphite electrodes.

The PAA film introduces a barrier for electron transfer at the electrode interface and an enhanced electron transfer resistance is obtained. An increase of charge-transfer resistance values due to a bigger repulsion between the negatively charged of the $[Fe(CN)_6]^{3-/4-}$ redox probe and the negatively charged polymer film was observed in according of what reported in [30].

The film coverage amount can be calculated using the following equation:

$$(1-\theta) = R_{ct}^{0}/R_{ct}$$

where θ represents the apparent electrode coverage; R_{ct}^{0} and R_{ct} are respectively the charge transfer resistance of bare and of a film-covered electrode. In the optimized condition, the coverage was calculated to be near 80%.

3.3 Optimization of monoclonal antibody anti-CA125 (mAb-CA125) immobilization

An increase of R_{ct} value was observed after the mAb-CA125 immobilization on the PAA-modified GSPEs (data not shown). The same behaviour was observed when the affinity reaction with CA125 was performed. This is due to the formation of protein insulating layer that reduce the electron transfer from the redox mediator solution to the electrode surface.

Different concentrations of primary antibody solution (20, 30 and 40 mg L^{-1}) were used to optimize the immunosensor response (Figure 4.7). An increase in the sensitivity was observed when primary mAb-CA125 solution of 30 mg $L^{-1}$was used (y=0.51x, R^2=0.98). A higher concentration of antibody solution did not improve the immunosensor sensitivity probably due to the higher steric hindrance that reduces the recognition or CA125 protein. A decrease of sensitivity was also observed using mAb-CA125 solution of 20 mg L^{-1}. For this reason, a primary antibody solution of 30 mg L^{-1} was chosen for further experiments (Figure 4.7).

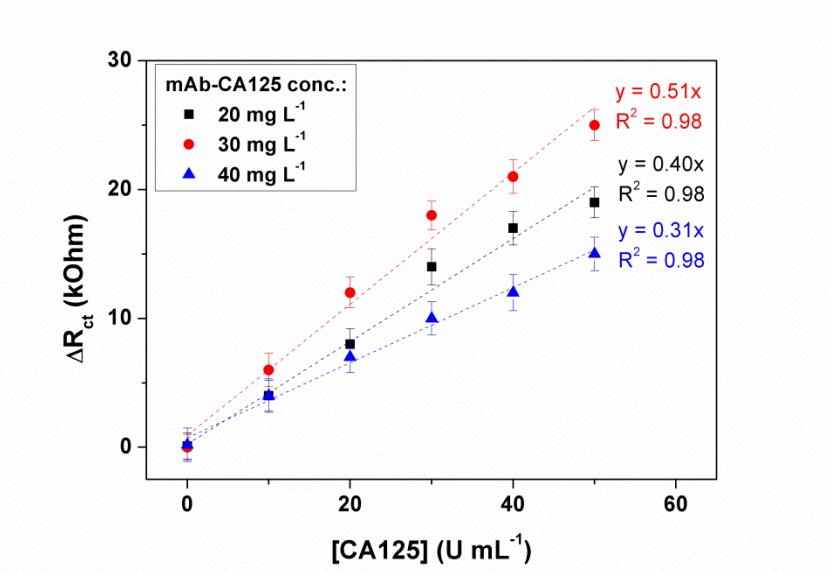

Figure 4.7. Optimization of primary antibody anti-CA125 (mAb-CA125) concentration: 20 mg L^{-1} (■), 30 mg L^{-1} (●), 40 mg L^{-1} (▲) on the EIS response for CA125 using 0.01 M $[Fe(CN)_6]^{3-/4-}$ prepared in TRIS 0.01 M pH 7.4. The values reported in the graphics represent the mean value of 3 different measurements.

3.4 Detection of CA125 by label-free immunosensor

The first approach developed was based on label free immunoassay as shown in Figure 4.2, route A. After the affinity reaction, the immunosensors were rinsed with 0.1 M PBS (pH 7.4) and then incubated with 10, 20, 30, 40 and 50 U mL^{-1} CA125 antigen as reported in the procedure. The impedance measurements for the immunocomplex detection were carried out applying +0.13 V using a 0.01 M equimolar solution of $[Fe(CN)_6]^{3-/4-}$ prepared in 0.01 M TRIS (pH 7.4).

Varying R_{ct} (ΔR_{ct} = $R_{ct,CA125}$ - $R_{ct,0}$) values were used as analytical signal in the CA125 calibration curve (Figure 4.8). A linear response was observed between 0 and 50 U mL^{-1},

with a slope value of 0.53 kOhm mL U^{-1}. The detection limit (LOD) of the label-free immunosensor, calculated as LOD = $3S_{blank}$/slope, was found 7.6 U mL^{-1}.

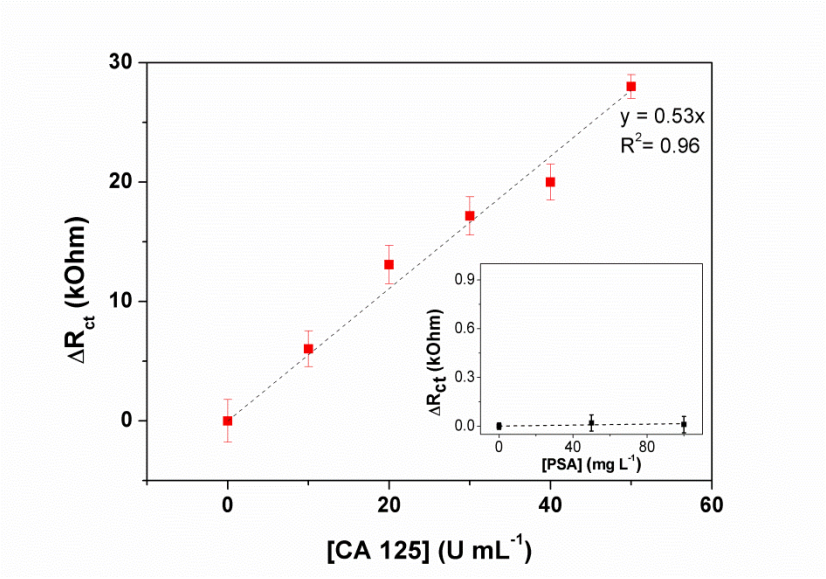

Figure 4.8. Calibration curve for label-free CA125 detection by EIS measurements performed in 0.01 M $[Fe(CN)_6]^{3-/4-}$ prepared in TRIS 0.01 M pH 7.4. Inset: aspecific test with PSA (0, 50, 100 mg L^{-1}). Each point was repeated at least 3 times using different modified graphite screen-printed electrodes.

Moreover, the limit of quantification, calculated as $10S_{blank}$/slope, was found 25.3 U mL^{-1}. A very similar R_{ct} value compared to the blank (0 U mL^{-1} of CA125) was achieved for PSA aspecific protein

3.5 CA125 detection by gold nanoparticles-silver enhancement

The second approach developed was based on sandwich immunoassay format as shown in Figure 4.2, route B.

Through a sandwich-type immunoreaction, the antibody-functionalized AuNPs could be captured on the immunosensor surface by the formation of immunocomplex. After the addition of silver deposition solution onto the sensor surface, the AuNPs could act as nuclei and catalysts to induce the reduction reaction of silver ion from the silver deposition solution. When CA125 concentration increased, the more amounts of AuNPs was captured on the sensor surface to produce more AgNPs.

Finally, anodic stripping analysis of the quantitatively deposited AgNPs on the corresponding immunosensors was used for CA125 detection.

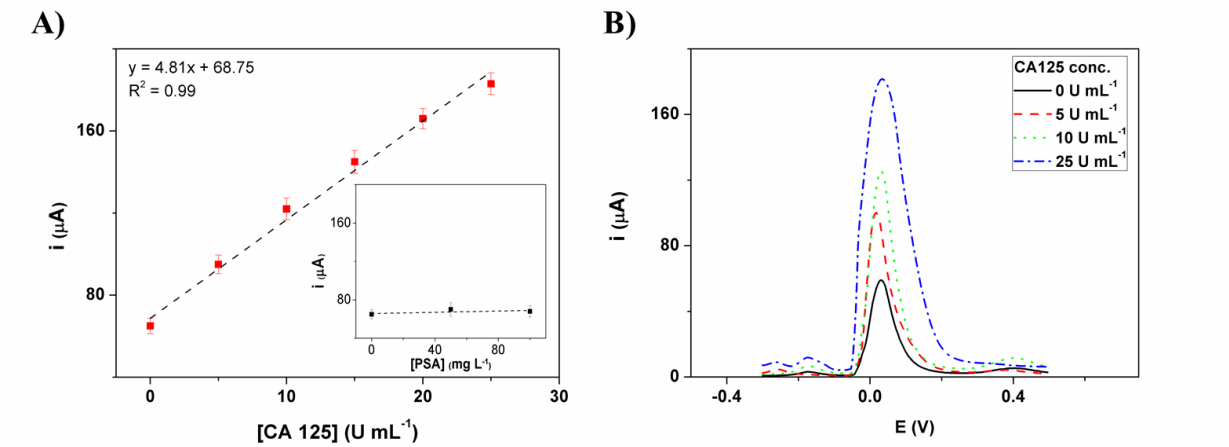

Figure 4.9. A) Calibration plots for CA125 detection through sandwich assay using pAb-CA125 antibody labelled-gold nanoparticles and silver enhancement. Inset: aspecific signal obtained with PSA (50, 100 mg L^{-1}). B) Voltammograms by differential pulse anodic stripping voltammetry of silver using different CA125 concentrations, from down to up: 0, 5, 10, 25 U mL^{-1}, respectively. Each point was repeated at least 3 times using different modified screen-printed graphite electrodes.

Calibration curves for the determination of CA125 protein by silver enhancement procedure were achieved under optimal conditions (Figure 4.9).

It is possible notice, a linear correlation between the current and the CA125 concentration in the range of 5 – 25.0 U mL^{-1} (y = 4.81x+68.75, R^2=0.99).

LOD and LOQ values, calculated as previously described, were estimated to be 2.0 U mL^{-1} and 7.0 U mL^{-1} respectively. Similar current value compared to the blank was achieved for PSA aspecific protein.

The analytical parameters of the proposed method based on gold nanoparticle silver enhancement was improved by both the AuNPs-induced silver deposition procedure and the well-defined stripping sharp peak of the deposited AgNPs in acid solution.

4. Conclusions

Two strategies for CA125 detection in this work were presented, by using poly-anthranilic acid modified graphite screen-printed electrodes.

In both cases, they were used as solid phase to build up a label free immunosensor and a sandwich format with gold nanoparticle silver enhancement.

A good sensitivity and reproducibility was achieved for CA125 detection, with a linear response, which matches the request of clinical needs. Future experiments will be performed in spiked and real sample to verify the responses of both immunosensors for their use in clinical analysis.

References

[1] Al-Khafaji QAM, Harris M, Tombelli S, et al. An Electrochemical Immunoassay for HER2 Detection. Electroanal 2012; 24:735-42.
[2] Zani A, Laschi S, Mascini M, Marrazza G. A New Electrochemical Multiplexed Assay for PSA Cancer Marker Detection. Electroanal 2011; 23:91-9.
[3] Peng NJ, Liou WS, Liu RS, Hu C, Tsay DG, Liu CB. Early detection of recurrent ovarian cancer in patients with low-level increases in serum CA-125 levels by 2-[F-18]fluoro-2-deoxy-D-glucose-positron emission tomography/computed tomography. Cancer biotherapy & radiopharmaceuticals 2011; 26:175-81.
[4] Bangar MA, Shirale DJ, Chen W, Myung NV, Mulchandani A. Single Conducting Polymer Nanowire Chemiresistive Label-Free Immunosensor for Cancer Biomarker. Anal Chem 2009; 81:2168-75.
[5] Ionescu AM. ELECTRONIC DEVICES Nanowire transistors made easy. Nat Nanotechnol 2010; 5:178-9.
[6] Rissin DM, Kan CW, Campbell TG, et al. Single-molecule enzyme-linked immunosorbent assay detects serum proteins at subfemtomolar concentrations. Nature biotechnology 2010; 28:595-9.
[7] Das J, Kelley SO. Protein Detection Using Arrayed Microsensor Chips: Tuning Sensor Footprint to Achieve Ultrasensitive Readout of CA-125 in Serum and Whole Blood. Anal Chem 2011; 83:1167-72.
[8] Chikkaveeraiah BV, Mani V, Patel V, Gutkind JS, Rusling JF. Microfluidic electrochemical immunoarray for ultrasensitive detection of two cancer biomarker proteins in serum. Biosensors and Bioelectronics 2011; 26:4477-83.
[9] Viswanathan S, Rani C, Ribeiro S, Delerue-Matos C. Molecular imprinted nanoelectrodes for ultra sensitive detection of ovarian cancer marker. Biosensors and Bioelectronics 2012; 33:179-83.
[10] Jagadeesan KK, Kumar S, Sumana G. Application of conducting paper for selective detection of troponin. Electrochem Commun 2012; 20:71-4.
[11] Mathebe NGR, Morrin A, Iwuoha EI. Electrochemistry and scanning electron microscopy of polyaniline/peroxidase-based biosensor. Talanta 2004; 64:115-20.
[12] Zhang J, Wang J, Zhu J, Xu J, Chen H, Xu D. An electrochemical impedimetric arrayed immunosensor based on indium tin oxide electrodes and silver-enhanced gold nanoparticles. Microchim Acta 2008; 163:63-70.
[13] Nguyen MT, Diaz AF. Water-Soluble Poly(aniline-co-o-anthranilic acid) Copolymers. Macromolecules 1995; 28:3411-5.
[14] Yan H, Wang H-J, Adisasmito S, Toshima N. Novel Syntheses of Poly(o-aminobenzoic acid) and Copolymers of o-Aminobenzoic Acid and Aniline as Potential Candidates for Precursor of Polyaniline. Bulletin of the Chemical Society of Japan 1996; 69:2395-401.
[15] Sriwichai S, Baba A, Phanichphant S, Shinbo K, Kato K, Kaneko F. Electrochemically controlled surface plasmon resonance immunosensor for the detection of human immunoglobulin G on poly(3-aminobenzoic acid) ultrathin films. Sensors and Actuators B: Chemical 2010; 147:322-9.
[16] Wang Y, Knoll W. In situ electrochemical and surface plasmon resonance (SPR) studies of aniline-carboxylated aniline copolymers. Anal Chim Acta 2006; 558:150-7.
[17] Preechaworapun A, Ivandini TA, Suzuki A, Fujishima A, Chailapakul O, Einaga Y. Development of Amperometric Immunosensor Using Boron-Doped Diamond with Poly(o-aminobenzoic acid). Anal Chem 2008; 80:2077-83.

[18] Fowler JM, Wong DKY, Brian Halsall H, Heineman WR, Chapter 5 - Recent developments in electrochemical immunoassays and immunosensors. In: Zhang X, Ju H, Wang J, editors. Electrochemical Sensors, Biosensors and their Biomedical Applications. San Diego: Academic Press, 2008: 115-43.
[19] Gao J, Liu D, Wang Z. Microarray-Based Study of Carbohydrate−Protein Binding by Gold Nanoparticle Probes. Anal Chem 2008; 80:8822-7.
[20] Guarise C, Pasquato L, De Filippis V, Scrimin P. Gold nanoparticles-based protease assay. P Natl Acad Sci USA 2006; 103:3978-82.
[21] Hou S-Y, Chen H-K, Cheng H-C, Huang C-Y. Development of Zeptomole and Attomolar Detection Sensitivity of Biotin−Peptide Using a Dot−Blot GoldNanoparticle Immunoassay. Anal Chem 2006; 79:980-5.
[22] Cheng W, Jin G, Zhang Y. Electrochemical Characteristics of Poly(o-Aminobenzoic Acid) Modified Glassy-Carbon Electrode and Its Electrocatalytic Activity towards Oxidation of Epinephrine. Russ J Electrochem 2005; 41:940-5.
[23] Gupta S, Huda S, Kilpatrick PK, Velev OD. Characterization and Optimization of Gold Nanoparticle-Based Silver-Enhanced Immunoassays. Anal Chem 2007; 79:3810-20.
[24] Pan Q, Zhang R, Bai Y, He N, Lu Z. An electrochemical approach for detection of specific DNA-binding protein by gold nanoparticle-catalyzed silver enhancement. Analytical Biochemistry 2008; 375:179-86.
[25] Frens G. Controlled nucleation for the regulation of the particle size in monodisperse gold suspensions. Nature 1973; 241:20-2.
[26] Haiss W, Thanh NTK, Aveyard J, Fernig DG. Determination of Size and Concentration of Gold Nanoparticles from UV−Vis Spectra. Anal Chem 2007; 79:4215-21.
[27] Ambrosi A, Castañeda MT, Killard AJ, Smyth MR, Alegret S, Merkoçi A. Double-Codified Gold Nanolabels for Enhanced Immunoanalysis. Anal Chem 2007; 79:5232-40.
[28] Cai H, Wang Y, He P, Fang Y. Electrochemical detection of DNA hybridization based on silver-enhanced gold nanoparticle label. Anal Chim Acta 2002; 469:165-72.
[29] Xu Y, Cai H, He P-G, Fang Y-Z. Probing DNA Hybridization by Impedance Measurement Based on CdS-Oligonucleotide Nanoconjugates. Electroanal 2004; 16:150-5.
[30] Liu J, Cheng L, Liu B, Dong S. Covalent Modification of a Glassy Carbon Surface by 4-Aminobenzoic Acid and Its Application in Fabrication of a Polyoxometalates-Consisting Monolayer and Multilayer Films. Langmuir 2000; 16:7471-6.

CHAPTER 5

Sandwich aptamers assay based on gold nanostructured graphite screen-printed electrodes for VEGF cancer biomarker detection

A. Ravalli [a], L. Rivas [b,c], A. de la Escosura-Muñiz [c], J. Pons [b], A. Merkoçi [c,d], G. Marrazza[a]

[a] Department of Chemistry "Ugo Schiff", University of Florence, Via della Lastruccia 3, 50019 Sesto F.no (FI), Italy.

[b] Unitat de Química Inorgánica, Departament de Química, Universitat Autónoma de Barcelona, Barcelona, Spain.

[c] Nanobioelectronics & Biosensors Group, CIN2 (ICN-CSIC), Catalan Institute of Nanotechnology, UAB Campus, Bellaterra, Barcelona, Spain.

[d] ICREA, Institució Catalana de Recerca i Estudis Avançats, Barcelona, Spain.

Abstract

In this work, an aptamers sandwich assay based on gold nanostructured (AuNPs) graphite screen-printed electrode for the determination of VEGF cancer biomarker was proposed. First, thiolated aptamer anti-VEGF (Apt1-VEGF) was covalently immobilized on the surface of gold nanoparticles-modified graphite screen printed electrodes (AuNPs/GSPEs) followed by the formation of a mixed self-assembly monolayer SAM. VEGF antigen was then incubated with the sensor and subsequently, the sandwich was completed by interaction with secondary biotinylated anti-VEGF aptamer (Apt2-VEGF). Streptavidin-alkaline phosphatase was finally incubated with the sensors and the electrochemical behaviour of alpha-naphthol (produced by alkaline phosphatase after the addition of alpha-naphthyl phosphate) was analysed by differential pulse voltammetry (DPV) in order to construct the calibration curve. Each phases involved in the assembly of the aptasensors were evaluated by electrochemical impedance spectroscopy (EIS) technique. The performance of the immunoassay in terms of sensitivity, reproducibility and selectivity has been also studied.

1. Introduction

The possibility of performing reliable cancer diagnosis even before any symptom of disease appears is crucial for increasing therapeutic treatment success and patient survival rates [1-3].

During the last decade, improved understanding of carcinogenesis and tumour metastasis revealed the ability of the tumoral cells to create new vasculatures in order to receive a large number of nutrient and oxygen necessary for their growth [4-7]. The main protein mediator of this process is the vascular endothelial growth factor, also known as VEGF [8-10].

New tumoral vasculatures formed are irregularly shaped, tortuous, with dead ends. This fact results in an insufficient supply of nutrient and oxygen to the tumoral cells with the consequent increase in the production VEGF [11, 12].

Thus, VEGF concentration in blood raise up and its values can be used as biomarker associated with diagnosis and prognosis of different type of cancer diseases [13-16].

VEGF is referred to a family of dimeric glycoprotein including five members: VEGF-A, VEGF-B, VEGF-C, VEGF-D and placenta growth factor (PLGF) [17]. Among these, VEGF-A (which includes three mainly isoforms: VEGF-121, VEGF-165, VEGF-189) represents the most abundant and the most studied protein of the family [18].

Traditionally, immunosensors were applied for the detection of a large number of biomarkers. Nevertheless these methods do not satisfy the rapidity requirement and the necessity to use simple instrumentation for point of care diagnostics. In this context, rapid non-immunochemical sensors based on electrochemical methods using aptamers as bioreceptors are emerging [19-21].

Aptamers (from Latin *aptus*, “to fit” and Greek, *merus*, “part”) are synthetic single strand oligonucleotide acids (DNA or RNA) or peptide fragment obtained through systematic evolution of ligands by exponential enrichment (SELEX) process [22].

Because they offer significant advantages over traditional bioreceptors (i.e. antibodies or enzymes), such as easy synthesis, easy chemical modification, good stability and resistance to denaturation, high specificity for target molecules and the possibility to distinguish between very similar targets [23], they were extensively used in many applications, in particular in biosensors field [24, 25].

In recent years, nanostructures have found a wide employment for different purposes [26]. Among these, gold nanoparticles (due to their particular properties such as high area/volume ratio, easily surface modification, high compatibility with biological molecules) were the most used [27-29]. A detailed review of gold nanoparticles-based biosensors can be found in ref. [30].

In this work, an aptamers sandwich assay based on gold nanostructured (AuNPs) graphite screen-printed electrode for the determination of VEGF cancer biomarker was proposed. First, thiolated aptamer anti-VEGF (Apt1-VEGF) was covalently immobilized on the surface of gold nanoparticles-modified graphite screen printed electrodes (AuNPs/GSPEs) followed by the formation of a mixed self-assembly monolayer SAM. VEGF antigen was the incubated with the sensors and then, the sandwich was completed by interaction with secondary biotinylated anti-VEGF aptamer (Apt2-VEGF).

Streptavidin-alkaline phosphatase was finally incubated with the sensor and the electrochemical behaviour of alpha-naphthol (produced by alkaline phosphatase after the addition of alpha-naphthyl phosphate) was analysed by differential pulse voltammetry (DPV) in order to construct the calibration curve. Each phases of the assembly of the immunosensor was evaluated by electrochemical impedance spectroscopy. The performance of the immunoassay in terms of sensitivity, reproducibility and selectivity has been also studied.

2. Materials and methods

2.1 Chemicals

Sodium chloride, tetrachloroauric (III) acid ($HAuCl_4$), 6-mercapto-1-hexanol (MCH), diethanolamine (DEA), 1-naphtyil phosphate, streptavidin-alkaline phosphatase, magnesium chloride, human Vascular Endothelial Growth Factor (VEGF) were obtained from Sigma-Aldrich (Milan, Italy). Human epidermal growth factor receptor 2 (HER2) protein (R&D Systems) were purchased from Space srl (Milan, Italy) and used as aspecific control.

Sulfuric acid, potassium chloride, potassium ferrocyanide ($K_4[Fe(CN)_6]$), potassium ferricyanide ($K_3[Fe(CN)_6]$), tris(hydroxymethyl)aminomethane hydrochloride (TRIS), ethylenediaminetetraacetic acid (EDTA) were purchased from Merck (Milan, Italy).

Aptamers used in this work were obtained from MWG Biotech, Germany. Sequences are reported in Table 1.

All chemicals were used as received without any further purification. Milli-Q water was used throughout this work.

Buffers used in this work include:

TBSE: TRIS 0.01 M, EDTA 0.05 mM, NaCl 0.1 M, pH 7.4

TBSE KCl: TRIS 0.01 M, NaCl 0.1 M, KCl 0.1 M, EDTA 0.05 mM, pH 7.4

TBS KCl: TRIS 0.01 M, NaCl 0.1 M, KCl 0.1 M, pH 7.4

DEA: Diethanolamine 0.1 M, KCl 0.1 M, $MgCl_2$ 0.001 M, pH 9.6

Table 5.1. List of the aptamers sequences (form 5' to 3') used in this work. 15 thymines nucleobases – T(15) – were used as spacer.

Aptamer	Sequence	Reference
Apt1-VEGF	5'-TGTGGGGGTGGACGGGCCGGGTAGA-T(15)-3'-SH	[31]
Apt2-VEGF	5'- GGGCCCGTCCGTATGGTGGGTGTGCTGGCC-T(15)-3'-Biot	[32]

Prior the use Apt1-VEGF and Apt2-VEGF were heated at 95 °C and then gradually cooled to 25 °C followed by fast cooling in freezer for to keep the folded structure of the aptamer.

2.2 Electrochemical instrumentations

Electrochemical experiments were performed in a digital potentiostat/galvanostat AUTOLAB PGSTAT 30(2)/FRA2 controlled with the General Purpose Electrochemical System (GPES) and Frequency Response Analyzer (FRA2) 4.9 software (Eco Chemie, Utrecht, The Netherlands). The sensor was assembled using graphite screen-printed cell, comprising of graphite and gold working electrode (2.5 mm in diameter) and counter graphite electrode and a pseudo-silver reference.

The screen-printed cells were produced in house on a DEK 248 screen-printing machine (DEK, Weymouth, UK). The printing was performed on a polyester film (Autostat CT5) from Autotype (Milan, Italy) using the polymeric inks (Electrodag PF-410 (silver)) and (Electrodag 423 SS (graphite)), which were purchased from Acheson (Milan, Italy) and gold-based ink (R-464 (DPM-78)) obtained from Ercon Inc. (MA, USA). Vinylfast 36-100 was used as the insulting ink and was obtained from Argon (Lodi, Italy).

2.2.1 Electrochemical impedance spectroscopy (EIS) measurements

EIS measurements were carried out using 0.01 M $[Fe(CN)_6]^{3-/4-}$ equimolar solution prepared in TBS KCl buffer as redox probe.

EIS spectra were acquired superimposing a voltage of 0.01 V in amplitude (peak-to-peak), within the frequency range 100 kHz – 10 mHz, at the bias voltage.

The DC potential was set up to + 0.13 V (*vs.* Ag/AgCl pseudo-silver reference), the formal potential of redox probe. Nyquist plot were fitted by a proper equivalent circuit using the facility of FRA2 4.9.004 (EcoChemie) software. Charge transfer resistance (R_{ct}) was taken as analytical parameter. All the potentials were referred to the screen-printed pseudo-reference electrode and the experiments were performed at room temperature (25 °C).

2.2.2 Differential pulse voltammetry (DPV) measurements

DPV experiments were performed from -0.3 V to 0.5 V (*vs.* Ag/AgCl pseudo-silver reference) using the following parameters: scan rate 0.1 V s^{-1}, modulation time 0.05 s, interval time 0.15 s, step potential 0.005 V, modulation amplitude 0.07 V. All the spectra were acquired at room temperature (25 °C).

2.2.3 Cyclic voltammetry (CV) parameters

Electrodeposition of gold nanoparticles (AuNPs) onto graphite screen-printed electrodes (GSPEs) was obtained by cyclic voltammetry in the range -0.2 and +1.6 V *vs.* screen-printed silver pseudo-reference using $HAuCl_4$ solution prepared in 0.5 M H_2SO_4.

2.3 Electrodeposition of gold nanoparticles on graphite screen-printed electrodes

Electrodeposition of gold nanoparticles (AuNPs) on the surface of graphite screen-printed electrodes (GSPEs), was realized in accordance with the optimized procedure reported in our previously work [33]. Briefly, 50 μL of 0.0006 M of $HAuCl_4$ solution (prepared in 0.5 M H_2SO_4) were placed onto GSPEs surface. Subsequently, the potential was cycled from -0.2 and +1.6 V *vs.* pseudo-reference silver screen-printed electrode for 25 cycles using a scan-rate of 0.1 V s^{-1}. AuNPs-modified GSPEs were then washed 3 times with Milli-Q water in order to remove the free ions from the GSPEs surface.

2.4 Functionalization of AuNPs-modified GSPEs with thiolated anti- VEGF aptamer (Apt1-VEGF) and with 6-mercapto-1-hexanol (MCH)

10 μL of 0.1 μM Apt1-VEGF solution prepared in TBSE KCl buffer, were placed on the working electrode surface of gold nanoparticle-modified graphite screen printed electrodes (AuNPs/GSPEs) and incubated overnight at 25 °C in a home-made wet chamber.

After, the Apt1-VEGF-modified electrodes were rinsed 3 times with TBSE KCl buffer and incubated for 60 minutes with 10 uL of 0.001 M 6-mercapto-1-hexanol (MCH).

Finally, the modified electrodes were washed 3 times with TBSE KCl.

2.5 Incubation with VEGF protein

The MCH/Apt1-VEGF-modified AuNPs/GSPEs were incubated with 10 μL with VEGF at various concentrations (0, 50, 100, 200, 500 nM), prepared in TBSE KCl buffer for 45 minutes at 25 °C. Then, the electrodes were washed 3 times with TBSE buffer in order to remove the unbound VEGF molecules.

Aspecific test was performed using human epidermal growth factor receptor 2 (HER2) protein at 50, 100 μg L^{-1} prepared in TBSE buffer instead of VEGF.

2.6 Binding with secondary biotinylated anti-VEGF aptamer and streptavidin alkaline-phosphatase

To complete the sandwich assay the VEGF-modified electrodes were incubate with 10 uL of 0.5 μM secondary biotinylated anti-VEGF aptamer (Apt2-VEGF) for 30’ at 25 °C. After three washing step performed with DEA buffer, streptavidin-alkaline phosphates (prepared in DEA buffer containing BSA 10 mg mL^{-1}) was added to the system and incubated for 15 minutes at 25 °C.

Finally, the sensors were washed three times with DEA buffer.

2.7 Differential pulse voltammetry (DPV) measurements

50 μL of alpha-naphthyl phosphate were placed on the sensors and incubated for 6 minutez at 25 °C. The redox peak of enzymatic product (alpha-naphthol) produced by the

enzyme was then determined by means of DPV technique and used to calculate the VEGF calibration curve.

3. Results and discussion

Electrodepostion of gold nanoparticles (AuNPs) on graphite screen-printed electrodes allows the formation of randomly distributed AuNPs (with size comprise between 40 and 100 nm) all over the working electrode surface.

Electrodeposed AuNPs provides a useful platform for the immobilization of the bioreceptors due to the high affinity and easy functionalization with thiols groups.

Because aptamers were directly synthesized with thiol functional groups, its immobilization on the gold electrode surface can be performed in a single step (decreasing the costs and the time request to complete the assay) without alteration of its folded structure, necessary for the recognition of the target protein.

In this work two different aptamers (Apt1-VEGF and Apt2-VEGF) were used to perform the sandwich assay in order to detect VEGF cancer biomarker.

Both aptamers were developed by Ikebukuro's groups and possess the ability to bind selectively with no cross-reactivity to different target domains present on VEGF molecules: in particular Apt1-VEGF (in a G-quadruplex folded structure) is capable to bind the receptor-binding domain (RBD) of VEGF, while Apt2-VEGF (in three stem loop folded structure) shown high affinity for the heparin-binding domain (HBD) of VEGF [31, 32].

Figure 5.1 shows the schematic representation of the steps involved in the development of aptamers sandwich assay based on gold nanoparticle-modified graphite screen printed electrodes for the determination of VEGF protein.

The protocol involves the following steps:

a) electrodeposition of gold nanoparticles AuNPs on graphite screen-printed electrodes (GSPEs) b) functionalization with thiolated primary anti-VEGF aptamer (Apt1-VEGF); c) Incubation with MCH; d) affinity reaction with VEGF protein; e) addition of biotinylated secondary anti-VEGF aptamer (Apt2-VEGF); f) incubation with streptavidin-alkaline phosphatase (streptavidin-AP); g) addition of the substrate (alpha-naphthyl phosphate) h) DPV analysis of enzymatic product alpha-naphthol.

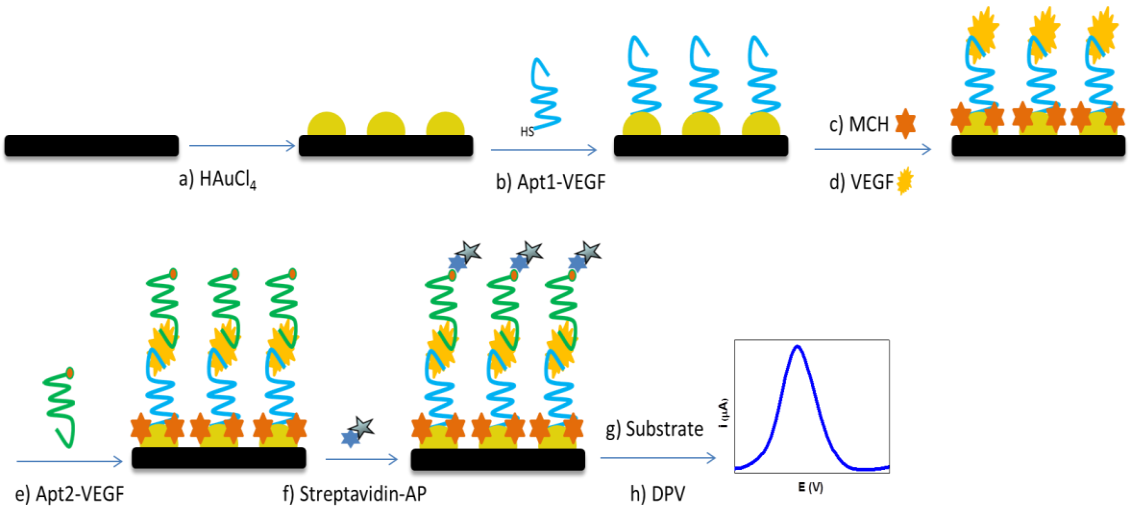

Figure 5.1. Schematic representation of the steps involved in the development of aptamers sandwich assay for VEGF detection: a) electrodeposition of gold nanoparticles AuNPs on graphite screen-printed electrodes (GSPEs); b) incubation with thiolated primary anti-VEGF aptamer (Apt1-VEGF); c) incubation with MCH protein; d) affinity reaction with VEGF; e) addition of biotinylated secondary anti-VEGF aptamer (Apt2-VEGF); f) incubation with streptavidin-alkaline phosphatase (streptavidin-AP); g) addition of the substrate (alpha-naphthyl phosphate) h) DPV measurements as described in materials and methods section.

3.1. Electrochemical impedance spectroscopy (EIS) surface characterization

Electrochemical impedance spectroscopy (EIS) measurements were used to characterize the modification of the graphite screen-printed electrode surface with AuNPs, to verify the functionalization of the electrodeposed AuNPs with thiolated Apt1-VEGF and the correct formation of a self-assembly monolayer (SAM) with MCH.

The measurements were performed using 0.01 M $[Fe(CN)_6]^{3-/4-}$ prepared in TBS KCl buffer (TRIS 0.01 M, NaCl 0.1 M, KCl 0.1 M, pH 7.4) as redox probe.

Resistance charge transfer (R_{ct}) was taken as analytical signal to characterize the modification of the electrode surface

Results are shown in the form of Nyquist plot, where the characteristic Faradic impedance shape can be observed in a semicircle region lying on x-axis (observed at high frequencies, corresponding to the kinetic control of the electron-transfer process), followed by a straight line (at low frequencies, related to the diffusive control of electron-transfer process) [34].

EIS spectra of bare graphite-screen printed electrode (GSPEs) and of the AuNPs-modified GSPEs (AuNPs/GSPEs) were reported in Figure 5.2.

A decrease in R_{ct} values from 22000 ± 250 Ohm (for bare GSPEs) to 750 ± 70 Ohm for (AuNPs/GSPEs) was observed. This result is in accordance with what reported in

literature confirming the formation of a randomly distributed AuNPs onto the entire electrode surface.

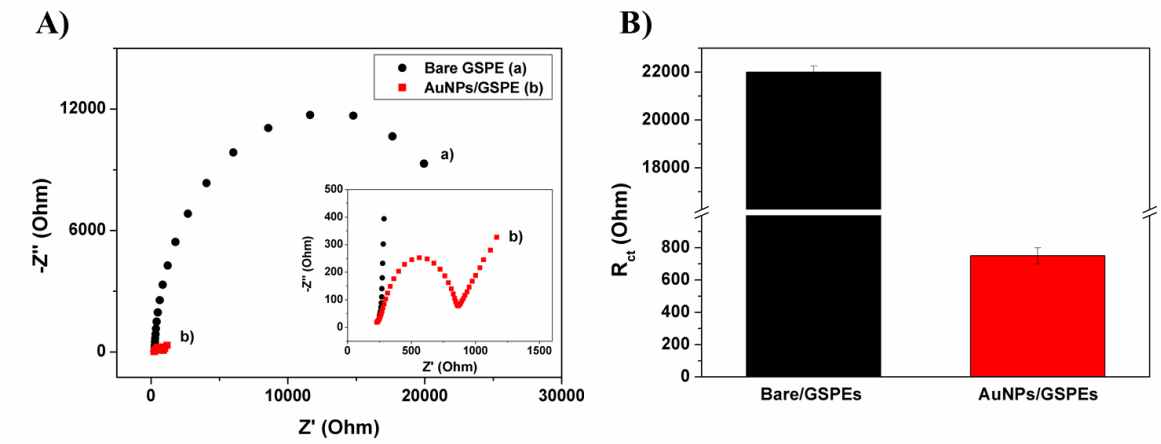

Figure 5.2. A) Nyquist plot of bare graphite screen-printed electrode (GSPE, ●) and of gold nanoparticles-modified graphite screen-printed electrode (AuNPs/GSPE, ■). Inset: magnification of AuNPs/GSPEs EIS spectrum. B) Average and standard deviation respect to the R_{ct} for bare GSPEs and for (AuNPs/GSPEs). EIS measurements were performed as reported in materials and methods section using 3 different electrodes.

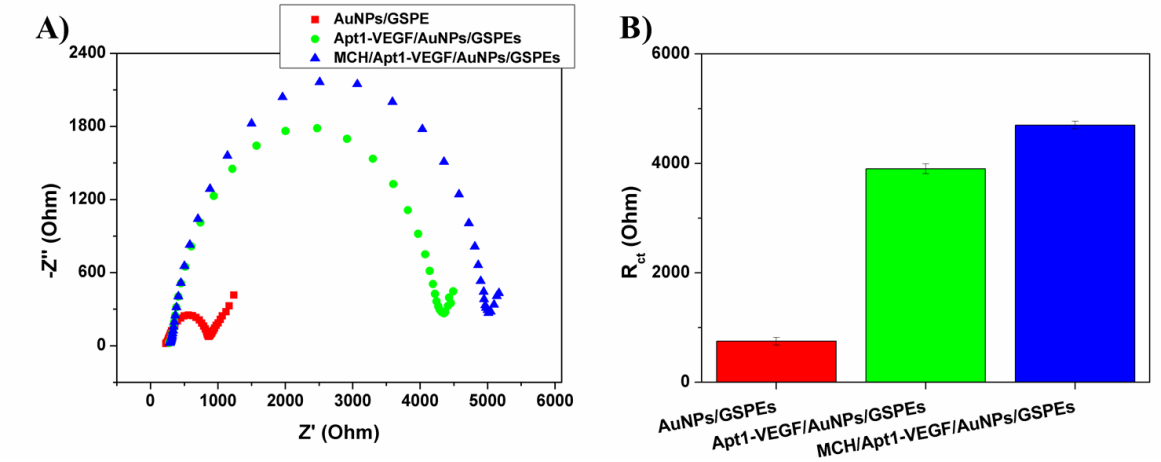

Figure 5.3. A) Nyquist plot of gold nanoparticles-modified graphite screen-printed electrodes (AuNPs/GSPEs, ■) and after the functionalization with thiolated primary anti-VEGF aptamer (Apt1-VEGF/AuNPs/GSPEs, ●) and after formation of mixed SAM monolayer with 6-mercapto-1-hexanol (MCH/Apt1-VEGF/AuNPs/GSPEs, ▲). B) Average and standard deviation respect to the R_{ct} for bare AuNPs/GSPEs, Apt1-VEGF/AuNPs/GSPEs and MCH/Apt1-VEGF/AuNPs/GSPEs. EIS measurements were performed as reported in materials and methods section using 3 different electrodes.

After the functionalization of AuNPs-modified GSPEs with thiolated Apt1-VEGF aptamer, an increase of R_{ct} up to 4000 ± 70 Ohm was determined.

This result is coherent with the fact that negative charged DNA sequence decrease the electron transfer from the solution of $[Fe(CN)_6]^{3-/4-}$ redox probe to the electrode surface

(thus increasing R_{ct} value) because the electrostatic repulsion between the negative backbone of the aptamer and the electrons of the redox mediator [35]. Moreover, after the incubation with MCH an increase of R_{ct} values up to 4700±80 Ohm was reported due to the formation of the mixed SAM necessary to prevent the non-specific adsorption of the protein on the electrode surface without altering the aptamer folding (Figure 5.3) [36].

3.2. Detection of VEGF by aptamers sandwich biosensor

After the functionalization with biotinylated secondary anti-VEGF aptamer (Apt2-VEGF), the assay was completed incubating the sensor with streptavidin-alkaline phosphatase and with redox substrate alpha-naphthyl phosphate.

The redox peak of enzymatic product alpha-naphthol was used to calculate the calibration curve using differential pulse voltammetry (DPV) technique.

Results are shown in Figure 5.4 A linear calibration curve ($y = 0.01x + 0.73$ $R^2 = 0.98$) was obtained in the range for 0 to 250 nM with a LOD (calculated as LOD = $3S_{blank}$/Slope) of 30 nM confirming the binding of VEGF protein between the two different aptamers.

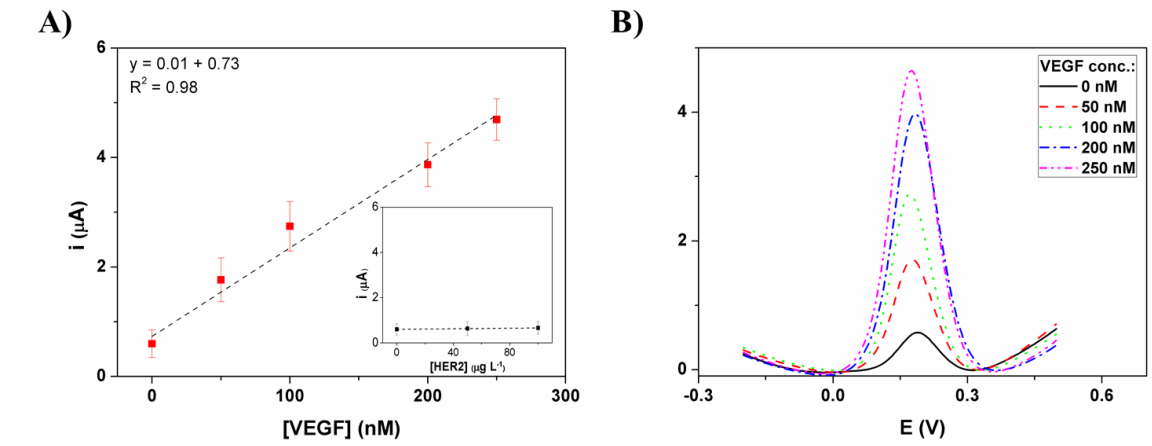

Figure 5.4. A) Calibration plots for VEGF detection through aptamers sandwich assay obtained by DPV measurements. Inset: aspecific signal obtained with HER2 protein (50, 100 µg L^{-1}). B) DPV voltammograms obtained through aptamers sandwich assay for VEGF concentration: 0, 50, 100, 200, 250 nM. Each point was repeated at least 3 times using different modified screen-printed graphite electrodes.

In order to evaluate the selectivity of the aptasensor, human epidermal growth factor receptor 2 (HER2) protein was used as non-specific antigen.

As can be observed in Figure 5.4 A inset, a very similar current values (compared to the blank) was obtained using HER2 (50 and 100 µg L^{-1}). This result confirms that the

observed increasing of current is originated from the specific recognition of VEGF by Apt1-VEGF and Apt2-VEGF.

4. Conclusions

In this work an aptamers sandwich assay based on gold-nanostructured graphite screen-printed electrodes for detection of VEGF cancer biomarker was realized.

Thiolated primary aptamer (Apt1-VEGF) and biotinylated secondary aptamer (Apt2-VEGF) bind with high affinity and selectivity two different domains present of VEGF molecule.

A good linear relationship between the current and the VEGF concentration in the range of 0 – 250 nM with a LOD of 30 nM and was obtained.

The sensitivity and the reproducibility achieved were adequate for the analysis of serum samples, since the VEGF levels in pathological conditions (although with high variability) is higher the 1 ng mL^{-1}.

Moreover the developed sandwich aptasensor shown good selectivity when HER2 protein was used instead of VEGF. Future experiments will be performed in spiked and real sample to verify the responses of both immunosensors for their use in clinical analysis.

References:

[1] Athey VL, Suckling RJ, Tod AM, Walters SJ, Rogers TK. Early diagnosis of lung cancer: evaluation of a community-based social marketing intervention. Thorax 2012; 67:412-7.
[2] Brenner H, Bouvier AM, Foschi R, et al. Progress in colorectal cancer survival in Europe from the late 1980s to the early 21st century: The EUROCARE study. International Journal of Cancer 2012; 131:1649-58.
[3] Ott JJ, Ullrich A, Miller AB. The importance of early symptom recognition in the context of early detection and cancer survival. European Journal of Cancer 2009; 45:2743-8.
[4] Carmeliet P. VEGF as a key mediator of angiogenesis in cancer. Oncology 2005; 69 Suppl 3:4-10.
[5] Gatenby RA, Gillies RJ. Hypoxia and metabolism - Opinion - A microenvironmental model of carcinogenesis. Nat Rev Cancer 2008; 8:56-61.
[6] Holash J, Wiegand SJ, Yancopoulos GD. New model of tumor angiogenesis: dynamic balance between vessel regression and growth mediated by angiopoietins and VEGF. Oncogene 1999; 18:5356-62.
[7] Liu W, Xu J, Wang M, Wang Q, Bi Y, Han M. Tumor-derived vascular endothelial growth factor (VEGF)-a facilitates tumor metastasis through the VEGF-VEGFR1 signaling pathway. International journal of oncology 2011; 39:1213-20.
[8] Hoeben A, Landuyt B, Highley MS, Wildiers H, Van Oosterom AT, De Bruijn EA. Vascular endothelial growth factor and angiogenesis. Pharmacological reviews 2004; 56:549-80.
[9] Inoue M, Hager JH, Ferrara N, Gerber HP, Hanahan D. VEGF-A has a critical, nonredundant role in angiogenic switching and pancreatic beta cell carcinogenesis. Cancer Cell 2002; 1:193-202.
[10] McMahon G. VEGF receptor signaling in tumor angiogenesis. The oncologist 2000; 5 Suppl 1:3-10.
[11] Harris AL. Hypoxia--a key regulatory factor in tumour growth. Nat Rev Cancer 2002; 2:38-47.
[12] Hendriksen EM, Span PN, Schuuring J, et al. Angiogenesis, hypoxia and VEGF expression during tumour growth in a human xenograft tumour model. Microvascular research 2009; 77:96-103.
[13] Jin-no K, Tanimizu M, Hyodo I, et al. Circulating vascular endothelial growth factor (VEGF) is a possible tumor marker for metastasis in human hepatocellular carcinoma. J Gastroenterol 1998; 33:376-82.
[14] Mitsuhashi A, Suzuka K, Yamazawa K, Matsui H, Seki K, Sekiya S. Serum vascular endothelial growth factor (VEGF) and VEGF-C levels as tumor markers in patients with cervical carcinoma. Cancer 2005; 103:724-30.
[15] Poon RT, Lau CP, Cheung ST, Yu WC, Fan ST. Quantitative correlation of serum levels and tumor expression of vascular endothelial growth factor in patients with hepatocellular carcinoma. Cancer Res 2003; 63:3121-6.
[16] Zhao J, Yan F, Ju H, Tang J, Qin J. Correlation between serum vascular endothelial growth factor and endostatin levels in patients with breast cancer. Cancer Letters 2004; 204:87-95.
[17] Ferrara N, Gerber HP, LeCouter J. The biology of VEGF and its receptors. Nature medicine 2003; 9:669-76.

[18] Park JE, Keller GA, Ferrara N. Vascular Endothelial Growth-Factor (Vegf) Isoforms - Differential Deposition into the Subepithelial Extracellular-Matrix and Bioactivity of Extracellular Matrix-Bound Vegf. Mol Biol Cell 1993; 4:1317-26.
[19] Strehlitz B, Nikolaus N, Stoltenburg R. Protein Detection with Aptamer Biosensors. Sensors 2008; 8:4296-307.
[20] McCauley TG, Hamaguchi N, Stanton M. Aptamer-based biosensor arrays for detection and quantification of biological macromolecules. Analytical Biochemistry 2003; 319:244-50.
[21] de-los-Santos-Álvarez N, Lobo-Castañón MaJ, Miranda-Ordieres AJ, Tuñón-Blanco P. Aptamers as recognition elements for label-free analytical devices. TrAC Trends in Analytical Chemistry 2008; 27:437-46.
[22] Ellington AD, Szostak JW. Invitro Selection of Rna Molecules That Bind Specific Ligands. Nature 1990; 346:818-22.
[23] Mascini M, Aptamers in bioanalysis. Hoboken, N.J.: J. Wiley & Sons, 2009.
[24] Song S, Wang L, Li J, Fan C, Zhao J. Aptamer-based biosensors. TrAC Trends in Analytical Chemistry 2008; 27:108-17.
[25] Mascini M, Palchetti I, Tombelli S. Nucleic Acid and Peptide Aptamers: Fundamentals and Bioanalytical Aspects. Angewandte Chemie International Edition 2012; 51:1316-32.
[26] de la Escosura-Muñiz A, Parolo C, Merkoçi A. Immunosensing using nanoparticles. Materials Today 2010; 13:24-34.
[27] Daniel MC, Astruc D. Gold nanoparticles: Assembly, supramolecular chemistry, quantum-size-related properties, and applications toward biology, catalysis, and nanotechnology. Chem Rev 2004; 104:293-346.
[28] Pérez-López B, Merkoçi A. Nanomaterials based biosensors for food analysis applications. Trends in Food Science & Technology 2011; 22:625-39.
[29] Merkoçi A. Nanoparticles-based strategies for DNA, protein and cell sensors. Biosensors and Bioelectronics 2010; 26:1164-77.
[30] Pingarrón JM, Yáñez-Sedeño P, González-Cortés A. Gold nanoparticle-based electrochemical biosensors. Electrochim Acta 2008; 53:5848-66.
[31] Nonaka Y, Sode K, Ikebukuro K. Screening and Improvement of an Anti-VEGF DNA Aptamer. Molecules 2010; 15:215-25.
[32] Hasegawa H, Sode K, Ikebukuro K. Selection of DNA aptamers against VEGF(165) using a protein competitor and the aptamer blotting method. Biotechnol Lett 2008; 30:829-34.
[33] Ravalli A, dos Santos GP, Ferroni M, Faglia G, Yamanaka H, Marrazza G. New label free CA125 detection based on gold nanostructured screen-printed electrode. Sensors and Actuators B: Chemical 2013; 179:194-200.
[34] Lisdat F, Schäfer D. The use of electrochemical impedance spectroscopy for biosensing. Anal Bioanal Chem 2008; 391:1555-67.
[35] Lucarelli F, Marrazza G, Turner APF, Mascini M. Carbon and gold electrodes as electrochemical transducers for DNA hybridisation sensors. Biosensors and Bioelectronics 2004; 19:515-30.
[36] Lucarelli F, Marrazza G, Mascini M. Enzyme-based impedimetric detection of PCR products using oligonucleotide-modified screen-printed gold electrodes. Biosensors and Bioelectronics 2005; 20:2001-9.

CHAPTER 6

Engineered protein scaffolds-based label-free gold nanostructured biosensor for HER2 breast cancer biomarker detection

A. Ravalli [a], C. G. da Rocha [b], H. Yamanaka [b], G. Marrazza [a]

[a] Department of Chemistry "Ugo Schiff", University of Florence, Via della Lastruccia 3, 50019 Sesto Fiorentino, Florence, Italy

[b] Department of Analytical Chemistry, São Paulo State University (UNESP), Rua Prof. Francisco Degni, 14800-900, Araraquara/SP, Brazil

Corresponding author. Tel.: +39 055-4573320
E-mail address: giovanna.marrazza@unifi.it

Abstract

In this work we reported the development of a label-free gold nanostructured biosensor using anti-HER2 engineered protein scaffolds as bioreceptor for the detection of HER2 breast cancer biomarker. The biosensor is based on the immobilization of the terminal cysteine-modified Affibody® on the surface of AuNPs-modified GSPEs *via* Au-SH bonds. After the formation of self-assembly monolayer, bioreceptor-antigen affinity reaction was evaluated by means of electrochemical impedance spectroscopy (EIS) technique. Linear calibration curve was obtained using HER2 concentration ranging from 0 to 40 μg L^{-1}. The proposed assay showed a limit of detection (calculated as $3S_{blank}$/Slope) of 6.7 μg L^{-1}.

Preliminary experiments in human serum samples spiked with HER2 protein were also conducted.

Each experimental step was characterized and evaluated by means of EIS measurements. Finally, the reproducibility and the selectivity of the affinity sensor were determined.

1. Introduction

Detecting cancer at early stage is one of the largest factors associated with successful treatment outcome. The classical methods (such as ELISA immunoassays) for diagnosis of cancer may take several hours, or even days from when tests are ordered to when results are received. These methods can be tedious, time consuming and often require extra care and expensive instruments making early diagnosis of cancer more difficult especially for the cancer patients who are admitted to an emergency department. Therefore, measurement of carcinomatous markers is critical in assisting the diagnosis of cancer and electrochemical biosensors can satisfy the rapid diagnosis requirements in cancer marker detection during early stages of the disease [1-4].

For this reason, the development of biosensors for the detection and monitoring of cancer biomarkers is a major area of recent researches [2].

Antibodies (Abs) have been the most used biorecognition elements. Antibodies are proteins produced in animals as an immune response to the presence of a foreign substance (called antigen) for which they have specific affinity [5, 6]. The quality of the designed immunosensor depends on the affinity and selectivity of the selected antibody to its antigen, as well as the proper immobilization of the antibody, with an optimum density and adjusted orientation for the antigen binding [7].

Despite the wide use of Abs for biosensing applications, some limitations still remain presents. In particular, antibodies (both monoclonal either polyclonal) are selected and produced using animals. Consequently, antibodies generation, as well as presenting ethical issues, becomes difficult with molecules which are toxic or not well tolerated by the host. In order to overcome immunoglobulin limitation, another field of investigation is represented by the development of alternative binding proteins (based either on scaffold with the immunoglobulin fold or on completely different protein topologies), called collectively engineered protein scaffolds [8-10].

Among this, Affibodies® received particular attentions and found application in several studies especially for *in vivo* diagnostic imaging [11, 12] and targeted cancer therapy applications [13, 14].

Affibody® molecules are being developed by a Swedish biotechnology company (Affibody® AB) and are an engineered version (Z domain) of one of the five stable three-a-helix bundle domains from the immunoglobulin Fc-binding region of staphylococcal

protein A. Affibody® molecules are constituted by only 58 amino acids without disulphide bonds and can therefore be produced in simpler organism such as prokaryote, rather than the animal system required in antibody synthesis [15].

Moreover, due to their small size they can also be chemically synthesised using solid phase peptide synthesis (SPPS), which eliminates the need for biological systems for production, but also means that specific site modification can be performed.

In fact, these biomolecules can include specific labels, such as fluorophores, radioactive labels and other moieties, such as biotin or cysteine groups, which can be used to couple the Affibody® to surfaces or other molecules, or surfaces. [16]

In this work, a label-free biosensors based on gold-nanoparticles (AuNPs) graphite screen-printed electrodes (GSPEs) using anti-HER2 Affibody® as bioreceptor was developed. We chose to use AuNPs as support both because their intrinsic properties (such as high area/volume ration, high biocompatibility) either because can be easily functionalized exploiting the high stability of Au-SH bonds.

HER2 is a cancer antigen that can be measured and evaluated as an indicator for normal biologic processes, pathogenic processes, or pharmacologic responses to therapeutic intervention. Specifically, the HER2 proto-oncogene is amplified and/or over expressed in approximately 20–25% of invasive breast cancers. Normal individuals have a HER2 concentration between 2 and 15 μg L^{-1} in the blood and breast cancer patients have blood HER2 levels from higher than 15 μg L^{-1}.The screening of HER2 on tumor biopsies is often used to evaluate whether a patient may successfully respond to therapy with Trastuzumab (Herceptin®), a monoclonal anti-HER2 antibody [17, 18].

In this work we reported the development of a label-free gold nanostructured biosensor using anti-HER2 Affibody® as bioreceptor for the detection of HER2 breast cancer biomarker. The assay is based on the immobilization of the terminal cysteine-modified Affibody® on the surface of AuNPs-modified GSPEs *via* Au-SH bonds.

After the formation of self-assembly monolayer, bioreceptor-antigen affinity reaction was evaluated by means of electrochemical impedance spectroscopy (EIS) technique. Preliminary experiments in human serum sample spiked with HER2 protein were also conducted.

Each phases of the construction of the assay was characterized and evaluated by means of EIS measurements. Finally, the reproducibility and selectivity were determined.

2. Materials and methods

2.1 Chemicals

Sodium chloride, tetrachloroauric (III) acid ($HAuCl_4$), 6-mercapto-1-hexanol (MCH), dithiothreitol (DTT), tris(hydroxymethyl)aminomethane hydrochloride (TRIS), human serum sample were obtained from Sigma-Aldrich (Milan, Italy).

Sulfuric acid, potassium chloride, potassium ferrocyanide ($K_4[Fe(CN)_6]$), potassium ferricyanide ($K_3[Fe(CN)_6]$), disodium hydrogen phosphate (Na_2HPO_4), sodium dihydrogenphosphate dehydrate ($NaH_2PO_4 \cdot 2H_2O$), sulphuric acid, potassium ferrocyanide ($K_4[Fe(CN)_6]$) and potassium ferricyanide ($K_3[Fe(CN)_6]$) were purchased from Merck (Milan, Italy).

Anti-HER2 Affibody® was purchased from Affibody® AB, Sweden. Human epidermal growth factor receptor 2 (HER2) protein (R&D Systems) was obtained from Space srl (Milan, Italy).

Human vascular endothelial growth factor (VEGF) (Sigma-Aldrich, Milan, Italy) was used as aspecific control. Illustra™ NAP-5 column were obtained from GE Healthcare Italy (Milan, Italy).

2.2 Electrochemical apparatus

Electrochemical experiments were performed in a digital potentiostat/galvanostat AUTOLAB PGSTAT 30(2)/FRA2 controlled with the General Purpose Electrochemical System (GPES) and Frequency Response Analyzer (FRA2) 4.9 software (Eco Chemie, Utrecht, The Netherlands).

The immunosensor was assembled using screen-printed cells, comprising of a graphite working electrode (2.5 mm in diameter) and counter graphite electrode and a pseudo-silver reference [6]. The screen-printed cells were produced in house on a DEK 248 screen-printing machine (DEK, Weymouth, UK).

The printing was performed on a polyester film (Autostat CT5) from Autotype (Milan, Italy) using the polymeric inks (Electrodag PF-410 (silver)) and (Electrodag 423 SS (graphite)), which were purchased from Acheson (Milan, Italy). Vinylfast 36–100 was used as the insulting ink and was obtained from Argon (Lodi, Italy).

2.3 Electrochemical measurements

Faradic impedance measurements were carried out in the presence of 0.01 M $[Fe(CN)_6]^{3-/4-}$ redox probe (equimolecular mixture prepared in 0.1 M PBS buffer pH 7.4). A voltage of 10 mV in amplitude (peak-to-peak), within the frequency range 100 kHz – 10 mHz, was superimposed to the applied bias potential. The DC potential was set up to +0.13V, the formal potential of $[Fe(CN)_6]^{3-/4-}$ redox probe. Experimental spectra, presented in the form complex plane diagrams (i.e. Nyquist plot), were fitted with proper equivalent circuits using the facilities of the FRA2 4.9.004 (EcoChemie) software. Both charge transfer resistance (Rct) and Δ charge transfer resistance (ΔRct) values were taken as analytical signals. All potentials were referred to the silver screen-printed pseudo-reference electrode; the experiments were carried out at room temperature (25°C).
Electrodeposition of gold nanoparticles (AuNPs) onto graphite screen-printed electrodes (GSPEs) was obtained by cyclic voltammetry in the range 0 and +1.3 V *vs.* screen-printed silver pseudo-reference using 0.006 M $HAuCl_4$ prepared in 0.5 M H_2SO_4 solution.

2.4 Experimental procedure for HER2 biosensor development

2.4.1 Electrodeposition of gold-nanoparticles onto graphite screen-printed electrodes

Electrodeposition of gold nanoparticles (AuNPs) on the surface of graphite screen-printed electrodes (GSPEs), was realized in accordance with the optimized procedure reported in our previously work [19]. Briefly, 50 μL of 0.0006 M of $HAuCl_4$ solution (prepared in 0.5 M H_2SO_4) were placed onto GSPEs surface. Subsequently, the potential was cycled from -0.2 and +1.6 V *vs.* pseudo-reference silver screen-printed electrode for 25 cycles using a scan-rate of 0.1 V s^{-1}. Finally, AuNPs-modified GSPEs were then washed 3 times with Milli-Q water.

2.4.2 Anti-HER2 Affibody® immobilization onto AuNPs-modified GSPEs

2.4.2.1 Procedure for reduction of the Affibody® cysteine residues

Anti-HER2 Affibody® molecule contains a C-terminal cysteine ideal for directed chemical modifications. However, tail-to-tail dimers are spontaneously generated via a disulfide bridge between the C-terminal cysteines.

Prior to immobilization of bioreceptor molecules onto AuNPs-modified GSPEs, C-terminal cysteine dimers were reduced.

As suggested from the producer, lyophilized anti-HER2 Affibody® was dissolved in 500 mL of 0.02 M dithiothreitol (DTT) prepared in 0.01 M TRIS buffer, pH 8.5 and left to incubate for 120 minutes.

After, the solution was injected into Illustra NAP-5 column (previously equilibrated with 10 mL of 0.1 M PBS, pH 7.4) and eluted with 1 mL of 0.1 M PBS, pH 7.4. This stock solution (100 μg L^{-1}) was then stored in freezer (-20 °C) and aliquoted for further experiments.

2.4.2.2 Functionalization on AuNPs/GSPEs with reduced anti-HER2 Affibody®

10 μL of 1 μg L^{-1} of cysteine-reduce anti-HER2 Affibody® prepared in 0.1 M PBS pH 7.4 buffer solution, were placed on the surface of AuNPs-modified GSPEs and incubated overnight in a home-made wet chamber at 25° C.

After, the anti-HER2 bioreceptors-modified electrodes were rinsed three times with 0.1 M PBS pH 7.4 buffer in order to remove unbound molecules.

2.4.3 Mixed SAM formation

Anti-HER2 Affibody®-modified AuNPs/GSPEs were incubated with 10 μL of 0.001 M MCH solution for 30 minutes at 25 ºC in order to block the free surface on AuNPs, thus reducing the aspecific adsorption of other molecules. Subsequently, the electrodes were washed three times with three times with 0.1 M PBS pH 7.4 buffer.

2.4.4 Affinity reaction with HER2 protein and aspecific protein control experiment

To develop the calibration curve, the sensors were incubated with different concentrations of HER2 (0, 10, 20, 30, 40 μg L^{-1}) protein for 60 minutes at 25 °C. The sensors were then rinsed with 0.1 M PBS pH 7.4 buffer solution.

Affinity reaction was determined by means of electrochemical impedance spectroscopy (EIS) measurements as reported in materials and method section.

The control experiments were performed using human vascular endothelial growth factor (VEGF) protein at 40 μg L^{-1}.

2.4.5 Serum samples analysis

Preliminary experiments for the determination of HER2 protein in serum samples were also performed.

The anti-HER2 Affibody® biosensor response was tested in 1/200 diluted (in PBS 0.1 M, pH 7.4) filtered (0.45 µm) human serum samples spiked with standard addition of HER2 protein (10, 20, 30 µg L^{-1}).

The response of the biosensor was the determined by EIS measurements in the same condition described in materials and methods section.

3. Results and discussion

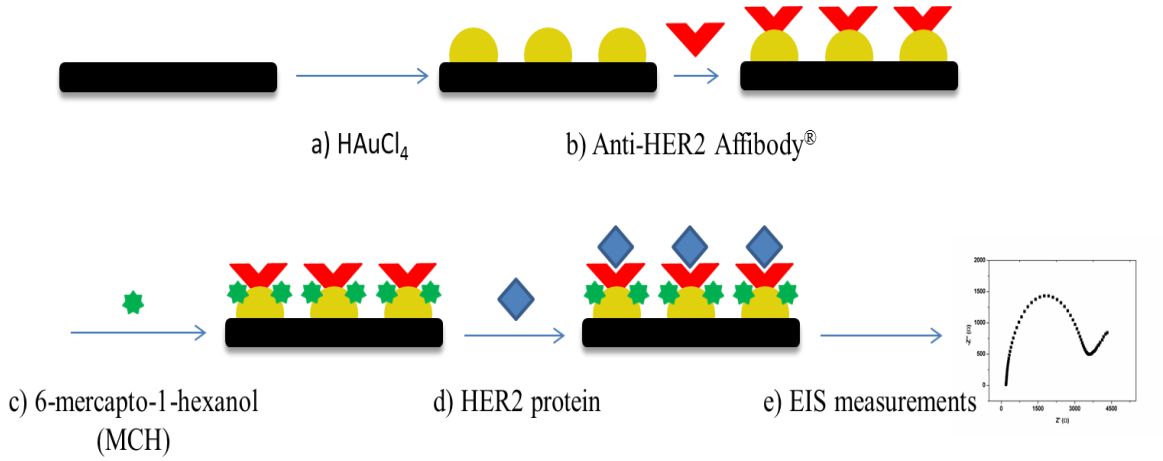

Figure 6.1. Schematic representation of engineered protein scaffolds-based label-free gold nanostructured biosensor for HER2 breast cancer biomarker detection: a) electrodeposition of gold nanoparticles (AuNPs) on graphite screen-printed electrodes (GSPEs); b) functionalization with anti-HER2 Affibody® molecules); c) Incubation with MCH; d) affinity reaction with HER2 protein; e) label-free HER2 determination by electrochemical impedance spectroscopy (EIS) measurements.

Figure 6.1 shows the schematic representation of the steps involved in the development of anti-HER2 Affibody® label-free assay based on gold nanoparticle-modified graphite screen-printed electrodes for the determination of HER2 cancer biomarker.

The protocol involves the following steps:

a) electrodeposition of gold nanoparticles (AuNPs) on graphite screen-printed electrodes (GSPEs); b) functionalization with anti-HER2 Affibody® molecules); c) Incubation with MCH; d) affinity reaction with HER2 protein; e) label-free HER2 determination by electrochemical impedance spectroscopy (EIS) measurements. EIS technique was also used to characterize each step necessary for the modification of the electrode surface.

3.1 Electrodeposition of AuNPs onto graphite screen-printed electrodes (GSPEs)

According with our previous work [19], AuNPs-modified GSPEs shown R_{ct} values about 30 time lower respect to bare GSPEs (respectively 750 ± 70 Ohm and 22000 ± 250 Ohm) demonstrating the formation of randomly distributed AuNPs (with size comprise between 40 and 100 nm) all over the working electrode surface of GSPEs.

3.2 Electrochemical impedance spectroscopy (EIS) surface characterization

Electrodeposed AuNPs represent a useful platform for the immobilization of the bioreceptors due to the high affinity and easy functionalization with thiols groups.

Because anti-HER2 Affibody® contains C-terminal cysteine, its immobilization on the AuNPs-modified electrode surface can be performed in a single step permitting also the correct orientation of the bioreceptor for the recognition of the target protein.

In order to prove the functionalization of the electrodeposed AuNPs anti-HER2 Affibody® and the following formation of mixed self-assembly monolayer (SAM) with 6-mercapto-1-hexanol (MCH), EIS measurements were performed using 0.01 M $[Fe(CN)_6]^{3-/4-}$ as redox probe prepared in PBS buffer (0.1 M, pH 7.4).

Resistance charge transfer (R_{ct}) was taken as analytical signal to characterize the modification of the electrode surface.

Nyquist plot of EIS measurements conducted on anti-HER2 Affibody®-modified electrodeposed gold nanoparticles (anti-HER2 Affibody®/AuNPs/GSPEs) and after the formation of SAM with MCH (MCH/anti-HER2 Affibody®/AuNPs/GSPEs) were reported in Figure 6.2.

After the modification of AuNPs/GSPEs with anti-HER2 bioreceptors an increase of R_{ct} values respectively form 750 ± 50 Ohm to 1700 ± 80 Ohm is observed.

Results is coherent with the presence onto the AuNPs/GSPEs surface of a layer of protein that hinders (because steric hindrance and electrostatic repulsions) the electron transfer from the redox probe solution to the electrode surface confirming the realization of the functionalization step.

The same behaviour was observed after the formation of the SAM with MCH (R_{ct} = 1900 ± 70 Ohm.

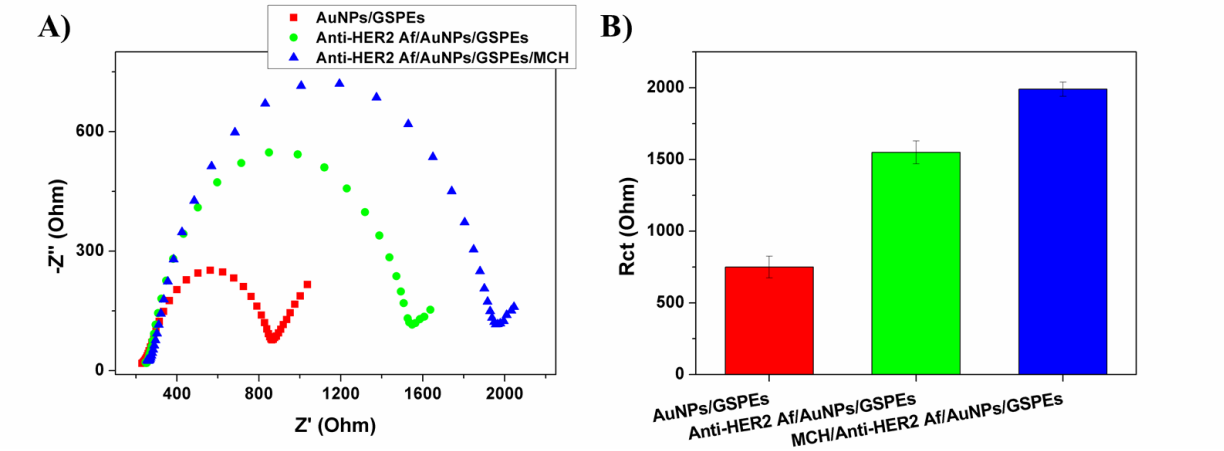

Figure 6.2. A) Nyquist plot of gold nanoparticles-modified graphite screen-printed electrodes (AuNPs/GSPEs, ■), after the functionalization with anti-HER2 Affibody® (anti-HER2 Af/AuNPs/GSPEs, ●) and with 6-mercapto-1-hexanol (MCH/anti-HER2 Af/AuNPs/GSPEs, ▲) obtained in 0.01 M $[Fe(CN)_6]^{3-/4-}$ equimolecular mixture in 0.1 M PBS, pH 7.4. B) Average and standard deviation respect to the R_{ct} for AuNPs/GSPEs, anti-HER2 Af/AuNPs/GSPEs, MCH/anti-HER2 Af/AuNPs/GSPEs. The measurements were repeated at least 3 times using different GSPEs.

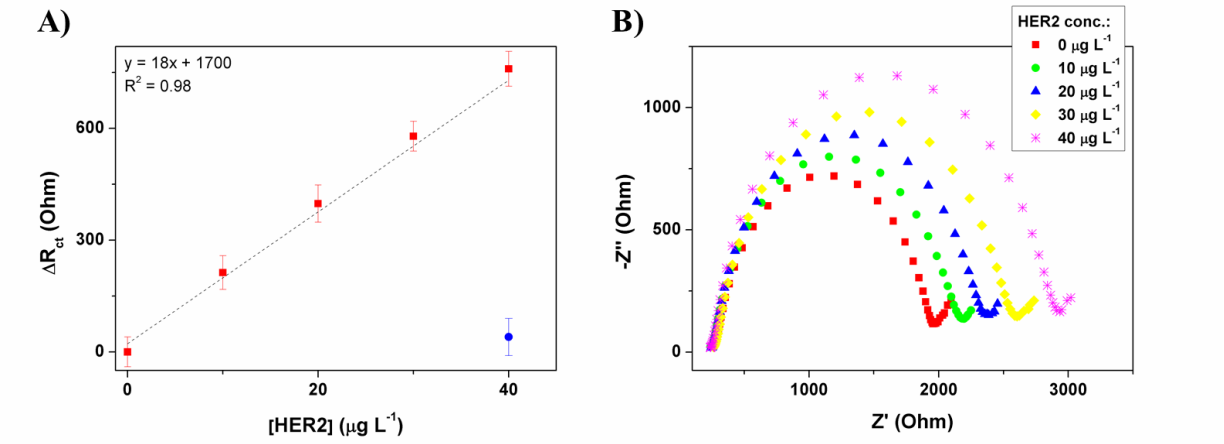

Figure 6.3. A) Calibration curve for HER2 cancer biomarker and aspecific test with 40 μg L^{-1} VEGF (●). B) Nyquist plot of Affibody®-HER2 affinity reaction obtained in 0.01 M $[Fe(CN)_6]^{3-/4-}$ equimolecular mixture in 0.1 M PBS, pH 7.4. The measurements were repeated at least 3 times using different GSPEs.

3.3 Label-free detection of HER2 cancer biomarker

The calibration curve for the detection of HER2 cancer biomarker was reported in figure 6.3 A.

Due to the affinity reaction between the antigen and the bioreceptor s(which led to the formation of a layer of protein that reduce the electron transfer from the redox mediator to the electrode surface), a proportional increase of R_{ct} was observed. A linear relationship ($y = 18x + 1700$, $R^2 = 0.98$) between the ΔR_{ct} (calculated as $\Delta R_{ct,HER2} - \Delta R_{ct,0}$) and concentration of HER2 was obtained in the range of 0 and 40 μg L^{-1} with a limit of detection (calculated as: $LOD = 3S_{blank}/Slope$) of 6.7 μg L^{-1}. The selectivity of the

proposed assay was evaluated using vascular endothelial growth factor (VEGF) 40 μg L^{-1} as aspecific protein. As can be observed in Figure 6.3 A, a very similar R_{ct} value compared to the blank was achieved, proving the selectivity of the developed biosensor.

3.4 Serum samples analysis

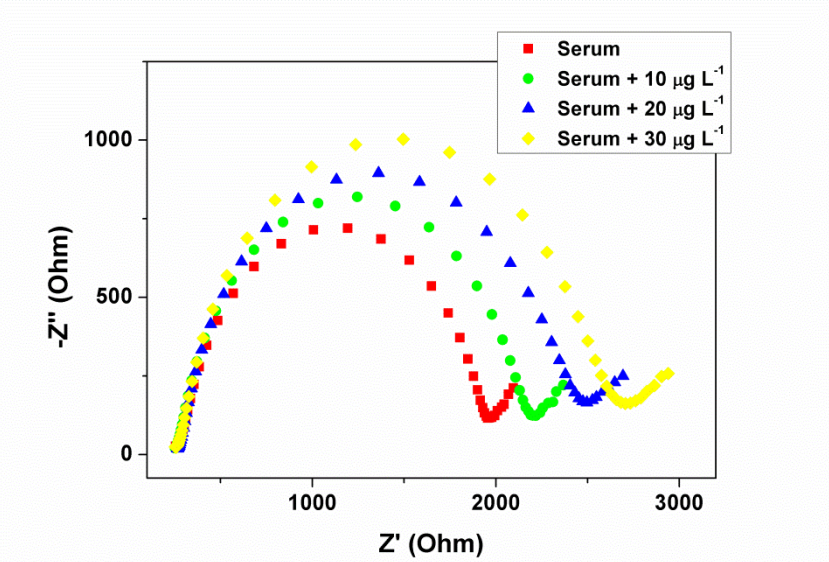

Figure 6.4. Nyquist plot of the biosensors response in serum samples spiked with HER2 (10, 20, 30 μg L^{-1}) obtained in 0.01 M $[Fe(CN)_6]^{3-/4-}$ equimolecular mixture in 0.1 M PBS pH 7.4. The measurements were repeated at least 3 times using different GSPEs.

In order to verify the suitability of the proposed biosensor in clinical applications, preliminary experiments using human serum samples was performed.

Experiments concerned 1/200 diluted and filtered human serum samples spiked with HER2 protein solution at a known concentration (10, 20, 30 μg L^{-1}).

Results are reported in the Figure 6.4. Increase of R_{ct} was proportional with the increase of HER2 concentration spiked in commercial serum samples, confirming the recognizing of HER2 cancer biomarker also in biological samples.

4. Conclusions

A label-free electrochemical biosensor based on the easy immobilization of anti-HER2 Affibody® bioreceptor on gold nanostructured graphite screen-printed electrode for the detection of HER2 cancer biomarker was developed. A good linear relationship between the electron transfer resistance (R_{ct}) and HER2 concentration in the range of 0 - 40 μg L^{-1}.

Limit of detection (calculated as LOD = $3S_{blank}$/Slope) was 6.7 μg L^{-1}, well below respect to the cut-off level of HER2 utilized in clinical analysis (15 μg L^{-1}).

The proposed Affibody®-based biosensors was also tested on the analysis of serum samples spiked with HER2 cancer biomarker, yielding promising results for use in clinical applications.

References

[1] Li J, Li S, Yang CF. Electrochemical Biosensors for Cancer Biomarker Detection. Electroanal 2012; 24:2213-29.
[2] Tothill IE. Biosensors for cancer markers diagnosis. Seminars in Cell & Developmental Biology 2009; 20:55-62.
[3] Soper SA, Brown K, Ellington A, et al. Point-of-care biosensor systems for cancer diagnostics/prognostics. Biosensors and Bioelectronics 2006; 21:1932-42.
[4] Laschi S, Tombelli S, Palchetti I, Mascini M, Marrazza G, New Affinity Biosensors as Diagnostic Tools for Tumour Marker Analysis. In: Baldini F, D'Amico A, Di Natale C, et al., editors. Sensors: Springer New York, 2014: 19-23.
[5] Ramirez NB, Salgado AM, Valdman B. The Evolution and Developments of Immunosensors for Health and Environmental Monitoring: Problems and Perspectives. Braz J Chem Eng 2009; 26:227-49.
[6] Wu J, Fu Z, Yan F, Ju H. Biomedical and clinical applications of immunoassays and immunosensors for tumor markers. TrAC Trends in Analytical Chemistry 2007; 26:679-88.
[7] Luppa PB, Sokoll LJ, Chan DW. Immunosensors—principles and applications to clinical chemistry. Clin Chim Acta 2001; 314:1-26.
[8] Binz HK, Amstutz P, Pluckthun A. Engineering novel binding proteins from nonimmunoglobulin domains. Nature biotechnology 2005; 23:1257-68.
[9] Gebauer M, Skerra A. Engineered protein scaffolds as next-generation antibody therapeutics. Curr Opin Chem Biol 2009; 13:245-55.
[10] Skerra A. Alternative non-antibody scaffolds for molecular recognition. Curr Opin Biotech 2007; 18:295-304.
[11] Lee SB, Hassan M, Fisher R, et al. Affibody molecules for in vivo characterization of HER2-positive tumors by near-infrared imaging. Clinical Cancer Research 2008; 14:3840-9.
[12] Orlova A, Magnusson M, Eriksson TLJ, et al. Tumor Imaging using a picomolar affinity HER2 binding affibody molecule. Cancer Res 2006; 66:4339-48.
[13] Tolmachev V, Orlova A, Nilsson FY, Feldwisch J, Wennborg A, Abrahmsen L. Affibody molecules: potential for in vivo imaging of molecular targets for cancer therapy. Expert Opin Biol Th 2007; 7:555-68.
[14] Tolmachev V, Orlova A, Pehrson R, et al. Radionuclide therapy of HER2-positive microxenografts using a 177Lu-labeled HER2-specific Affibody molecule. Cancer Res 2007; 67:2773-82.
[15] Nygren PA. Alternative binding proteins: affibody binding proteins developed from a small three-helix bundle scaffold. The FEBS journal 2008; 275:2668-76.
[16] Harris M, Tombelli S, Marrazza G, Turner AP, Affibodies as an alternative to antibodies in biosensors for cancer markers. In: Higson S, editor. Biosensors for medical applications: Woodhead Publishing Limited, 2012: 217-32.
[17] Gutierrez C, Schiff R. HER2: biology, detection, and clinical implications. Archives of pathology & laboratory medicine 2011; 135:55-62.
[18] Tai W, Mahato R, Cheng K. The role of HER2 in cancer therapy and targeted drug delivery. Journal of controlled release : official journal of the Controlled Release Society 2010; 146:264-75.

[19] Ravalli A, dos Santos GP, Ferroni M, Faglia G, Yamanaka H, Marrazza G. New label free CA125 detection based on gold nanostructured screen-printed electrode. Sensors and Actuators B: Chemical 2013; 179:194-200.

CHAPTER 7

Bioassays for multiplex detection of MUC1 tumor marker addressable to hospital patients for cancer screening

A. Florea[a,b], A. Ravalli[a], C. Cristea[b], R. Sandulescu[b], G. Marrazza[a]

[a] Department of Chemistry "Ugo Schiff", University of Florence, Via della Lastruccia 3, 50019, Sesto Fiorentino, Florence, Italy

[b] Department of Analytical Chemistry, Faculty of Pharmacy, University of Medicine and Pharmacy, Iuliu Hatieganu", Pasteur 4, Cluj-Napoca, Romania

*Corresponding author: tel. +39 055 4573320, fax +39 055 4573396, e-mail:
E-mail: giovanna.marrazza@unifi.it

Abstract

In this work, different electrochemical bioassays for Mucin1 (MUC1) tumor marker using magnetic beads coupling screen-printed arrays were developed and used for analysis in biological samples. The bioassays are based on a sandwich format in which aptamers or antibodies were coupled respectively to Streptavidin or Protein G-modified magnetic beads. The MUC1 protein was captured by bioreceptor-modified beads followed by the addition of a secondary aptamer or antibody to complete the sandwhich. The enzyme alkaline phosphatase (AP) and its substrate (1-naphthyl phosphate) are then used for the electrochemical detection by differential pulse voltammetry (DPV). The analytical performance of the designed assays was compared in terms of sensitivity, selectivity and reproducibility. Under the optimal conditions, a linear response was obtained ranging from 0 to 10 ng mL^{-1} in MUC1 buffered solution for all three assays, with detection limits: 2.5, 2.4 and 1.36 ng mL^{-1}, respectively for antibodies-based, aptamer-antibody-based and aptamers-based sandwich assays. The results showed that the aptamer-based approaches exhibit higher selectivity for MUC1, allowing the detection of the protein in complex matrices. The developed aptasensor for multiplex detection was applied on serum samples obtained from cancer patients, providing promising perspectives for clinical applications.

Keywords: immunosensor, MUC1, magnetic beads, aptamer, multiarray, electrochemical detection

1. Introduction

In recent years, increasing efforts have been focused on the development of affinity sensors for biomedical, food-safety and environmental applications [1-4].

A key step in the construction of affinity sensors is represented by the selection of an appropriate biorecognition element that binds the target molecule. Antibodies have been widely applied as recognition elements [5-7]. The quality of the designed immunosensor depends on the affinity and selectivity of the selected antibody to its antigen, as well as the proper immobilization of the antibody, with an optimum density and adjusted orientation for the antigen binding [8].

To overcome problems relating to stability of antibodies and to improve specificity and sensitivity of affinity biosensors, synthetic molecules such as peptides and nucleic aptamers or molecularly imprinted polymers have been explored [9, 10].

In recent years aptamers have been studied intensively because they offer significant advantages over antibodies such as easy synthesis, easy labelling, good stability and resistance to denaturation, high specificity for target molecules and the possibility to distinguish between very similar targets [11-14].

Different affinity sensors have been designed improving the analytical performances in real samples. The use of micro- and nano-particles either as immobilization platforms [15, 16] or as labels [17, 18] has attracted major attention lately. Their use as a solid support for the immobilization of the recognition element has many advantages such as fast and specific immobilization of a wide amount of bioelements due to the large binding surface conferred by their geometry and small size, leading therefore to an improved sensitivity, easy separation after the washing and reaction steps, easy manipulation, reduction of the analysis time and reagents consumption. In addition magnetic beads-based assay could be successfully applied to biological samples without the requirement of any purification steps, reducing at the same time the matrix effect due to the improved washing steps [19, 20]. The proposed approaches uses disposable screen-printed arrays as transducers and a simple target capturing step by aptamers or antibodies functionalised magnetic beads. Screen-printed cells (SPCs) are widely used as electrochemical sensing due to their simple, rapid and inexpensive manufacturing process, the possibility of mass production and the ability to print the entire electrode system on one solid support to obtain disposable devices. In the fabrication process of carbon SPCs are particularly of interest

due to their advantages of being relatively inexpensive and leading to low background currents and broad potential windows. SPC arrays have the advantage of simultaneous analysis of different samples, reducing the analysis time. Several disposable immunosensors have been developed on SPC arrays in the field of clinical or food analysis [21-24].

Given the fact that immunosensors for tumor markers detection attracted considerable interest lately, MUC1 tumor marker was selected as model molecule. MUC1 is a trans-membrane glycoprotein expressed on the apical surface of various epithelial cells, which loses its apical distribution in case of malignant neoplasm, becomes over expressed and it is secreted into the blood circulation [25] serving therefore as potential tumor marker and prognosis factor in different types of cancer such as ovarian [26], breast [27], lung [28] or pancreatic cancer [29].

In this study three different approaches were employed in a sandwich format using magnetic beads as solid support and antibodies or aptamers as biorecognition molecules. The aptamers used in this work were selected from a library of aptamers, designed by SELEX, that were shown to have the ability to recognize MUC1 protein, the affinity for MUC1 being tested by ELISA tests and SPR [30, 31].

The target molecule is captured between the primary antibody or aptamer immobilized on the magnetic beads and a secondary antibody or secondary aptamer. The affinity reaction is labelled with Alkaline Phosphatase (AP) in different assay configurations. All variables concerning the all bioassays were optimized. The electrochemical multidetection is achieved on graphite based eight screen-printed cells, by DPV, through the addition of the enzymatic substrate (1-naphtyl phosphate) and its subsequent conversion to the electrochemical active compound 1-naphthol. In order to assess the suitability of the developed aptasensor and to evaluate the influence of the matrix effect, commercial serum samples spiked with different known concentration of MUC1 protein were also analysed. Moreover, serum samples obtained from hospital patients were analysed and the obtained results were compared with the histological diagnosis, demonstrating the potential applications for cancer screening.

2. Materials and methods

2.1. Chemicals and instrumentation

Dynabeads Protein G-coated magnetic beads and Streptavidin-coated magnetic beads were purchased from Invitrogen (Milan, Italy).

MUC1 protein, MUC1 monoclonal mouse antibody (Ab1), MUC1 polyclonal rabbit antibody (Ab2), MUC4 protein, MUC16 protein, polyclonal antibody anti-rabbit IgG labeled with alkaline phosphatase (Ab3-AP) were provided by Novus Biological (Cambridge, UK).

Two different aptamers were used in this work, having the sequences:

5'-GCAGTTGATCCTTTGGATACCCTGGTTTTTTTTTTTTTTT-3` - Biotin (Apt1)

5`-GAAGTGAAAATGACAGAACACAACATTTTTTTTTTTTTTT-3` - Biotin (Apt2)

The aptamers were purchased from AlphaDNA (Canada) and Eurofins (Germany).

1-naphthyl phosphate, diethanolamine, sodium chloride, potassium chloride, magnesium chloride, polyoxyethylene sorbitan monolaureate (Tween 20), biotin, bovine serum albumin, streptavidin-alkaline phosphatase, commercial non-pathological human serum were purchased from Sigma-Aldrich (Milan, Italy).

Tris(hydroxymethyl)amino-methane (TRIS) and ethylene-diamine-tetra-acetic acid (EDTA) were purchased from Merck (Milan, Italy).

The sample mixer was purchased from Dynal Biotech (Milan, Italy)

All solutions were prepared using water from Milli-Q Water Purification System (Millipore, UK) .

The following buffers were used in the experiments:

Buffer A: PBS 0.1 M, pH=7.4 with 0.005% w/w Tween 20

Buffer B: TRIS Buffer 50mM, NaCl 10 mM, pH=8.0 with or without 0.005% w/w Tween 20

Buffer C: TRIS 10mM, EDTA 1mM, NaCl 2 M, pH=7.5 with 0.005% w/w Tween 20

Buffer D: TRIS 10mM, NaCl 100mM, KCl 100 mM, $MgCl_2$ 5mM, pH=7.2 with 0.005% w/w Tween 20

Buffer E: DEA Buffer DEA 0.1 M, KCl 0.1 M, $MgCl_2$ 1 mM, pH=9.6 with 0.005% w/w Tween 20

Eight screen-printed cells were used in the experiments. Each cell is based on graphite working electrode (2.0 mm in diameter) each with a graphite counter electrode and a silver pseudo-reference electrode, produced on a DEK 248 (DEK,Weymouth, UK) screen printing machine. The printing was performed on a polyester film (Autostat CT5) from Autotype (Milan, Italy) using the polymeric inks (Electrodag PF-410 (silver)) and (Electrodag 423 SS (graphite)), which were obtained from Acheson (Milan, Italy). Vinylfast 36-100 was used as the insulting ink and was obtained from Argon (Lodi, Italy). An 8-holes methacrylate box is fixed onto the strip by using a double layer adhesive. Each hole is 8 mm diameter and it is positioned exactly in correspondence of each cell.
Electrochemical measurements were performed with μAutolab type II PGSTAT (Methrom, The Netherlands) with General Purpose Electrochemical System (GPES) 4.9 software and PalmSens handheld potentiostat (PalmSens BV, The Netherlands).
Differential pulse voltammetry (DPV) was employed as electrochemical technique using the following parameters: potential range: - 0.2 V to + 0.5 V; pulse amplitude 0.070 V; scan rate 0.033 V s^{-1}. The measurements were carried out at room temperature.

2.2. Electrochemical sandwich assays for MUC1 detection

Three different sandwich assays were employed for the detection of MUC1 tumor marker, using various bioreceptors (Fig. 7.1. A).
In the first assay, MUC1 monoclonal mouse antibody (Ab1) was immobilized on the surface of Protein G-coated magnetic beads followed by the addition of protein, secondary MUC1 polyclonal rabbit antibody (Ab2) and the third polyclonal anti-rabbit IgG labeled with alkaline phosphatase (Ab3-AP) (Fig. 7.1. A, a).
In the second approach, the primary antibody was replaced with the aptamer (Apt1).
The biotinylated aptamer immobilized on the surface of streptavidin-coated magnetic beads binds specifically the MUC1 protein, followed by the reaction with Ab2 and Ab3-AP (Fig. 7.1. A, b).
In the third assay, the antibodies were replaced with two different aptamers.

After the immobilization of primary biotinylated aptamer (Apt1) on streptavidin-magnetic beads and interaction with MUC1 protein, a secondary biotinylated aptamer (Apt2) binds the complex. Streptavidin-AP was used for labeling the formed Apt1-MUC1-Apt2 complex (Fig. 7.1. A, c).

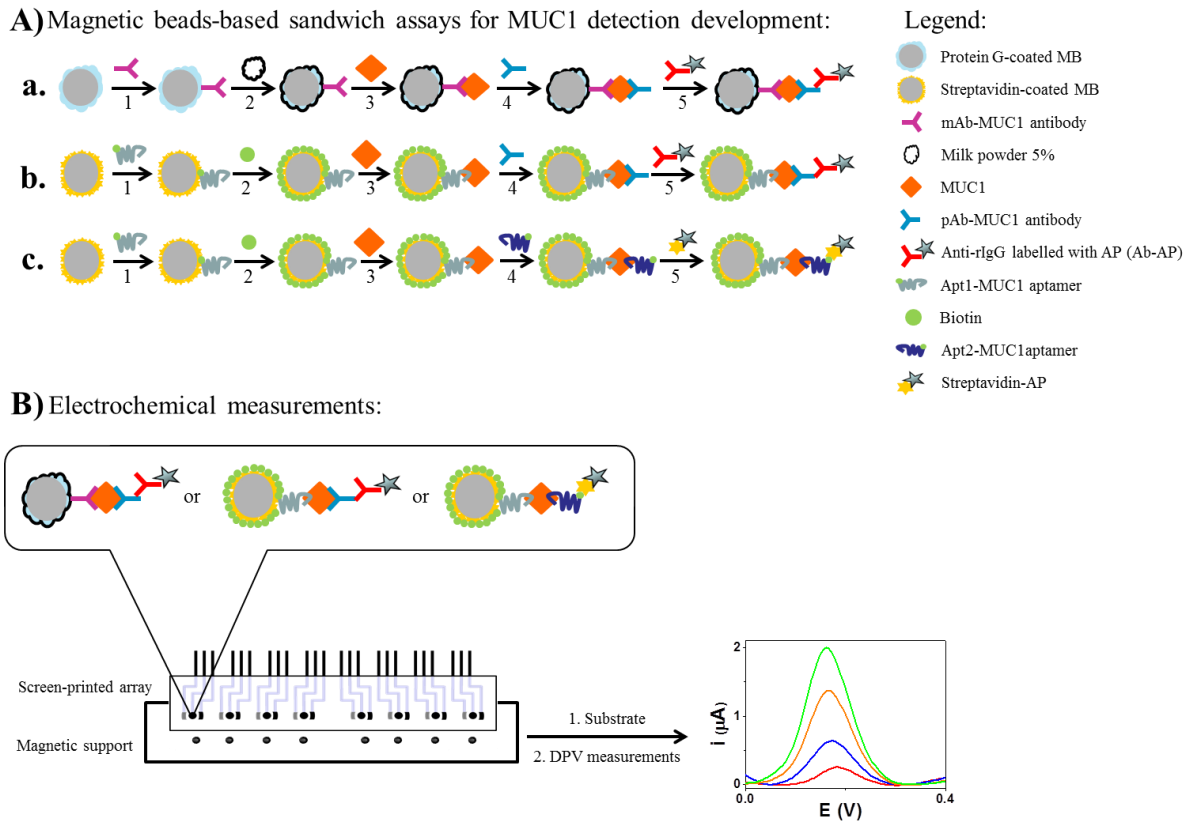

Figure 7.1. A) Schematic representation of the steps involved in the development of different MUC1 assays: a. Antibody – Antibody assay (Ab – Ab): 1) incubation of protein G-modified magnetic beads with primary anti-MUC1 antibody (mAb-MUC1); 2) blocking step with milk powder 5% prepared in 0.1 M PBS buffer pH 7.4; 3) affinity reaction with MUC1 protein; 4) incubation with secondary anti-MUC1 antibody (pAb-MUC1); 5) incubation with alkaline phosphatase (AP)-labelled anti-rabbit IgG tertiary antibody (Ab-AP). b. Aptamer – Antibody assay (Apt – Ab): 1) incubation of streptavidin-modified magnetic beads with biotinylated primary anti-MUC1 aptamer (Apt1-MUC1); 2) blocking step with biotin; 3) incubation with MUC1 protein; 4) incubation with secondary anti-MUC1 antibody (pAb-MUC1); 5) incubation with alkaline-phosphatase (AP) labelled anti-rabbit IgG tertiary antibody (Ab-AP). c. Aptamer – Aptamer assay (Apt – Apt): 1) incubation of streptavidin-modified magnetic beads with biotinylated primary anti-MUC1 aptamer (Apt1-MUC1); 2) blocking step with biotin; 3) incubation with MUC1 protein; 4) incubation with secondary biotinylated anti-MUC1 aptamer (Apt2-MUC1); 5) incubation with streptavidin-alkaline phosphatase.B) Electrochemical measurements: screen-printed array were placed on an magnetic support and modified-magnetic beads were deposited on the surface of each working electrode of the array.

In case of all three assays, the amount of protein captured by the bioreceptor, was quantified by measuring the electrochemical signal obtained by differential pulse voltammetry (DPV) after the conversion of enzymatic substrate 1-naphtyl phosphate to 1-naphthol electroactive product. For the measurements, 10 µL of the final beads

suspension were placed onto each working electrode of the array, using a magnetic support to concentrate the magnetic beads on the working electrode. Thus, each well of the array was filled with 60 µL of a solution containing 1 mg mL^{-1} of 1-naphthyl phosphate prepared in buffer E. After 6 min of incubation time, DPV measurements were carried out for each electrochemical cell.
Control experiments in all bioassays were also performed omitting the MUC1 protein from the assay.

2.3. Protocol of antibody - antibody sandwich assay

2.3.1. Immobilization of primary antibody

For the functionalization of the magnetic beads, 100 µL of the beads suspension were taken from the stock solution of Protein G-coated magnetic beads (30 mg mL^{-1}), added in a vial and washed with Buffer A for three times. For the washing step the beads were re-suspended in 500 µL buffer and mixing by vortex.
Then the tube was placed in a magnetic separation stand to capture the magnetic beads on the bottom of the tube, allowing the removal of the supernatant.
After the washing steps 200 µL of Ab1 solution 50 µg mL^{-1} prepared in buffer A was added to the beads and incubated for 120 minutes in the rotating stand at room temperature.

2.3.2. Blocking of free binding-sites

In order to reduce the non-specific adsorption of the reagents used in the following steps of the immunoassay, the free binding-sites of the beads were blocked using casein in milk powder as a blocking agent.
For the blocking step the functionalized beads were first washed for three times with 500 µL buffer A. Afterwards 1 mL milk powder solution 5% prepared in buffer A was added and incubated for 120 minutes in the rotating stand at room temperature. The beads were washed and reconstituted in 1 mL buffer A.
The functionalized beads suspension was stored at 4ºC temperature for up to one week for further experiments.

2.3.3. Capturing of MUC1 protein

To obtain a calibration curve, 50 µL of the functionalized magnetic beads suspension were placed in a vial, in magnetic stand separator and, after removing the supernatant, 500 µL of MUC1 protein solution in buffer B was added in the concentration range of 0 – 10 ng mL^{-1}.
The samples were incubated for 60 minutes in the rotating stand at room temperature and then washed with buffer A.

2.3.4. Binding of secondary antibody and third antibody labeled with alkaline phosphatase

200 µL of Ab2 solution 5 µg mL^{-1} prepared in buffer A were added to the beads and incubated for 60 minutes in the rotating stand at room temperature.
The beads were then washed three times with buffer E. Then, 200 µL of a solution containing Ab3-AP (0.5 µg mL^{-1}) with 1% mg mL^{-1} BSA were added to the beads and incubated for 10 minutes. After a washing step, the beads were reconstituted in 50 µl buffer E, proceeding with the electrochemical measurements.

2.4. Protocol of aptamer - antibody sandwich assay

2.4.1. Immobilization of the primary aptamer

In order to unfold the aptamer strand, a thermal treatment was applied to the aptamer solution before the immobilization on magnetic beads. The biotinylated aptamer solution was heated at 90 ºC and then gradually cooled at 25 ºC followed by fast cooling in freezer for to keep the folded structure of the aptamer.
Afterwards 100 µL of suspension were taken from the stock solution of streptavidin – magnetic beads (10 mg mL^{-1}), added in a vial and washed with buffer C for three times using the magnetic separation stand.
The beads were re-suspended in 200 µL buffer C and 200 µL solution of biotinylated aptamer (Apt1) in water was added, to reach the final concentration of the aptamer of 5 µM, followed by an incubation step of 30 minutes in the rotating stand at room temperature and then washed with buffer A.

2.4.2. Blocking of free binding-sites

For the blocking of the remaining active sites, Apt1 modified magnetic beads were incubated for 30 minutes with 500 µL biotin 1 mM prepared in buffer A in the rotating stand at room temperature. The beads were washed three times with buffer C and reconstituted in 1 mL buffer C.

2.4.3. Capturing the MUC1 protein

To obtain a calibration curve, 50 µL of the functionalized magnetic beads suspension were incubated with 500 µL of MUC1 protein solution in buffer D in the concentration range of 0 – 10 ng mL^{-1} for 45 minutes in the rotating stand at room temperature and then washed three times with buffer D.

2.4.4. Binding of secondary antibody and third antibody labeled with alkaline phosphatase

Apt1-MUC1 modified beads were incubated with 200 µL of Ab2 solution 5 µg mL^{-1} prepared in buffer D for 30 minutes in the rotating stand at room temperature. Subsequently, 200 µL of a solution containing Ab3-AP with 1% mg mL^{-1} BSA were added to the beads and incubated for 10 minutes. The beads were washed with buffer E and were reconstituted in 50 µL buffer E for the electrochemical measurements.

2.5. Protocol of aptamer – aptamer sandwich assay

For the immobilization of the primary biotinylated aptamer (Apt1) on streptavidin-magnetic beads and the capturing of MUC1 protein the experiments were performed in the same way as described in the protocol of aptamer-antibody assay in section 2.5. In the following section, the labeling of the affinity reaction with the secondary biotinylated aptamer (Apt2) and streptavidin-alkaline phosphatase is reported.

2.5.1. Binding of secondary aptamer and streptavidin-alkaline phosphatase

200 µL secondary aptamer (Apt2) solution 1 µM prepared in buffer D was incubated for 10 min with the beads modified with the affinity complex Apt1-MUC1, at room

temperature, under stirrer. Then, the beads were washed with buffer E and incubated with 200 µL streptavidin conjugated with AP solution in buffer D for 15 minutes. At last, after washing, the beads were suspended in 50 µL buffer D.

2.6. Analysis of human serum samples

When testing human serum, firstly the serum was filtered (Filtropur S, diameter of filter pores 0.2 µM), then diluted 1:200 with the buffer D for the incubation step with MUC1 solution. 50 µl beads suspension, functionalized with aptamer (Apt1), was incubated with 500 µl of the solutions above carrying out the experiments as previously described in the protocol in section 2.3.3.

Experiments were carried out on commercial normal human serum spiked with different MUC1 concentrations.

Pathological serum samples from cancer patients were also analyzed. Standard addition method was performed to quantify the amount of antigen in the samples.

2.7. Measurement with screen-printed 8-sensor arrays

10 µL of beads suspension were deposited onto the surface of each working electrode of the array, and kept in its position through the magnet holding block.

Thus, each well of the array was filled with 60 µL of a solution containing 1 mg mL^{-1} of 1-naphthyl phosphate prepared in buffer E.

After 6 min of incubation time, DPV measurement was left to start. DPV was carried out sequentially for each channel.

3. Results and discussion

In case of each configuration of the bioassays for the detection of MUC1 tumor marker, the experimental parameters were optimized in order to find the best conditions for the assay.

Experimental parameters such as the concentration of antibodies and aptamers, incubation time with antibodies, aptamers and protein, as well as the type, concentration and incubation time with blocking agents, were tested for 0 ng mL^{-1} and 5 ng mL^{-1} MUC1.

For this purpose, the measurements were performed for one concentration of MUC1 (5 ng mL^{-1}) and compared with the blank (0 ng mL^{-1}).

The best parameters were chosen taking in consideration the current ratio between 5 ng mL^{-1} MUC1 and the blank (I_{MUC1}/I_{blank}) and on the CV% obtained.

3.1. Optimization of antibody – antibody assay parameters

The concentration and incubation time with the primary antibody had to be first optimized (Table 7.1.). The magnetic beads were functionalized with 50 and 100 µg mL^{-1} Ab1 solution and the assay was carried out as previously described. No increase in the I_{MUC1}/I_{blank} ratio (1.36 for 50 µg mL^{-1} respects to 1.19 for 100 µg mL^{-1}) was observed with the increase of the concentration of primary antibody solution, thus 50 µg mL^{-1} Ab1 solution was chosen for further experiments.

Table 7.1. Experimental parameters optimization for antibody – antibody sandwich assay. $I_{MUC}1/I_{blank}$ represent the ration between the current obtained using respectively 5 ng mL^{-1} and 0 ng mL^{-1} MUC1 buffered solution. Letters and numbers present in Assay step column are referred in accordance of Figure 7.1 A.

Assay. step	Prameters		Current ratio (I_{MUC1}/I_{blank})	Average CV%
a.1	Ab1 concentration	50 µg mL^{-1}	1.36	7
		100 µg mL^{-1}	1.19	8
a.2	Milk powder 5% incubation time	120 min	1.30	7
		overnight	0.90	6
	rIgG (10 µg mL^{-1})	120 min	0.82	8
		overnight	0.92	7
a.3	MUC1 incubation time	60 min	1.40	7
		90 min	1.02	6
a.4	Ab 2 concentration (60 min)	2 µg mL^{-1}	1.00	8
		5 µg mL^{-1}	1.40	7
		10 µg mL^{-1}	0.83	5
	Ab2 incubation time (5 µg mL^{-1})	30 min	0.90	7
		60 min	1.40	9
		90 min	1.00	6

Average CV% was calculated by means of three bioassay repetition for each concentration.

Various blocking agents were investigated in order to reduce nonspecific adsorption on the free sites of the beads in different steps of the assay and the results are also reported in Table 7.1. Milk powder 5% and bovine IgG 10 µg mL^{-1}, were used as blocking agents after the functionalization of protein G beads with the primary antibody. To observe the

effectiveness of using bovine IgG as blocking agent the beads were incubated, after the functionalization with primary antibody, with 1 mL 10 µg mL^{-1} bovine IgG solution in buffer A, for 120 minutes and overnight at 4ºC and the experiments were carried out as previously described. The incubation time with milk powder 5% was also optimized, incubating the functionalized beads with milk powder solution 5% in buffer A, for 120 minutes and overnight. In the case of rabbit IgG in different incubation times and milk powder 5% overnight the signals obtained for the blank and one concentration MUC1 (5 ng mL^{-1}) were not improved, the best results being obtained in case of 120 minutes incubation time with milk powder 5%.

The optimization of the incubation time with protein was also performed. For this, the modified beads were incubated for 60 and 90 minutes with 5 ng mL^{-1} MUC1 protein. The ratio between the signal and the blank was 1.4 and 1.02 respectively, indicating that for 60 minutes a steady-state is achieved.

In order to achieve the best conditions for the complete formation of the immunocomplex, the concentration (2, 5 and 10 µg mL^{-1}) and incubation time (30, 60 and 90 minutes) with secondary antibody was further optimized. The concentration of 2 µg mL^{-1} and the incubation time of 30 minutes was insufficient for binding the whole amount of protein in the sample to form an immunocomplex. For a higher concentration (10 µg mL^{-1}) and a longer incubation time (90 minutes) the secondary antibody binds probably directly on the beads that were not completely covered by the primary antibody and blocking agent, leading to a nonspecific adsorption of the following reagents added and a lower current ratio between 5 ng mL^{-1} MUC1 and blank. Therefore the intermediate concentration of 5 µg mL^{-1} and incubation time of 60 min were considered optimum for further experiments.

3.2. Optimization of aptamer-antibody assay parameters

To further improve the performance of the biosensor and overcome the back draws of antibodies use, the primary antibody was replaced with an aptamer, in the second approach. The immobilization of the primary aptamer on the surface of the magnetic beads with an appropriate orientation and flexibility for binding the target protein is of paramount importance for the performance of the assay. In order to optimize the concentration and incubation time with the primary aptamer 1 µM and 5 µM of Apt1 solution were incubated for 30 min and overnight with the streptavidin beads, followed by

a blocking step and the reaction with protein, Ab2 and Ab3-AP. The assay showed better response for a higher concentration of aptamer (5 µM) and lower incubation time (30 min): these conditions assuring a proper conformation of the aptamer for capturing the protein.

Taking in consideration that streptavidin modified magnetic beads were used to bind the biotinylated aptamer, biotin was chosen as blocking agent. Concentrations of 100 µM and 1 mM of biotin solution at different incubation times were investigated. The results showed that 1 mM solution used with incubation time of 30 minutes ensured an optimum magnetic beads-surface blocking.

Table 7.2. Experimental parameters optimization for aptamer – antibody sandwich assay. $I_{MUC}1/I_{blank}$ represent the ration between the current obtained using respectively 5 ng mL^{-1} and 0 ng mL^{-1} MUC1 buffered solution. Letters and numbers present in Assay step column are referred in accordance of Figure 7.1 A.

Assay step	Prameters		Current ratio (I_{MUC1}/I_{blank})	Average CV%
b.1	Apt1 concentration (30 min)	1 µM	1.3	8
		5 µM	3.3	9
	Apt1 incubation time (5 µM)	30 min	3.3	12
		overnight	1.2	10
b.2	Biotin concentration (30 min)	100 µM	0.8	14
		1 mM	5.5	7
	Biotin incubation time (1mM)	30 min	5.5	7
		overnight	5.2	7
b.3	MUC1 incubation time	30 min	2.0	6
		45 min	5.0	7
		60 min	5.2	7
b.4	Ab2 incubation time (5 µg mL^{-1})	10 min	2.7	8
		30 min	5.3	10
		60 min	5.0	8

Average CV% was calculated by means of three bioassay repetition for each concentration.

The best conditions for binding the protein to the immobilized aptamer were then investigated.

The functionalized beads were left to incubate with the target for 30, 45 and 60 minutes. The incubation time of 30 min was not sufficient, whereas a similar higher signal to blank ratio being obtained after 45 and 65 minutes. Thus, an incubation time of 45 minutes was

selected (Table 7.2.). Incubation time of Ab2 was then optimized. It was possible notice that with this assay configuration a lower incubation time (30 minutes), respect of Ab2 incubation time for antibody – antibody assay, was found to be sufficient to bind the MUC1 protein.

This can be probably related to the fact that the smaller dimensions of the Apt1 (in comparison with the dimension of Ab1) increase the availability of the secondary epitope of MUC1 (Table 7.2.).

3.3. Optimization of aptamer - aptamer assay parameters

To accomplish the analysis of various possible formats of the magnetic beads based assay for MUC1 detection, a further assay was developed based on two different aptamers in a sandwich format.

To appraise the influence of the concentration and incubation time with secondary aptamer, the Apt1-MUC1-modified beads were left to incubate with different concentrations of Apt2 solution for 10, 15 and 30 minutes.

Increasing the concentration of the secondary aptamer from 0.5 to 1 μM resulted in an increase in the signal/blank ratio from 2.7 to 5.3, whereas a lower incubation time of 10 min seemed to be sufficient for the complete formation of the Apt1-MUC1-Apt2 complex.

Table 7.3. Experimental parameters optimization for aptamer – aptamer sandwich assay. $I_{MUC}1/I_{blank}$ represent the ratio between the current obtained using respectively 5 ng mL^{-1} and 0 ng mL^{-1} MUC1 buffered solution. Letters and numbers present in Assay step column are referred in accordance of Figure 7.1 A.

Assay step	Prameters		Current ratio (I_{MUC1}/I_{blank})	Average CV%
c.4	Apt2 concentration (15 min)	0.5 μM	2.0	7
		1.0 μM	5.3	8
	Ap2 incubation time (5 μg mL^{-1})	10 min	5.3	8
		15 min	4.9	10
		30 min	4,7	8

Average CV% was calculated by means of three bioassay repetition for each concentration

The last step, of incubation with the enzymatic conjugate had to be optimized as well.

The modified beads were incubated with streptavidin-AP solution for 10 and 15 min. 10 min incubation time was insufficient, a higher current being obtained in this case for the blank respect to 5 ng mL^{-1} (0.33±0.01 µA, 0.053±0.004 µA respectively), thus the incubation time of 15 min was chosen for further experiments.

3.4. Calibration curve of MUC1 in buffered solutions

A dose-response curve has been obtained under the optimized experimental conditions in MUC1 buffered solution for each assay and the analytical performance of the optimized sensors is reported in Table7.4.

A linear response was obtained in the range of 0 - 10 ng mL^{-1}, which is also the important range from the clinical point of view. In order to test the reproducibility three determinations on different screen-printed cells were assayed for each concentration and the average CV% was calculated.

Table 7.4. Analytical performances of antibody – antibody (Ab – Ab), aptamer – antibody (Apt – Ab), aptamer – aptamer (Apt – Apt) assays performed in MUC1 buffered solutions. Letters a, b., c. are referred in accordance of Figure 7.1 A.

Type of assay	LOD (ng mL^{-1})*		R^2	Average CV %**
a. Ab – Ab	2.5	y = 0.06x+1.57	0.88	7
b. Apt – Ab	2.4	y = 0.05x+0.10	0.93	11
c. Apt – Apt	1.36	y = 0.10x+0.55	0.96	5

* LOD (limit of detection) was calculated by the ratio between three times the blank ($3S_{blank}$) standard deviation and the slope of calibration curve: LOD = $3S_{blank}$/Slope

** Average CV% was calculated by means of three bioassay repetition for each concentration

Results show a better reproducibility and a lower detection limit using aptamer sandwich assay respect to dual antibody and antibody – aptamer assay.

3.5. Selectivity of the assays

Nonspecific proteins, members of the mucins family, which have been studied as tumor markers, such as MUC4 and MUC16 were analyzed in order to evaluate the selectivity of the three developed assays. For this purpose, the above described procedures were employed for 5 ng mL^{-1} MUC1, 5 ng mL^{-1} MUC4 and 35 U mL^{-1} MUC16.

The concentrations were chosen with respect to the threshold value of MUC1, MUC4 and MUC16 tumor marker.

The results (Figure 7.2.) showed that the antibody - antibody immunoassay is not specific for MUC1 protein, while a higher signal being obtained for both MUC4 and MUC16 proteins probably due to the similar structures of the three mucins, which the antibodies are not able to discriminate.

When antibodies were replaced with aptamers, the signal obtained for the non-specific proteins was approximately the same as the signal of the blank showing that the aptamer-based assays are highly specific for MUC1 tumor marker.

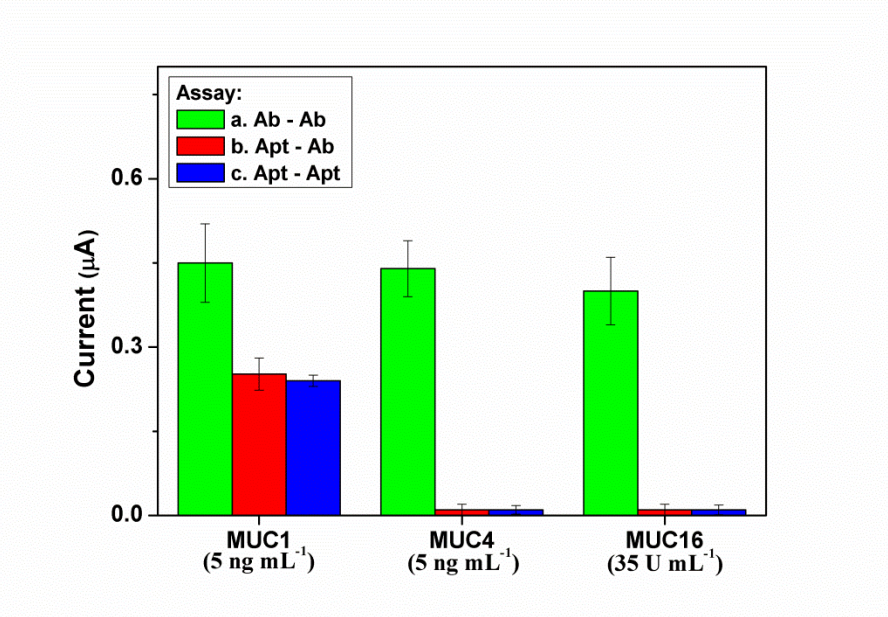

Figure 7.2. Selectivity of the different developed assays performed in MUC1 (5 ng mL^{-1}), MUC4 (5 ng mL^{-1}) and MUC16 (35 U mL^{-1}) buffered solution (a. Ab – Ab assay; b. Apt – Ab assay; c. Apt – Apt assay). Blank signal was substracted from each measurement.

Thus, in accordance with the results obtained from the development of the calibration curves in buffered solution for the three different assays, aptamer sandiwich assay was selected for the analysis of non-pathological and pathological patient serum samples.

3.6. Serum samples analysis

Once verified the suitability of the aptamer-aptamer assay to detect MUC1 in standard solutions, preliminary experiments using normal human serum samples were carried out.

With this aim, batches of a non pathologic serum AB group from women were spiked with MUC1 in order to have different final concentrations.

The obtained results show an increase of the current between serum alone and serum added with different concentration of MUC1 protein (Figure 7.3.). These experiments further demonstrated the selectivity of the aptasensor, since, despite the high complexity of serum, the measurements allowed the discrimination between the MUC1 spiked serum samples. Moreover, good reproducibility in terms of CV% was also obtained (average CV% = 7).

Phatological serum samples were also analyzed. The samples were from hospital women patients who have been subjected to breast and ovarian carcinoma: tissue samples were analyzed by histological diagnosis. Standard addition method was used in order to quantify the amount of the MUC1 in the serum samples using the aptamer sandwich assay (Table 7.5). Qualitative correlation between MUC1concentration and malignancy stage can be done.

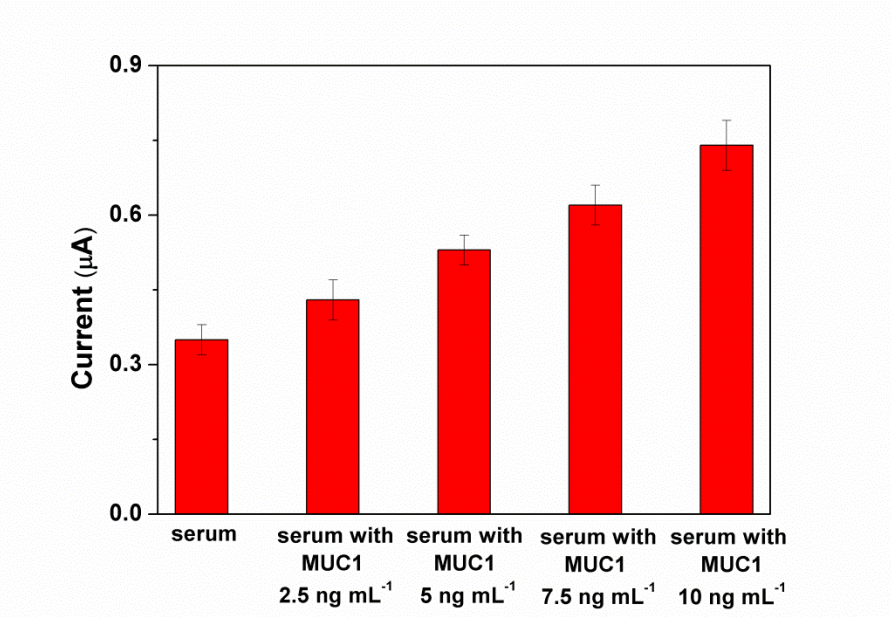

Figure 7.3. Exepriments with commercial serum sample 1:200 diluted spiked with MUC1 at different concentrations using sandwich aptamer assay.

The serum samples of different ovarian pathological conditions were analyzed (Table 5: from 1 to 4 sample). A higher MUC1 concentration in the sample 3 respect to others was detected. This could be due to the fact that both ovaries are affected by the tumor.

Moreover, the MUC1 lower value obtained for sample 4 is related to the presence of a non-malignant pathology.

Serum samples from patients affected by invasive ductal breast carinoma were also analyzed (Table 5: from 5 to 9 sample). The samples were characterized by the Nottingham Prognostic Index (NPI), which is used to determine the prognosis following surgery for breast cancer. Is calculated using three criteria: the size of the lesion, the number of involved lymph nodes and the grade of tumor. A 93% 5-year survival rate is associated with score 2, whereas for score 3 the 5-year survival rate is 85%. Comparable MUC1 concentrations were obtained in the samples 5 and 7 corresponding serum samples of patients with 2 NPI value. On the contrary, resulted a higher MUC1 concetration could be detected in the samples 6, 8 and 9 with 3 NPI value.

The proposed aptassay demonstrated to be a potential test to screen clinical samples for the evaluation to distinguish the stage of the tumours.

Table 7.5.MUC1 determination in 1:200 diluted serum sample form cancer patients performed with aptamers sandich assay using standard addition method.

Serum samples	Histological Diagnosis	MUC1 concentration (ng mL^{-1})	Average CV%
1	Left ovarian carcinoma	169	12
2	Right ovarian tumor	274	12
3	Bilateral ovarian carcinoma	500	14
4	Right ovarian cyst	25	13
5	Invasive ductal breast carcinoma	121	17
6	Invasive ductal breast carcinoma	639	13
7	Invasive ductal breast carcinoma	105	14
8	Invasive ductal breast carcinoma	234	11

9	Invasive ductal breast carcinoma	198	13

Average CV% was calculated by means of three bioassay repetition for each concentration.

4. Conclusions

In this work, three affinity sensors were developed for the detection of MUC1 tumor marker magnetic beads modified with various bioreceptors and SPC arrays. The first approach was an antibody - antibody ELISA-like assay. To obtain a higher specificity for MUC1 protein the antibodies were subsequently replaced with aptamers. The designed aptasensor showed a good sensitivity with limits of detection 1.36 ng mL^{-1} in the linear range of 0-10 ng mL^{-1} in buffered solutions.

Moreover, the proposed aptasensor was tested in human pathological women serum samples for the detection of MUC1 protein, demonstrating the potential practical applications in biological samples and offering a promising tool in biomedical applications.

Acknowledgements:

The authors are grateful for the financial support to Ministero dell'Istruzione, dell'Università e della Ricerca, Italy, PRIN 2009 and UMF "Iuliu Haţieganu" research grant (27027/3/15.11.2011), PNII IDEI grant no. 338/2011 and SC PolisanoPharma SRL.

The authors thank the Oncology Institute "Ioan Chiricua" for kindly providing the serum samples from hospital patients.

References

[1] D'Orazio P. Biosensors in clinical chemistry — 2011 update. Clin Chim Acta 2011; 412:1749-61.
[2] Pérez-López B, Merkoçi A. Nanomaterials based biosensors for food analysis applications. Trends in Food Science & Technology 2011; 22:625-39.
[3] Turner APF. Biosensors: sense and sensibility. Chem Soc Rev 2013; 42:3184-96.
[4] Perfezou M, Turner A, Merkoci A. Cancer detection using nanoparticle-based sensors. Chem Soc Rev 2012; 41:2606-22.
[5] Chikkaveeraiah BV, Bhirde AA, Morgan NY, Eden HS, Chen X. Electrochemical Immunosensors for Detection of Cancer Protein Biomarkers. Acs Nano 2012; 6:6546-61.
[6] Diaconu I, Cristea C, Hârceagă V, Marrazza G, Berindan-Neagoe I, Săndulescu R. Electrochemical immunosensors in breast and ovarian cancer. Clin Chim Acta 2013; 425:128-38.
[7] Ricci F, Adornetto G, Palleschi G. A review of experimental aspects of electrochemical immunosensors. Electrochim Acta 2012; 84:74-83.
[8] Makaraviciute A, Ramanaviciene A. Site-directed antibody immobilization techniques for immunosensors. Biosensors and Bioelectronics 2013; 50:460-71.
[9] Harris M, Tombelli S, Marrazza G, Turner AP, Affibodies as an alternative to antibodies in biosensors for cancer markers. In: Higson S, editor. Biosensors for medical applications: Woodhead Publishing Limited, 2012: 217-32.
[10] Berti F, Todros S, Lakshmi D, et al. Quasi-monodimensional polyaniline nanostructures for enhanced molecularly imprinted polymer-based sensing. Biosens Bioelectron 2010; 26:497-503.
[11] Centi S, Tombelli S, Mascini M. Electrochemical Aptamer-Based Biosensors. Electrochemical DNA biosensors 2012:29.
[12] Mascini M, Palchetti I, Tombelli S. Nucleic Acid and Peptide Aptamers: Fundamentals and Bioanalytical Aspects. Angewandte Chemie International Edition 2012; 51:1316-32.
[13] Soper SA, Brown K, Ellington A, et al. Point-of-care biosensor systems for cancer diagnostics/prognostics. Biosensors and Bioelectronics 2006; 21:1932-42.
[14] Amaya-González S, de-los-Santos-Álvarez N, Miranda-Ordieres A, Lobo-Castañón M. Aptamer-Based Analysis: A Promising Alternative for Food Safety Control. Sensors 2013; 13:16292-311.
[15] Berti F, Laschi S, Palchetti I, et al. Microfluidic-based electrochemical genosensor coupled to magnetic beads for hybridization detection. Talanta 2009; 77:971-8.
[16] Ravalli A, dos Santos GP, Ferroni M, Faglia G, Yamanaka H, Marrazza G. New label free CA125 detection based on gold nanostructured screen-printed electrode. Sensors and Actuators B: Chemical 2013; 179:194-200.
[17] Taleat Z, Ravalli A, Mazloum-Ardakani M, Marrazza G. CA 125 Immunosensor Based on Poly-Anthranilic Acid Modified Screen-Printed Electrodes. Electroanal 2013; 25:269-77.
[18] Ambrosi A, Castañeda MT, Killard AJ, Smyth MR, Alegret S, Merkoçi A. Double-Codified Gold Nanolabels for Enhanced Immunoanalysis. Anal Chem 2007; 79:5232-40.
[19] Al-Khafaji QAM, Harris M, Tombelli S, et al. An Electrochemical Immunoassay for HER2 Detection. Electroanal 2012; 24:735-42.

[20] Mendes RK, Laschi S, Stach-Machado DR, Kubota LT, Marrazza G. A disposable voltammetric immunosensor based on magnetic beads for early diagnosis of soybean rust. Sensors and Actuators B: Chemical 2012; 166–167:135-40.
[21] Chikkaveeraiah BV, Mani V, Patel V, Gutkind JS, Rusling JF. Microfluidic electrochemical immunoarray for ultrasensitive detection of two cancer biomarker proteins in serum. Biosensors and Bioelectronics 2011; 26:4477-83.
[22] Zani A, Laschi S, Mascini M, Marrazza G. A New Electrochemical Multiplexed Assay for PSA Cancer Marker Detection. Electroanal 2011; 23:91-9.
[23] Erdem A, Congur G. Impedimetric detection of in situ interaction between anti-cancer drug bleomycin and DNA. International Journal of Biological Macromolecules 2013; 61:295-301.
[24] Erdem A, Congur G, Eksin E. Multi channel screen printed array of electrodes for enzyme-linked voltammetric detection of MicroRNAs. Sensors and Actuators B: Chemical 2013; 188:1089-95.
[25] Van Elssen CH, Frings PW, Bot FJ, et al. Expression of aberrantly glycosylated Mucin-1 in ovarian cancer. Histopathology 2010; 57:597-606.
[26] Vlad AM, Diaconu I, Gantt KR. MUC1 in endometriosis and ovarian cancer. Immunologic research 2006; 36:229-36.
[27] Mukhopadhyay P, Chakraborty S, Ponnusamy MP, Lakshmanan I, Jain M, Batra SK. Mucins in the pathogenesis of breast cancer: implications in diagnosis, prognosis and therapy. Biochimica et biophysica acta 2011; 1815:224-40.
[28] Kaira K, Nakagawa K, Ohde Y, et al. Depolarized MUC1 expression is closely associated with hypoxic markers and poor outcome in resected non-small cell lung cancer. International journal of surgical pathology 2012; 20:223-32.
[29] Winter JM, Tang LH, Klimstra DS, et al. A novel survival-based tissue microarray of pancreatic cancer validates MUC1 and mesothelin as biomarkers. Plos One 2012; 7:e40157.
[30] Ferreira CS, Matthews CS, Missailidis S. DNA aptamers that bind to MUC1 tumour marker: design and characterization of MUC1-binding single-stranded DNA aptamers. Tumour biology : the journal of the International Society for Oncodevelopmental Biology and Medicine 2006; 27:289-301.
[31] Ferreira CS, Papamichael K, Guilbault G, Schwarzacher T, Gariepy J, Missailidis S. DNA aptamers against the MUC1 tumour marker: design of aptamer-antibody sandwich ELISA for the early diagnosis of epithelial tumours. Anal Bioanal Chem 2008; 390:1039-50.

General conclusions

In this work various nanostructured electrochemical biosensors for the detection of tumoral biomarkers (in particular for CA125, HER2, VEGF, and MUC1) related to ovarian and breast cancers were developed employing different types of bioreceptors (antibodies, aptamers and Affibodies®) and different electrochemical techniques.

In particular gold nanoparticles (AuNPs) were used as sensing/signal amplification platform in two different approaches.

In the first one, AuNPs were electrodeposed on the surface of graphite screen-printed electrodes (GSPEs) in order to be functionalized with more capture probe allowing the recognition of a higher number of targets of interest.

Electrodeposition was performed by simple cyclic voltammetry procedure. In optimized condition GSPE surface was covered by randomly distributed AuNPs with dimensions ranging from 40 to 100 nm.

Electrodeposed AuNPs were subsequently functionalized with the bioreceptor and then the affinity reaction with analyte was evaluated by means of electrochemical impedance spectroscopy (EIS), in a label-free strategy, or by differential pulse voltammetry (DPV), in a sandwich-based approach.

AuNPs-based CA125 and HER2 label-free biosensors were developed using respectively anti-CA125 antibody anti-HER2 Affibody® as bioreceptors. Both label-free biosensors allowing the determination of these cancer biomarkers in a useful clinical range of concentration (from 0 to 100 U mL^{-1} for CA125 and from 0 to 40 µg L^{-1} for HER2) with a limit of detection below the clinical threshold values (6.7 U mL^{-1} and 6.7 µg L^{-1} respectively for CA125 and HER2 label-free biosensors).

Moreover, an unambiguous identification of the related cancer biomarker (no significant non-specific signal was detected in the case of all negative controls) coupled with successfully detection of these cancer related protein in biological matrices were verified.

Gold nanostructured-based aptamers sandwich biosensor was also developed for the determination of VEGF cancer biomarker.

VEGF was successfully sandwiched by a thiolated capture aptamer and a biotinylated detection aptamer. Streptavidin-alkaline phosphatase was then incubated with the sensors and the electrochemical behaviour of alpha-naphthol was analysed by differential pulse

voltammetry (DPV). The sensitivity and the reproducibility achieved were adequate for the analysis of VEGF cancer biomarker (linear range 0 – 250 nM, limit of detection 30 nM). Moreover, the developed sandwich aptasensor showed good selectivity.

In a second approach, AuNPs colloidal solutions were synthetized by citrate reduction methods, conjugated with anti-CA125 detection antibodies and used to complete a sandwich assay for the detection of CA125 cancer biomarker.
After the immobilization of the capture probe on polyanthranilic acid-modified GSPEs, AuNPs-conjugated anti-CA125 detection antibodies were introduce in the system.
The AuNPs captured onto immunosensor surface induced the silver deposition from a silver enhancer solution which allows the detection of the deposited AgNPs by anodic stripping analysis. A high sensitivity with a detection limit of 2 U mL^{-1} of human CA125 protein was achieved. This level of detection could be attributed to the sensitive electrochemical determination of silver ions and to the catalytic precipitation of a large number of silver ions on the gold nanoparticles- labelled antibody.

Finally, different electrochemical bioassays for Mucin1 (MUC1) tumor marker using magnetic beads coupling screen-printed arrays were developed and used for analysis in biological samples.
The bioassays are based on a sandwich format in which aptamers or antibodies were coupled respectively to Streptavidin or Protein G-modified magnetic beads.Under the optimal conditions, a linear response was obtained ranging from 0 to 10 ng mL^{-1} in MUC1 buffered solution for all three assays, with detection limits: 2.5, 2.4 and 1.36 ng mL^{-1}, respectively for antibodies-based, aptamer-antibody-based and aptamers-based sandwich assays.
The results showed that the aptamer-based approaches exhibit both an high sensibility and an high selectivity for the detection of MUC1 protein. Thus, the proposed aptasensor was tested in human pathological women serum samples for the recognizement of MUC1 cancer biomarker.
Comparison with histological analysis demostrated the potential practical applications of the deveolped aptasensor dfor the detection of MUC1 in biological samples and offering a promising tool for biomedical applications.

In summary, this work proposed the description of several strategies for the development of nanostructured biosensors for the detection of a pattern of breast and ovarian cancer biomarkers.

Nanostructures (gold and magnetic nanoparticles) provide a useful suitable platform for biomolecules immobilization (which retain their biological activity) and facilitate the electron transfer between the immobilized proteins and electrode surfaces which result in an enhancement of analytical performance of the biosensor for the detection of the cancer-related proteins of interest.

Finally, because the analysis of a single cancer biomarker lacks in sensitivity and the ability to optimally combine information on multiple markers becomes necessary for useful mass screening, the developed nanostructured biosensors offer promising tools in clinical applications.